UNIVERSITY OF OKLAHOMA

GRADUATE COLLEGE

EXPERIMENTAL STUDY OF EFFECT OF PROPPANT CONCENTRATION, TYPES, SIZES, ROCK MINERALOGY AND OVERBURDEN STRESS ON FRACTURE CONDUCTIVITY

A THESIS

SUBMITTED TO THE GRADUATE FACULTY

in partial fulfillment of the requirements for the

Degree of

MASTER OF SCIENCE

By

ABHISHEK KUMAR GUPTA
Norman, Oklahoma
2019

EXPERIMENTAL STUDY OF EFFECT OF PROPPANT CONCENTRATION, TYPES, SIZES, ROCK MINERALOGY AND OVERBURDEN STRESS ON FRACTURE CONDUCTIVITY

A THESIS APPROVED FOR THE
MEWBOURNE SCHOOL OF PETROLEUM AND GEOLOGICAL ENGINEERING

BY THE COMMITTEE CONSISTING OF

Dr. Chandra Rai, Chair

Dr. Carl Sondergeld

Dr. Deepak Devegowda

Acknowledgements

I would like to express my sincere gratitude to my advisors Dr. Chandra Rai and Dr. Carl Sondergeld for providing me this amazing opportunity to work with them in their world class lab facility and their valuable guidance throughout the course of my thesis. I am thankful to my family for their continuous support to fulfill my dream of higher studies. I am thankful to Dr. Deepak Devegowda for being a part of my thesis committee.

I am deeply grateful to Dr. Richard Larese for his valuable SEM analysis. I would also like to thank Jeremy Jernigen and Gary Stowe for helping me with the experimental setup. I am thankful for the Unconventional shale consortium for their financial support to make this research possible. I would also like to thank Abinav, Ishank, Sayantan and Son for their help during my research. Last but not least, I would like to thank my friends Bhairav, Alpha, Rod and Aditi for being in my life and making this journey, a memorable one.

Table of Contents

List of tables

List of Figures

Abstract

Hydrocarbon production from unconventional reservoirs, particularly shales, requires massive hydraulic fractures to expose the large surface areas within the formation and provide a conduit to the wellbore. Proppants are pumped along with the fracturing fluids during hydraulic fracturing to keep the fractures open. For the economic production of hydrocarbon, maintaining the conductivity of such fractures is critical. However, there are different mechanisms such as proppant crushing, fines migration, proppant embedment and proppant diagenesis etc., which can lead to the significant reduction in fracture conductivity with time. The severity of each mechanisms varies substantially depending on the rock mineralogy, proppant type, proppant concentration, proppant size and overburden stress. Field observations reveals the overall performance of well productivity depends on fracture conductivity which is influenced by the combination of these factors. Lab experiments conducted under simulated reservoir conditions can help to systematically evaluate the effect of different parameters on fracture conductivity. This study focuses on the effect of proppant concentration, proppant type, proppant size, rock mineralogy and overburden stress on the propped fracture conductivity under simulated reservoir conditions. Different damage mechanisms including proppant crushing, embedment and diagenesis and their severity to the conductivity reduction have also been evaluated.

Experiments were conducted with shale platens machined from Eagle Ford and Meramec formations. Proppants with different concentration (varying form 1.5 lb/ft^2 to 4 lb/ft^2), different sizes (20/40, 40/70, 60/100), different types were placed between the two platens and propped fracture conductivity is measured over the period of 7-60 days. Axial stress of 5000 psi was applied to simulate the closure stress which was also varied from 1500 to 7500 psi in different experiments

to evaluate the effect of overburden stress on conductivity. The brine composed of 3% NaCl, 0.5% KCl was flowed at a constant rate of 3 ml/min throughout the experiment. In some experiments, 0.05 molar Na_2CO_3 was added to raise the pH of the brine up to 10.

Testing was done to study the effect of proppant concentration using 60/100 mesh Ottawa sand placed between metal platens; result shows significant reduction in permeability at lower concentration of 2 lb/ft^2 compared to higher concentration of 4 lb/ft^2. Within a unit drop in porosity, permeability declines up to 98% with 2 lb/ft^2 concentration while conductivity decline of 80% and 60% observed with increased concentration of 3 lb/ft^2 and 4 lb/ft^2 respectively. Particle sizes analysis showed 13% fines generation at lower concentration compared to 8% at higher concentration.

Effect of particle size evaluated at different closure stress by placing the Ottawa sand (20/40 and 60/100 mesh) between metal platens shows higher crushing and proppant width reduction with higher stress. However, finer mesh (60/100) mesh shows relatively higher compaction and crushing compared to coarser sand (20/40) at each compaction pressure. Effect of particle size on conductivity evaluated using long term flow through conductivity tests with Meramec formation platens shows higher decline in conductivity with finer (60/100 mesh) sand compared to coarser (20/40 mesh sand). Compaction up to 17% observed with 20/40 sand compared to 25% compaction with 60/100 sand over the flow period of 10 days.

Experiments with different types of proppant shows higher initial permeability with ceramic proppant compared to Ottawa sand under similar conditions. Over the period of 8 days, experiment with Ottawa sand shows up to 60% fracture width reduction compared to 30% with ceramic

proppant. Ceramic proppant also shows uniform distribution of embedded grains and formation extrusion. However, significant diagenetic growth is observed with ceramic proppant.

Over the life of a well, due to the production, pore pressure decreases leading to increase in effective stress on fractures. To study the effects of different stress condition on conductivity, experiments were conducted at 1500, 3000 and 7500 psi closure stress keeping all other test conditions the same. Conductivity was observed to decrease significantly at higher stress. Over the flow period of 10 days, fracture width reduces up to 50% at 7500 psi whereas up to 18% and 21% fracture width reduction observed at 1500 and 3000 psi respectively. Surface scans and SEM images shows higher degree of proppant crushing and embedment with increased closure stress. Exit brine composition also shows higher silica concentration at 7500 psi throughout the period of experiment indicating significant proppant crushing and dissolution.

Experiments with different rocks machined form Meramec, Vaca Muerta and Eagle Ford suggests higher decline in conductivity with higher clay and lower quartz content formations. Assuming the matrix permeability of (50 nd) and fracture half-length (100 ft), the dimensionless fracture conductivity (FCD) observed to decline at a very high rate and goes below 20 after 18 days in Eagle Ford, 35 days in Vaca Muerta and 75 days in Meramec.

Chapter 1: Introduction

1.1 Synopsis

This thesis is divided into 4 chapters. Chapter 1 gives the brief introduction about hydraulic fracturing, proppant types, their characteristics and fracture conductivity. It will also introduce the different conductivity degradation mechanism, historical development of conductivity measurements and objective of this research. Chapter 2 will discuss the experimental set up and procedure. Chapter 3 will describe the results of all the experiments conducted along with the discussions of the results. Chapter 4 will provide the conclusions from this study and recommendations. Step by step instruction for carrying out the experiments are given in Appendix A.

1.2 Unconventional reservoirs

Unconventional reservoirs cover a wide range of hydrocarbon-bearing formations that require special recovery operations like hydraulic fracturing for the economic production of hydrocarbons. Unconventional reservoirs include reservoirs such as tight gas sands, gas and oil shales, coal bed methane, gas hydrate deposits, etc. The United States is rich in unconventional oil and gas resources which has contributed tremendously to its oil and gas production. As per the EIA estimates, the production from the unconventional reservoirs contributed up to 54% of the total 9.3 million BOPD in 2017. Production from the unconventional reservoirs continues to grow leading to the highest annual average production of 10.7 million BOPD in 2018 and surpassed the previous record of 9.6 million BOPD in 1970. It is expected that production will continue to grow and reach ~12 million BOPD in early 2040s (EIA 2019). As per the latest EIA report, the United States will become a net energy exporter in 2020 and remains so throughout the projection period

till 2050 (**Fig.1**.) This has been a result of increased crude oil, natural gas and natural gas plant liquids production.

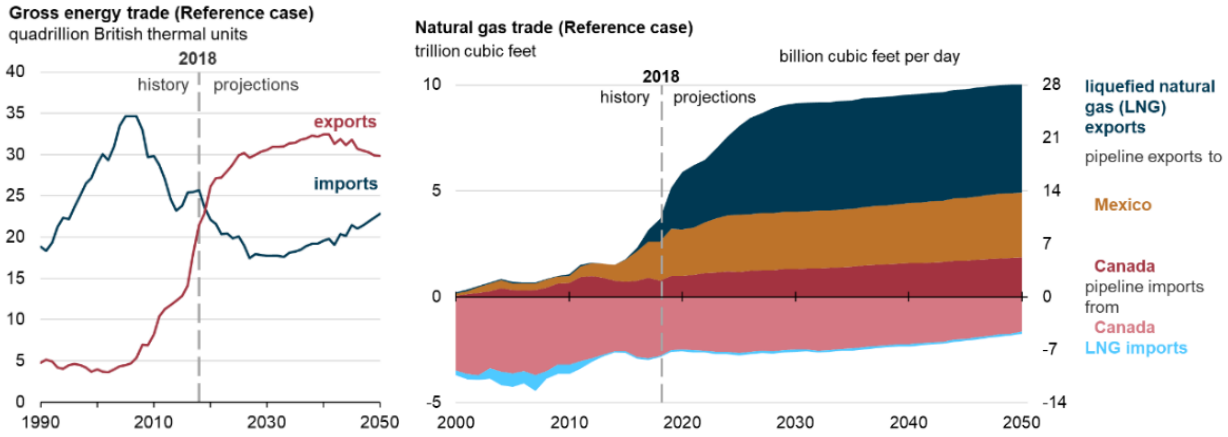

Figure 1: U.S becomes a net exporter due to continued development of tight oil and shale gas resources (EIA 2019).

1.3 Hydraulic fracturing

Hydraulic fracturing is a well stimulation technique used in low permeability reservoirs like tight sandstone, shale, coal beds, etc. to increase the flow of fluid from the reservoirs. The process typically involves injecting water, sand and chemicals at high pressure with an intention to create new fractures in the rock as well as increase the size, extent and connectivity of the existing fractures.

The combination of horizontal drilling technology and hydraulic fracturing has led to the significant growth of the oil and gas production from unconventional shale plays in U.S. Horizontal drilling along with hydraulic fracturing allows access to a greater area of the producing formation leading to higher oil and gas recovery. In 2016, out of 13 million feet of total drilled footage, around 10.7 million were horizontally drilled and hydraulically fractured (EIA 2018).

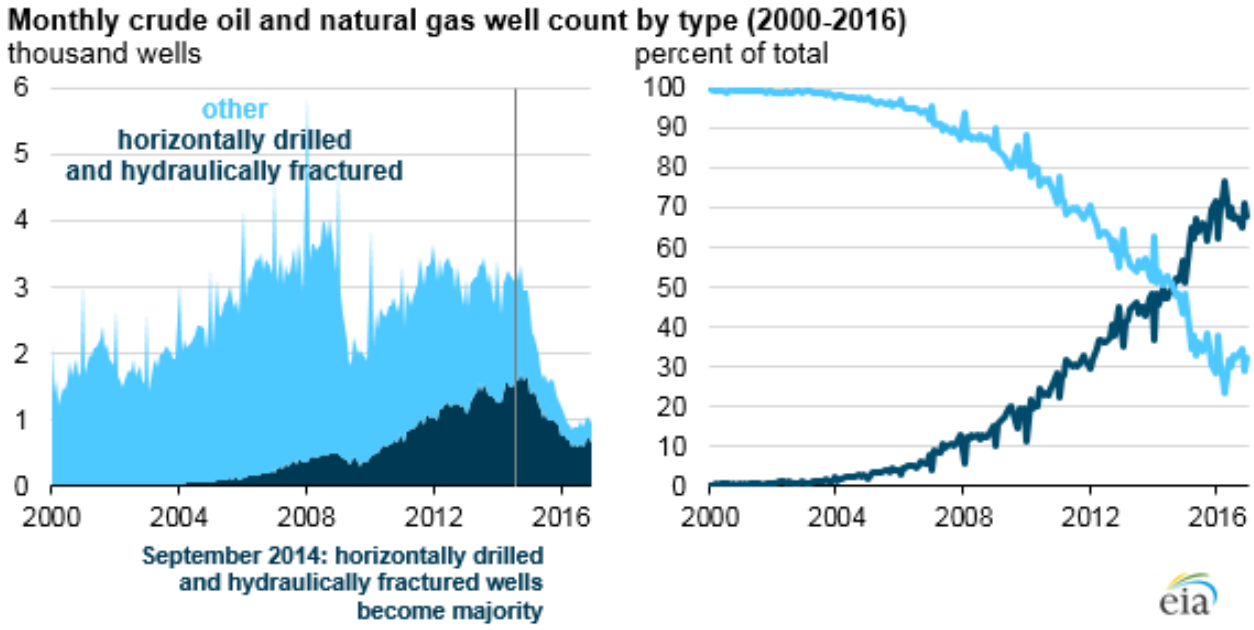

Figure 2: Increasing number of horizontally drilled and hydraulically fractured wells (EIA 2018)

Hydraulically fractured horizontal wells account for most of the new wells drilled and completed since late 2014 **(Fig. 2)**. As per EIA (2016) out of 977,000 producing wells, 670,000 were horizontally drilled and hydraulically fractured.

1.4 Proppant types

To create hydraulic fractures in unconventional reservoirs, fluids are pumped at a very high pressure. Proppants are pumped to keep the fracture propped open to provide the conduit of the reservoir fluids to the well bore. Sand obtained from Arkansas River was first introduced as proppant to hydraulic fracturing in 1947 (Montgomery and Smith 2010). However, over the next 30-40 years, many new proppants, such as uncoated sand, resin coated sand and ceramics, have been developed to meet the operational needs. Gallagher (2011) classified the proppant in three major categories. Tier 1 comprised of ceramic proppants, tier 2 resin coated sand and tier 3 sand.

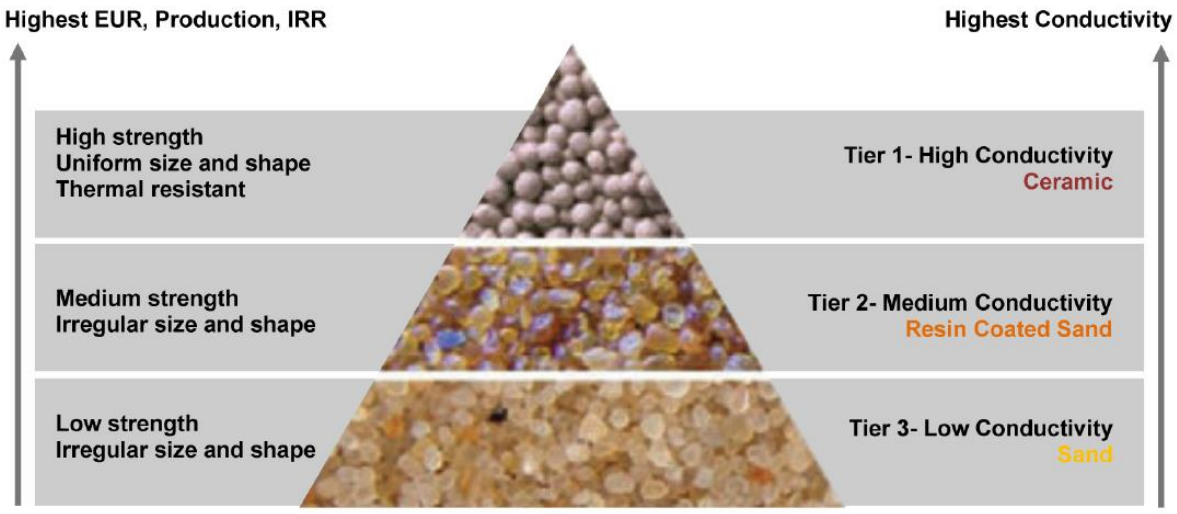

Figure 3: The hierarchy of different types of proppant and their conductivities (Gallagher 2011)

High tier proppants provide higher conductivity which will lead to higher production. However, the increase is governed by several factors such as proppant shape, size uniformity and strength (Gallagher 2011).

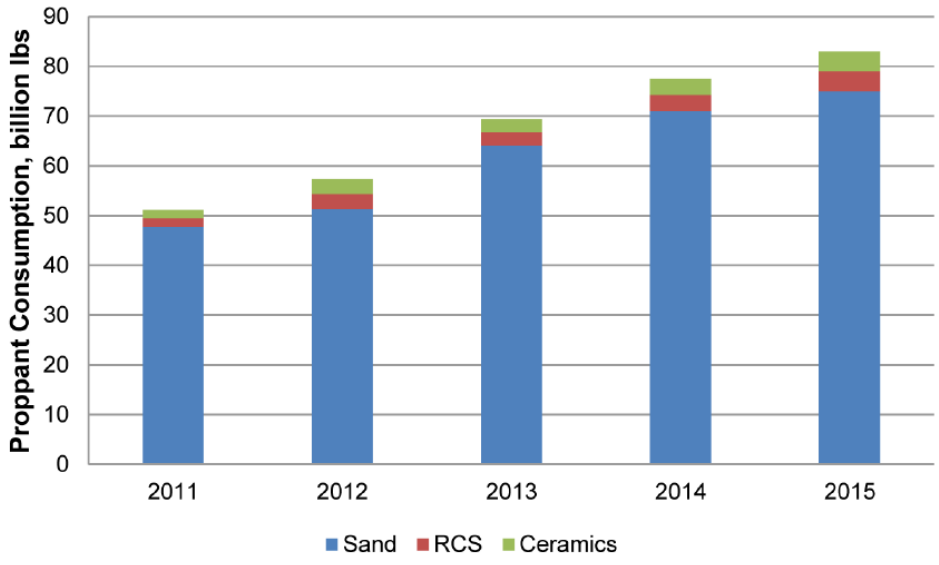

Figure 4: Proppant consumption in U.S (Source: PacWest proppant market analysis 2013 with a forecast for year till 2015)

Even though, highest fracture conductivity is obtained with ceramic proppants, untreated sands remain the most commonly used proppant (PacWest, 2013). However, shale fracturing operations have dramatically increased the demand for proppant.

1.4.1 Frac sand

Since Stanolind Oil carried out the first hydraulic fracturing in Hugoton field utilizing Arkansas River sand in 1947, sand remains the most commonly used proppant for fracturing (Liang 2015) as shown in **Fig.5** because it is most commonly available and relatively cheap. Sand is usually mined and used as a proppant post processing which include washing, cleaning, drying and sizing of the sand grains.

Common frac sand is classified as either white or brown. Most of the white sand is mined from the Midwest region of the United States (Stephenson et al. 2003). Because they contain fewer impurities, they are light in color and hence called white sand. On the other hand, brown sand has relatively high impurity content and does not contain as much silicon dioxide as white sand resulting in lower strength. However, brown sand is cheaper and has gained popularity in recent years (Yang et al. 2019).

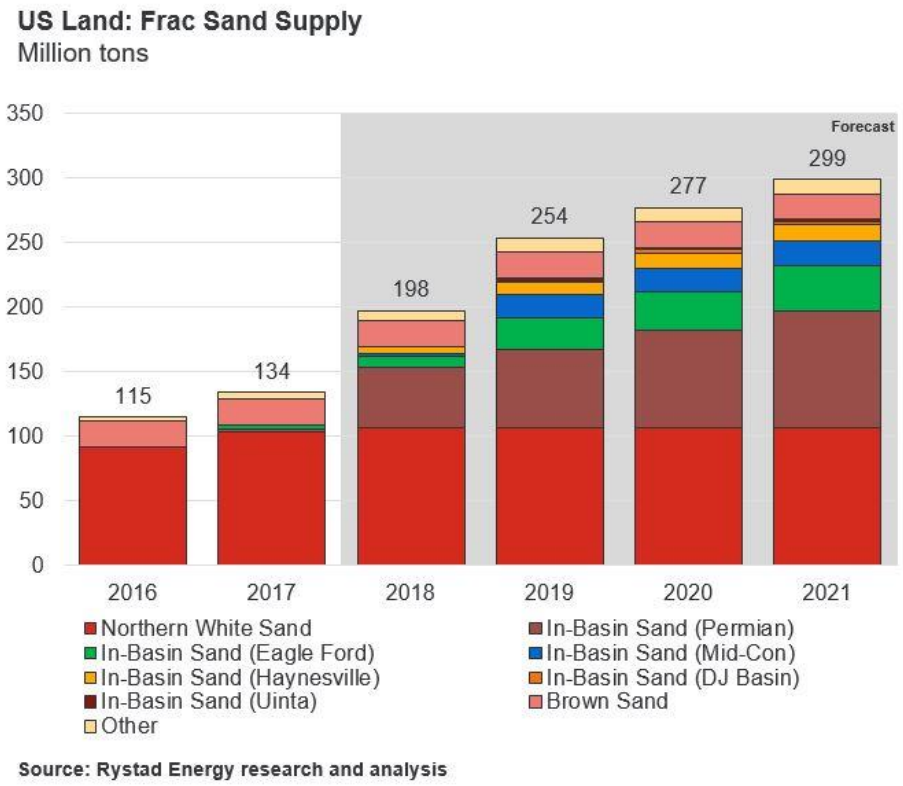

Figure 5: Increase in "in-basin" sand compared to the white sand to reduce hydraulic fracturing costs (Source: Yang et al. 2019)

1.4.2 Resin coated sand (RCS)

Since frac-sands are easily friable which creates fines under high stress conditions, resin coated sands were developed to reduce fines production and the decline in fracture conductivity. Proppants can be either used as pre-coated with resin in the production facility or brought to the hydraulic fracturing site and coating done on site. (Murphey and Totty 1989; Underdown et al. 1980). Resin coated sand traps the broken pieces of sand within the coating and reduces the fines blocking of the pores which can reduce fracture conductivity.

1.4.3 Ceramic proppant

Commonly used frac sands usually fails under high stress conditions. Ceramic proppants are synthetic proppants designed to withstand high stress conditions. They are manufactured from sintered bauxite, kaolin, magnesium silicate or blends of kaolin and bauxite. Since they are synthetic, ceramic proppants tends to be more spherical and rounder, and they have high strength and crush resistance compared to frac sand or resin coated sand.

Ceramic proppants can be broadly categorized in to three categories: lightweight ceramics (LWC), intermediate density ceramics (IDC) and high-density ceramics (HDC). The light weight ceramics have densities similar to sand.

1.5 Proppant characteristics

Proppant selection is the key decision in hydraulic fracturing stimulation. The choice of proppant can significantly impact the treatment size, job economics, well productivity and overall field development economics. Therefore, the different characteristics, discussed below, of the proppant need to be evaluated before selection.

1.5.1 Proppant Size

Proppant size plays an important role in hydraulic fracturing treatment. Proppant sizes are usually given as a mesh size which is the number of openings across one inch of a screen. The proppant is usually described as the size in microns such as 20/40 mesh is 420 µm to 841 µm; 30/50 mesh is 297 µm to 595 µm; 40/70 is 210 µm to 420 µm etc. The typical fracturing treatment starts with smaller sized proppant and tailed with bigger size proppant to maximize near well productivity. The particle mesh size is measured using the dry sieve analysis or laser diffraction particle size analyzer. Kumar et al. (2013) did the comparison of both the methods and found that both gives

the comparative particle size up to 500 µm but recommended to use sieve analysis for particle size higher than 500 µm.

1.5.2 Shape of the proppant

The shape of the proppant is evaluated for its sphericity and roundness. The chart in **Fig.6** shows the visual estimation of sphericity and roundness of grains (Krumbein and Schloss 1963). The lower Krumbein number represents more angular grains while a number closer to 1 suggests higher circularity and roundness. The high angular proppants tend to undergo greater crushing, leading to lower conductivity.

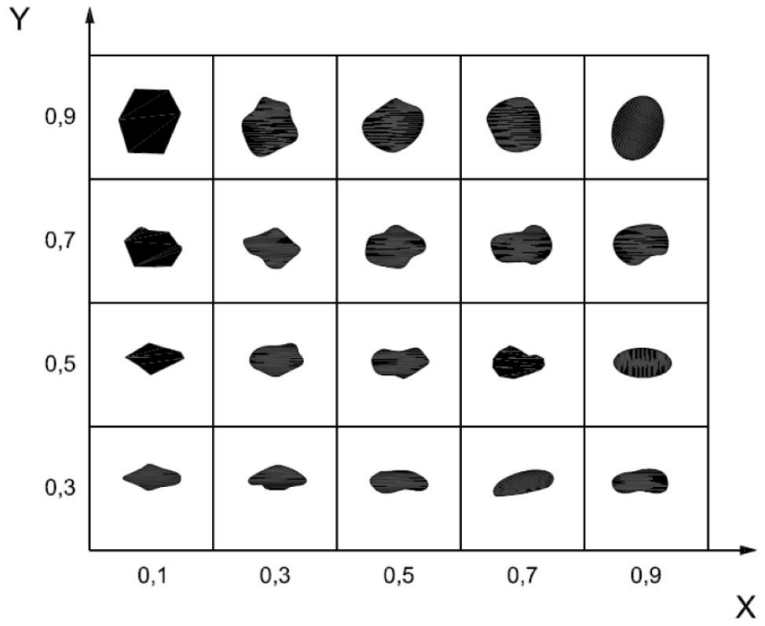

Figure 6: The chart showing roundness in the X-axis and sphericity in Y-axis used for visual estimation of sphericity and roundness. The closer the value to 1, the more spherical and round the particle is. (Krumbein and Schloss 1963)

1.6 Dry crush test: methods, advantages and disadvantages

Dry crush tests are one of the inexpensive methods to obtain some of the mechanical properties of the proppants and are readily available for most of the proppants. Crush test is an important parameter used in the industry for quality control applications. API proposed the crush test (API RP 56; ISO 13502-2) to evaluate proppant using the "percent crush" parameter (Palisch et al. 2009).

As per the API methodology, before the dry crush test, the proppant should be sieved properly to meet the required size specification. For example, for 20/40 mesh proppant, 90% of the proppant should fall in the size range of 420 µm to 841 µm. The test should be conducted at the proppant concentration of 4 lb/ft^2 and the cell should be loaded at a rate of 2000 psi/min to the desired load and maintained for 2 minutes. After the crushing test, the proppant should be sieved and the fines smaller than the native size should be reported as crush material. For example, particle size less than 420 µm will be considered as a crushed material if 20/40 mesh proppants used in dry crush test.

Several improvements in the dry crush tests have been proposed after the API test. Freeman et al. (2009) conducted crush test at higher temperature after saturating proppant in liquid. Raysoni et al. (2013) conducted single grain crush test on ceramic proppant with 30 grains of uniform shape and size and determined the crush strength statistically using Weibull distributions. Simo et al. (2013) proposed a new crushing method approach and studied the crushing using increasing load at a constant displacement rate rather than constant loading rate. Taneja (2016) conducted several dry crush tests with different proppant concentration at different temperature using different types of proppants.

Although the dry crush tests provide some information about the strength of the different proppant, it should be used carefully to compare different proppant properties for hydraulic fracturing stimulation job. Palisch et al. (2009) broke several myths about the blind application of crush test as a primary criterion in proppant selection. They suggested the steel crush cell used in the API should not be used as they do not account for the proppant embedment happening in the rock formations. Moreover, the concentration of 4 lb/ft^2 is not representative of proppant density in fractures which are mostly limited to 0.5-2 lb/ft^2. The API crush test gives the crush percent which is the percentage of smaller crushed particles compared to native particles. This method only gives what volume percent of broken particles are smaller than native particles. Many particles break which are not small enough and are not accounted in the crush percent but can have adverse in proppant pack conductivity. They also suggested that modification of the crush test to test other variables like temperature, concentration etc. However, these should be done cautiously as it might significantly increase/decrease the crush percent or may affect repeatability. They also showed that crushing is indeed detrimental to conductivity. However, crush test only is insufficient to quantify the relationship with conductivity. (**Fig.7**). Therefore, conductivity tests should be carried out at simulated reservoir conditions to directly measure the conductivity incorporating the effect of particle crush, concentration, temperature, etc.

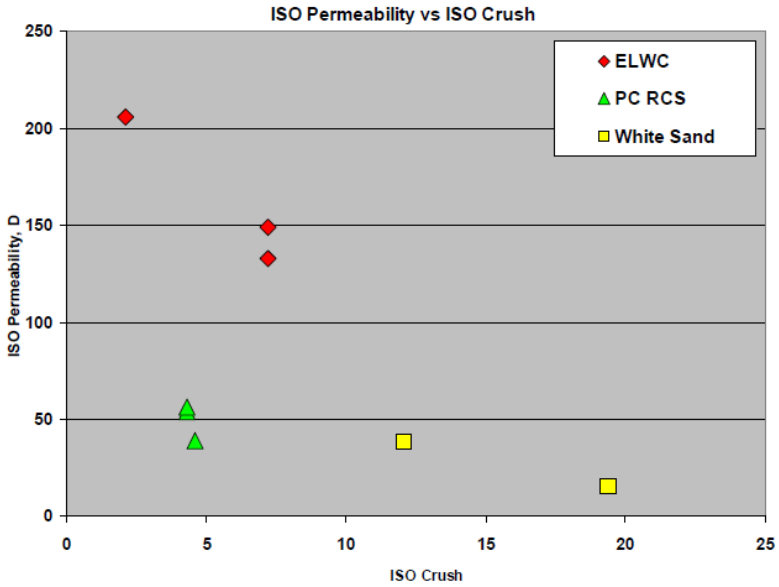

Figure 7: Comparison of permeability of economy light weight ceramic (ELWC), pre-cured resin coated sand (PC RCS) and white sand obtained through ISO conductivity test (conducted at a concentration: 4 lb/ft^2) with ISO crush test (conducted at a concentration: 2 lb/ft^2, Palisch 2009)

1.7 Fracture conductivity

Fracture conductivity is defined as the product of the fracture permeability and fracture width as shown in the equation 1.

$$conductivity = k_{frac} * W_{frac} \quad \text{Eq.1}$$

This conductivity is used to determine the dimensionless fracture conductivity which is a ratio of flow capacity of the fracture to the flow capacity of the reservoir and is given by equation 2.

$$F_{CD} = \frac{k_{frac} * W_{frac}}{k * X_f} \quad \text{Eq.2}$$

Where,

F_{CD} = Dimensionless fracture conductivity

k_{frac} = Fracture permeability, md

W_{frac} = Width of the fracture, ft

k = Rock matrix permeability, md

X_f = Fracture half-length, ft

1.8 Effect of concentration

Proppant concentration plays an important role in degree of proppant embedment at high stress; with increase in proppant concentration, overall stress between particles is reduced due to stress distribution (Palisch 2009; Tang 2018). There has been a growing trend of pumping overall higher proppant and more than 4 times proppant amount per lateral length has been pumped in Delaware basin between 2012 to 2018 (Xu et al. 2019). Field observations by Jaripatke et al. (2016) show increase in production was associated with increased in proppant amount. Moreover, the drill back studies conducted in HFTS experiment showed the proppant concentration varying from 0.5-1 cm thick and at times 0 (Elliot and Gale 2018; Raterman et al. 2017) which corresponds up to 2-3.5 lb/ft^2 proppant concentration. Higher proppant concentration at pump using highly viscous and proppant suspending frac fluid leads to increased proppant concentration in the fractures (Coulter et al. 1972). Due to overall lower embedment and less proppant crushing, it is believed that higher proppant concentration would lead to high sustained production (Penny 1987; Coulter et al. 1972; Holditch et al. 1973).

1.9 Stress effects on conductivity

Propped fracture conductivity depends upon several factors like proppant type, rock mineralogy, frac fluid additives, etc. One of the major components is the *in-situ* stress. The effective stress increases with time due to the decline in pore pressure (Terzaghi 1925; Biot 1941) with production as explained by the below equation:

$$\sigma' = \sigma - \alpha p \qquad \text{Eq. 3}$$

where,

σ' = Effective stress, psi

σ = Total stress, psi

α = Biot's coefficient

p= Pore pressure, psi

Numerical simulations of conventional reservoirs (Davies et al. 2001) indicate that fracture permeability was strongly dependent on stress in both consolidated and unconsolidated rocks. However, the permeability decline showed huge variation with different samples (Porosities: 25-40%) of the same rock type with little difference in burial depth and no unique relationship could be established. To understand the reasons for these differences and different mechanisms leading to such variations in permeability, controlled lab experiments under similar conditions with only one changing parameter (stress) need to be conducted.

1.10 Conductivity reduction mechanisms

It has been established that simplified lab experiments cannot provide the realistic estimates of propped fracture conductivity (Penny 1975, 1987; Palisch 2007). When API published the recommended procedure for the conductivity tests in 1989, they released it with a caution that these tests are not designed to provide absolute conductivity under reservoir condition, but to be used qualitatively after considering other factors such as temperature, frac fluid residues, fines migration, etc., which can account for up to 90% or more reduction in conductivity. Nevertheless, people just use these test results with manual adjustments to predict conductivity giving poor estimates of fracture conductivity. Palisch et al. (2007) demonstrated the cumulative effects of different damage mechanisms on fracture conductivity reduction as shown in the **Fig. 8**.

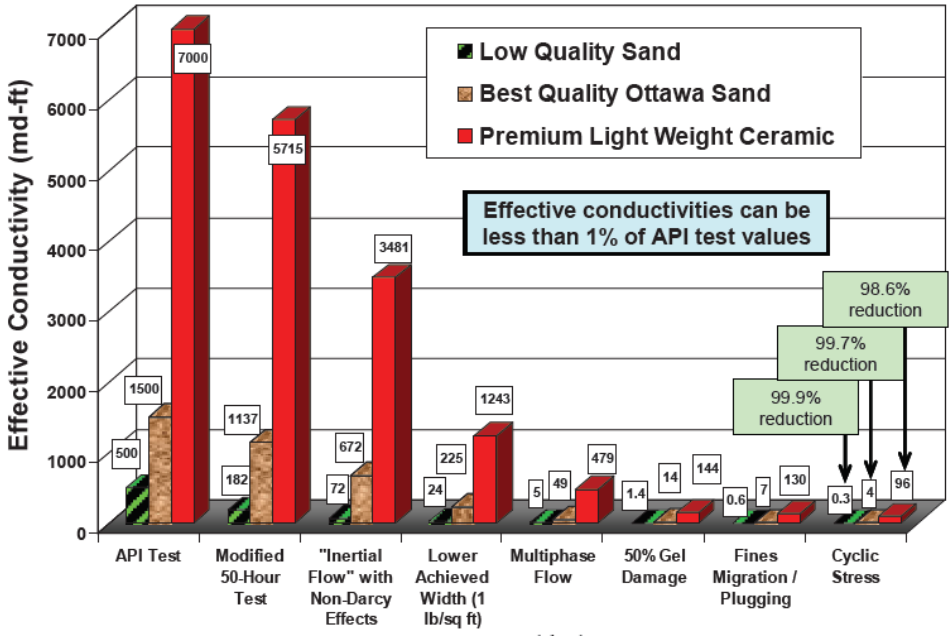

Figure 8: Cumulative effect of different conductivity reduction mechanisms on propped fracture conductivity (Palisch 2007)

There are several mechanisms leading to the reduction in proppant conductivity as shown in the **Table 1** (Duenckel 2011). Major damage mechanisms including proppant crushing, fines migration, fracture width reduction, proppant embedment and proppant diagenesis are investigated in this study.

Category of Damage	Damage Mechanism Causing Higher Pressure Losses
Physical loss of porosity and/or fracture width	Particle crushing, pack rearrangement, compaction Particle embedment into fracture face Spalling of formation material, contaminating proppant pack Cyclic stress loading increasing particle crush and rearrangement Low achieved proppant concentration yielding narrower fracs Gel filter cake at frac face resulting in loss of effective width Dispersed gel residue occupying porosity
Complex fluid flow regimes causing higher pressure losses than reported in low velocity flow tests	Fluid inertia causing non-Darcy pressure losses due to curvilinear flowpath around proppant grains (significant even at modest laminar production rates) Fluid turbulence (significant only at high production rates) Multiphase flow Emulsions, foams, froths, mist flow causing higher pressure losses
Non-linear fracture geometry	Complex fracture geometry would be expected to increase total flowpath length and flowpath tortuosity
Imperfectly uniform proppant distribution	Irregular packing should result in greater proppant crush and embedment and also result in bottlenecks or regions of aperture restriction
Uncertain or multiple mechanisms	Continued degradation over time Thermal degradation of some proppant types
Chemical degradation of proppant	Proppant dissolution causing reduction in particle diameter or strength (especially in acid or steam injection) Stress corrosion, pressure solutioning, static fatigue Deposition of sulfate or carbonate scales Precipitation of waxes or asphaltenes

Table 1: Classification of different proppant conductivity damage mechanisms (Duenckel 2011)

1.10.1 Proppant Crushing

Presence of *in-situ* stress in the reservoirs can lead to the proppant crushing (Wang et al. 2014; Ghosh et al. 2014; Mittal et al. 2017). This crushing will lead to the generation of finer particles which will move in the direction of the flow (fines migration) blocking the pore throats. This blockage can have a serious impact on the proppant conductivity and needs to be evaluated for different proppants and at reservoir conditions. Even 5% of crushed particles can lead to the reduction in fracture conductivity of up to 62% (Wells and Coulter 1972). Dry crush test could help to compare the crushing strength of different proppants (Palisch 2009; Simo et al. 2013; Taneja 2016) but should be used with caution when correlating with proppant pack conductivity

(Schubarth 2004, Palisch 2009). Migration of fines and their effect on conductivity has been studied experimentally and found to cause severe conductivity degradation (Terracina et al. 2010; Mittal et al. 2018).

1.10.2 Proppant embedment

Gidley et al. (1989) and Lacy et al. (1998) have studied proppant embedment. The embedment depth in unconsolidated rocks was found to be limited to ½ of the grain diameter (Duenckel et al. 2017). However, due to the presence of unconsolidated material and fluids interaction, greater depths of embedment have also been observed (Simon et al. 1982; Lacy et al. 1998). Embedment of proppant leads to the up lifting or extrusion of the formation material which can further adds to the fines in the proppant pack.

1.10.3 Proppant diagenesis

Although the dissolution of proppant has been observed during conductivity tests by Penny (1987) and McDaniel (1986), the term "proppant diagenesis" was first introduced by Weaver et al. (2005). Diagenesis is a geological term defined as "physical, chemical or biological changes that a sediment undergoes after initial deposition, and during and after lithification", excluding weathering and metamorphism. The proppant diagenesis refers to the growth of minerals due to the interaction of proppant, formation and formation/frac fluids over time. Yashuhara et al. (2003); Weaver et al. (2007) reported that diagenesis in proppant can occur in a fraction of years and the rate of reactions can be accelerated at high temperatures (Weaver et al. 2008). Proppant diagenesis leads to porosity and permeability reductions in the proppant pack. Proppant diagenesis depends on the type of proppant, mineralogy of the formation and composition of formation fluids (Weaver at al. 2009). The formation of needle, tabular shaped mineral growths were observed (Weaver et

al. 2009) when ceramic proppant pack was kept in presence of crushed shale at an elevated temperature of 500 ^{o}F for 2 months. The growth of diagenetic minerals was also observed by Raysoni et al. (2013) when high strength proppant and shale mixture was heated up to 450 ^{o}F in a static cell over the period of 15-180 days. These growths were observed to increase with time and caused the reduction in permeability. Lee et al. (2010) conducted lab experiments and did numerical simulation to study the effects of diagenesis on porosity and permeability and observed a decline up to 27% in permeability depending upon proppant, formation and fluid type. LaFollete and Carman (2010) conducted several experiments on different types of ceramic proppants sandwiched between the Haynesville shale at 300 ^{o}F and aged over the period of 30, 60, 120 and 240 days and observed diagenetic activity developing over that period. Ghosh et al. (2014) conducted several flow-through experiments with Ottawa sand, resin coated sand and ceramic proppant with shales of different mineralogy (one clay rich and other carbonate rich) and observed secondary mineral growths. Mittal et al. (2018) demonstrated the higher mineral growth rate at high pH (~10) in presence of crushed basalt (simulating volcanic ash). These secondary growths, in the long term, are believed to further add to the reduction in proppant pack permeability. The compatibility of proppant, formation and fluid needs to be evaluated to minimize the proppant diagenesis and should be one of the important criteria for proppant selection in hydraulic fracturing (Elsarawy et al. 2018).

1.11 Historical development timeline of conductivity measurement

Cooke (1975) conducted proppant experiments at various stresses to study the effects of different fluids at high temperature. His experimental set up is shown in the **Fig. 9**. The proppant was placed between a heated platen of a press used to apply the required stress. The cell had a width of 1.5" and proppant pack was 0.5" in height. The permeability of 8-12 mesh sand under the stress condition of 2000 - 10000 psi was evaluated using different fluids (**Fig.10**). He observed higher decline in permeability at higher stress in presence of high temperature brine. At temperature 250 ^{o}F, a significant difference in proppant pack permeability was observed in presence of water compared to oil.

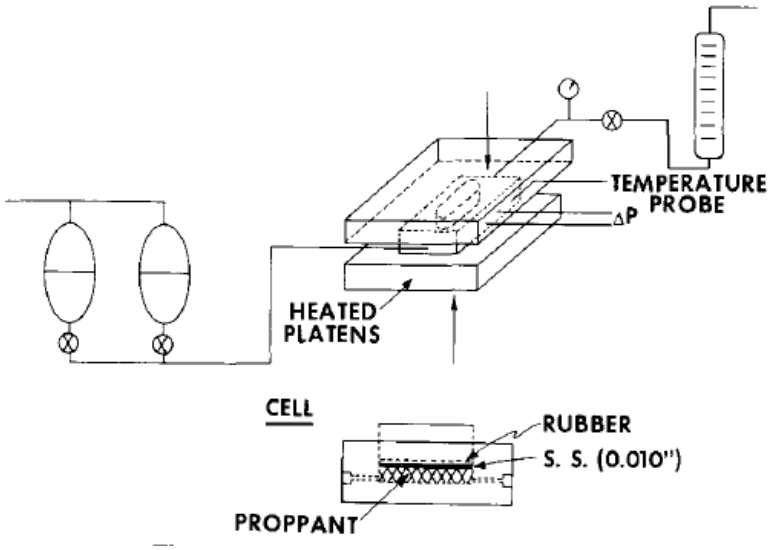

Figure 9: Apparatus designed and used by Cooke (1975) to measure the proppant conductivity at different temperatures and at different stress conditions.

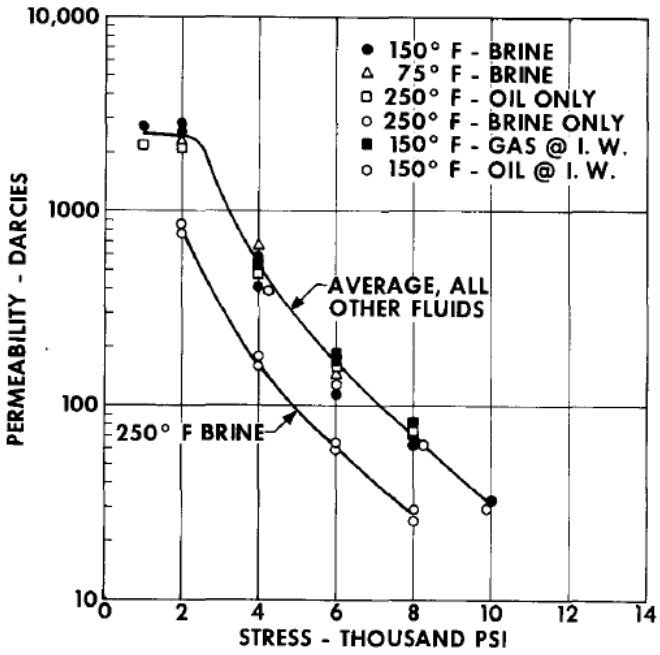

Figure 10: The results of the conductivity tests conducted by Cooke (1975) to evaluate the effect of stress, fluids and temperature on proppant conductivity

Cutler et al. (1985) measured the fracture conductivity using resin coated and ceramic proppant at different stress conditions. They observed bauxite-based proppant gave higher conductivity at high stress and recommended their use for deeper wells.

Parker and McDaniel (1987) conducted experiments with 20/40 Ottawa sand and found that filter cake formed by the frac fluid can have harmful effect on the proppant conductivity. They also reported that even at lower stress, intermediate strength proppant and regardless of proppant type, higher proppant concentration should be used to get desired conductivity in fractures.

The first industry standard for measuring proppant conductivity was published in 1989 by American Petroleum Institute (API RP61) which was commonly referred as the short-term conductivity test. However, it was realized that long-term conductivity showed conductivity reduction up to 90% or more at elevated temperature due to embedment and fines generations.

Penny (1987) conducted experimental modification to overcome several deficiencies in the API recommendations. The modifications were:

- Use of Ohio sandstone platens instead of stainless-steel platens to allow for proppant embedment.
- Use of 2% KCl water instead of deionized water. The brine was also saturated with silica to avoid sandstone dissolution over the long-term tests.
- Increased time to 50 hours after as sharp decline in conductivity was observed initially which tend to stabilize after 50-100 hours.
- Use of elevated temperature of 150-250 ^{o}F.

The use of sandstone eliminated the regions of high porosity and high permeability due to "Wall effect" observed at the proppant-metal interface. The procedures outlined by Penny (1987) were recognized as a long-term conductivity test compared to the short-term conductivity test proposed by API.

Fredd at al. (2001) conducted conductivity experiments using Texas Valley formation cores. They observed that in absence of proppant, displacement of rough fracture walls can significantly affect the fracture conductivity. Kassis et at. (2010) conducted several permeability measurements on Barnett shale as a function of proppant type, closure stress propped and unpropped fractures. They observed fracture offsets were as effective as propping a fracture and propped fracture showed higher closure stress dependency to conductivity. They also observed significant proppant crushing and embedment on the rock surface.

Rivers et al. (2012) conducted experiments with resin coated and uncoated proppants and observed lower conductivity with resin coated proppant as resins from the coated proppant blocked the pore

throats of the proppant pack. Ghosh et al. (2014) conducted several conductivity tests with different types of proppant placed between shales at different flow rates. Although higher proppant crushing was observed with Ottawa sand compared to ceramic proppant, extensive secondary mineral growth in ceramic proppant was observed. Mittal et al. (2017) designed a new conductivity cell which measured the proppant conductivity and compaction over the longer duration of testing period. Effects of fines migration, rock mineralogy, frac fluids, etc., were evaluated where higher volumes of fines observed near the outlet of the proppant pack. High pH (~10) lead to the accelerated growth of secondary minerals on the rock and proppant (Ottawa sand) surface. Summary of the mentioned historical developments is presented in table 2:

Author	**Platens type**	**Proppant used**	**Experimental conditions**	**Observations**
Cooke (1975)	Metal platens	8-12 mesh, Brady sand	Stress: 2000-10000 psi Temp: 75-250 ^{o}F	Higher decline in permeability at high stress. At 250 ^{o}F, brine permeability was lower than oil
Cutler (1985)	Hastelloy platens	20/40 mesh, Resin coated sand, Ottawa sand, Ceramic proppant	Stress: 1000-14000 psi Temp: 122 ^{o}F	Bauxite based proppant have higher conductivity at higher stress and is suitable for deeper wells
Parker and McDaniel (1987)	Ohio sandstone platens	20/40 Ottawa sand	Stress: 2000-8000 psi Temp: 75-275 ^{o}F	In presence of gel filter cakes, lower conductivity was observed. Low proppant concentration increases problems caused by filter cake
Penny (1987)	Ohio sandstone platens	20/40 Jordan sand, ceramic proppant	Stress: 4000-10000 psi Temp: 175-300 ^{o}F	Use of sandstone eliminated the high permeability due to “wall effect” observed at proppant-metal interface.
Fredd et al. (2001)	Texas valley formation cores	20/40 Jordan sand, ceramic proppant	Stress: 1000-7000 psi Temp: 250 ^{o}F	In absence of proppant, displacement of rough fracture surfaces can significantly affect the fracture conductivity

Kassis (2010)	Barnett shale cores	40/70 Ottawa sand, ceramic proppant	Stress: 6000 psi Temp: 73 ^{o}F	Fracture offsets are as effective as propping a fracture. Propped fracture shows higher dependency of stress on conductivity
Rivers et al. (2012)	Berea sandstone core	16/30 ceramic uncoated, resin coated ceramic proppant	Stress: 3000-10000 psi Temp: 250 ^{o}F	Lower conductivity observed with resin coated proppant as resins blocked the pore throats of proppant pack
Ghosh et al. (2014)	Barnett shale cores	20/40, 40/70 Ottawa sand, 40/70 ceramic, 30/50 resin coated sand	Stress: 5000 psi Temp: 225-275 ^{o}F	Extensive crushing in Ottawa sand and extensive mineral growth in ceramic proppant observed
Mittal et al. (2017)	Eagle Ford, Vaca Muerta shale platens	20/40, 40/70, 60/100 Ottawa sand	Stress: 5000 psi Temp: 250 ^{o}F	Finer mesh sand leads to higher reduction in permeability. Presence of higher clay content leads to higher proppant embedment depths

Table 2: Summary of historical development timeline of conductivity measurement

1.12 Motivation

With the decline in oil prices, use of high-quality synthetic proppants have reduced and frac sands have become more common. Low priced frac sands allows the operators to pumped higher concentration of sand during hydraulic fracturing stimulation. Xu et al. (2019) showed the volume of proppant per foot of lateral length has increases up to 4 times from 2012 to 2018. The increased proppant volume is believed to increase production (Jaripatke at al. 2018). Moreover, drill back studies by Eliot and Gale (2018) and Raterman et al. (2017) shows the proppant concentration in complex fracture network could vary from 0 to 3.5 lb/ft^2. Therefore, factors leading to the

difference in conductivity with different proppant concentration and different damage mechanism affecting the fracture conductivity need to be evaluated.

The main function of the proppant is to keep the fracture propped open after the completion of the hydraulic fracturing stimulation. The proppant has to withstand the *in- situ* and drawdown stresses to maintain the conductivity after the fracture stimulation. Stress variations can also adversely affect the proppant conductivity over time. The study of proppant conductivity with varying stress can help understand the extent of different damage mechanisms over the life of the well.

1.13 Objective

The objective of this study is to investigate the effect of different parameters such as proppant concentration, proppant types and size, overburden stress, and rock mineralogy on propped fracture conductivity at simulated reservoir conditions. To simulate the presence of complex ions present in the shales from volcanics, basalt and obsidian has been used in the experiments conducted with Eagle Ford shale platens. Different conductivity reduction mechanisms such as crushing, embedment and proppant diagenesis will also be evaluated for each experiment to understand their role and extent in conductivity reduction.

Chapter 2: Experimental setup and procedures

2.1. Schematic of experimental setup

The schematic of the experimental setup used in the experiment is illustrated in **Fig.11**. The setup is designed to measure the conductivity of the proppant placed between the metal or rock platens. In the setup, fluid is pumped using the two computer-controlled syringe pumps connected in parallel to the inlet to provide continuous flow over the duration of the experiment. Flow of the pump is regulated to an accuracy of 0.01 ml/min. The fluid is subsequently collected at the outlet after passing through the conductivity cell. The back-pressure valve connected near the outlet provides a pressure which the inlet fluid must overcome to establish the flow through the conductivity cell. The pressure drop across the conductivity cell is measured using a differential pressure gauge (calibrated for a range of 0 - 45 psi with an accuracy of ±0.01 psi) connected at both the ends of the cell.

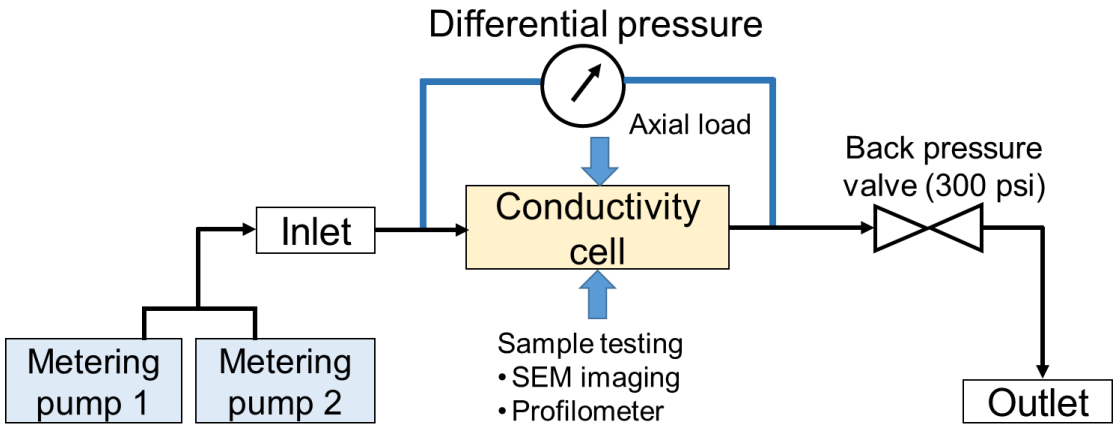

Figure 11: Experimental setup schematic showing the conductivity cell where continuous flow is maintained using two syringe pumps and the pressure differential is measured using the differential pressure gauge. (Mittal 2017)

The cross-sectional view of the conductivity cell is shown in the **Fig. 12**. The body of the conductivity cell is made using Hastelloy C-276 which is a nickel-chromium -molybdenum based alloy containing 5% iron. This material is resistant to pitting and stress corrosion (Haynes 2016). The LVDT attached to the cell is used to measure the compaction of the proppant pack over time with an accuracy of ± 0.0001 inch. Heating tape is wrapped around the conductivity cell to raise the temperature to the desired level and the attached thermocouple gives continuous temperature reading during the experiment. The whole conductivity cell is covered with glass wool to provide the thermal insulation.

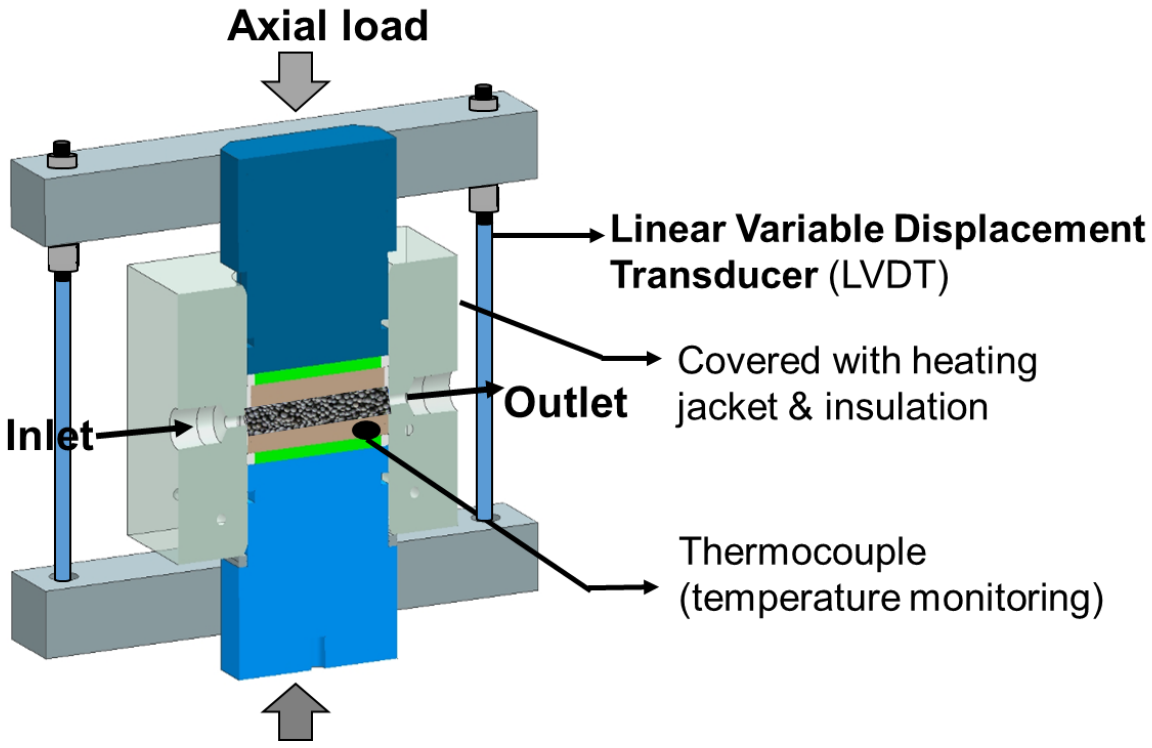

Figure 12: Cross sectional view of the conductivity cell made up of Hastelloy C-276. The proppant pack is placed in the center to allow the flow of fluid through the inlet and outlet ports. The LVDT at both the ends is used to measure the proppant pack width reduction throughout the period with an accuracy of ± 0.0001 inch. (Mittal 2017)

Fig. 13. Shows the cross-sectional view of the proppant pack. Proppant of required concentration varying from 0.75 to 3 lb/ft^2 can be used in conductivity cell. Proppant is sandwiched between the metal or machined rock platens. The rock/metal platens are of 2" length, 1.25" width and 0.25" thickness. The Teflon seals around the platens help prevent any fluid loss during the flow-through experiment.

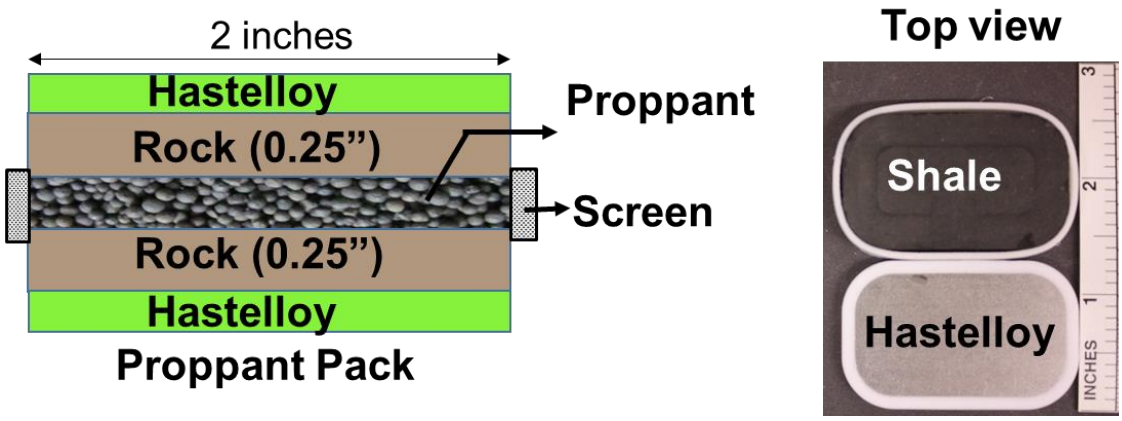

Figure 13: Enlarged view of the proppant pack where proppant is placed between the rock platens (2" X 1.25" X 0.25"). Teflon ring around the metal and rock platens (right) provides seals to prevent any fluid leak during the flow-through experiment (Mittal 2017).

The apparatus was calibrated using the rock platens which were machined from Berea sandstone having 22.7 % porosity and 315 md permeability. The permeability from the apparatus was compared to the Klingenberg-corrected permeability and found to be within 15%. The repeatability of the experimental setup has also been verified by conducting the experiment in which 20/40 Ottawa sand was placed between the metal platens. The detailed explanation of the setup, calibration and repeatability experiments are described by Mittal et al. (2018).

2.2. Experimental procedure

2.2.1. Rock platen preparation

Rocks platens were machined using the diamond saw to the required dimension of 2" long, 1.25" wide and 0.25" thick. After that, the surface of the shale platens was polished using 220, 400, 600, 800, 1200 and1500 grit emery paper to make the surface smooth before the start of the experiment. The surface roughness was measured using the profilometer.

2.2.2. Rock mineralogy

The mineralogy of the rock and shale platens were determined using transmission Fourier Transform Infrared Spectroscopy (Sondergeld and Rai 1993; Ballard 2007). Using FTIR, sixteen minerals including quartz, calcite, aragonite dolomite, siderite, oligoclase, orthoclase, albite, illite, kaolinite, chlorite, smectite, mixed clays, anhydrite, pyrite and apatite can be quantified. Before measuring FTIR mineralogy, the crushed sample was placed in plasma asher to remove any organic matter (Kale 2009).

2.2.3. Surface scan using profilometer

The surface of the shale sample before and after the experiment was scanned using the confocal microscope (Keyence VK-X250). For all the scans, 20x lens was used which has a resolution of 0.5 nm and an accuracy of 0.2 + L/100 μm (L = measuring length). The microscope operates incorporating two light sources. White light source is used to gather color and laser source is used to scan the surface and acquire heights. Both light sources are combined to give high resolution surface profile up to nanometer accuracy. The schematic of the microscope is shown in the **Fig. 14**.

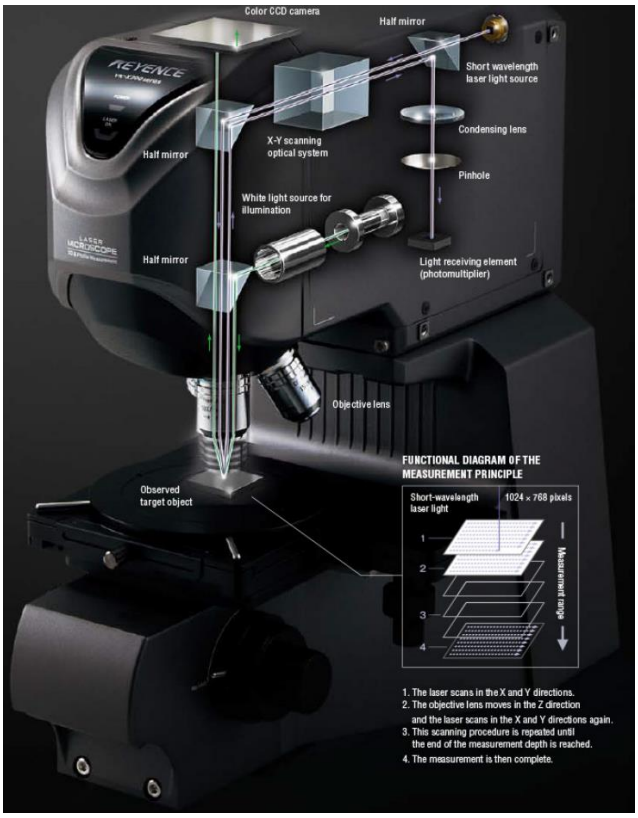

Figure 14: Schematic of the microscope Keyence VK-X250

2.2.3. Proppant sieve shaker

Proppant of desired mesh range (20/40, 40/70 and 60/100) was sieved using the Restch AS shaker shown in the **Fig. 15**. The sieving is done by placing the proppant on the top of the coarse mesh. Finer mesh sieves are placed in sequence and the pan at the bottom to collect the proppant size finer than the smallest mesh used. The vibratory sieve is brought in to motion utilizing the spring mass system operated by an electromagnetic drive providing the sieving of the proppant to the required sieve distribution (Restch 2015).

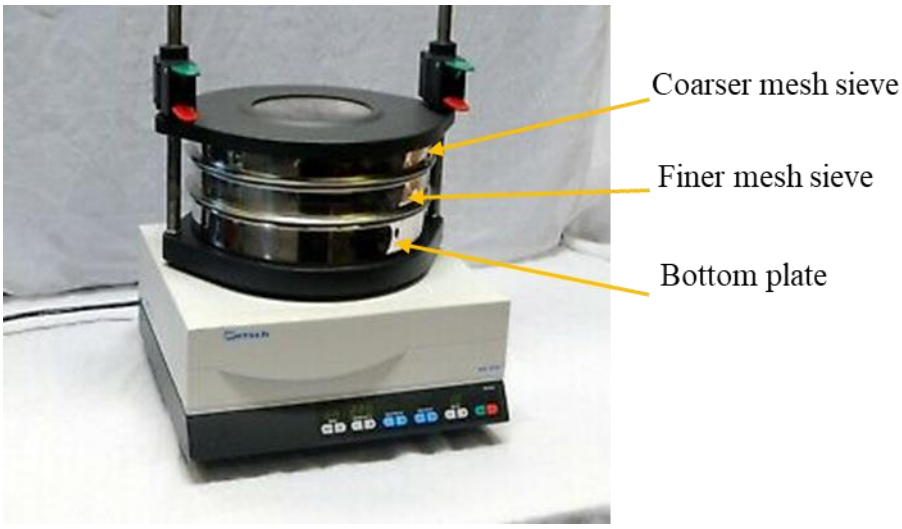

Figure 15: Restch AS 200 vibratory sieve shaker (Restch 2015)

2.2.4. Lase particle size analyzer

The laser particle size analyzer (Beckman Coulter LS 13 320) as shown in the **Fig. 16** was used before and after the experiment to characterize the particle size distribution of the proppant. The LS 13 320 utilizes the pattern of the light scattered by the particle called "scattering pattern" to measures its size. Particles scattering pattern is the characteristic property of its size (Beckman Coulter, 2011). Smaller particles scatter light at larger angles and vice versa. The particle size of the range 0.4 to 2000 µm can be measured using this laser particle size analyzer with the repeatability of 1% about the mean size.

Figure 16: Dry laser particle size analyzer (Beckman Coulter 2013)

2.2.5 Cell preparation

The detailed steps of cell preparation are discussed in Appendix A.

Chapter 3: Results and Discussion

3.1. Dry crush tests

To understand the mechanisms leading to difference in conductivity of coarser and finer sands, dry crush tests have been performed. Experiments were conducted by placing 20/40 and 60/100 mesh between the metal platens at a concentration of 2 lb/ft^2 at 60 ^{o}F. The compaction at 1500, 3000 and 5000 psi has been used to study the effect of stress on overall compaction and proppant crushing.

Fig. 17 shows compaction percentage in three different pressures with 20/40 Ottawa sand. At 1500 psi, compaction of 3% is observed. At 3000 psi, compaction of 5% observed and at 5000 psi, overall compaction of 8% is observed.

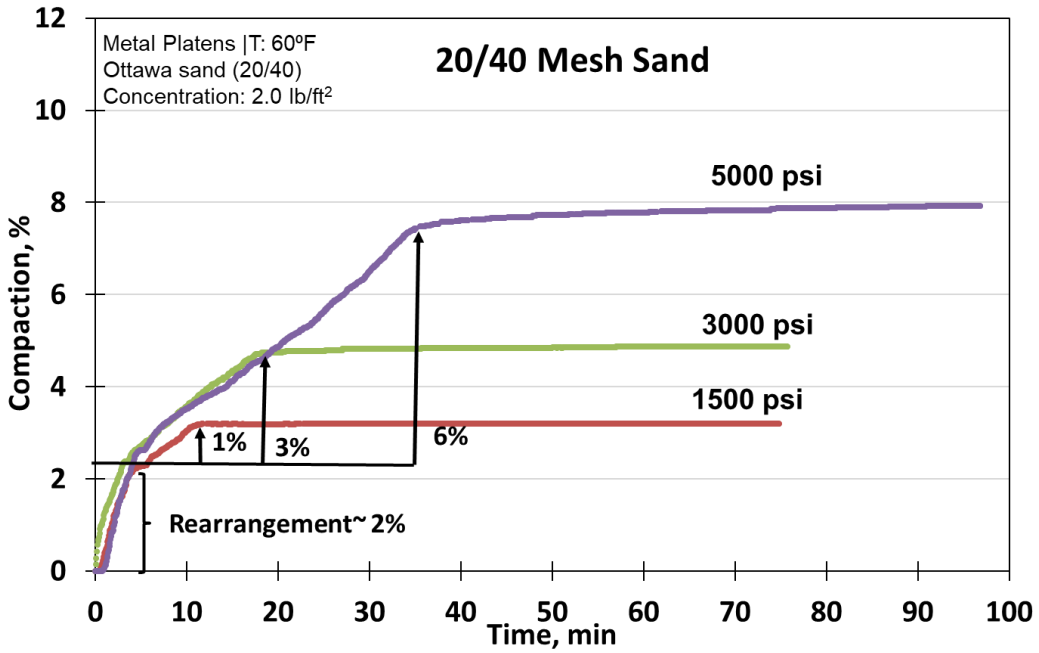

Figure 17: Compaction percentage of 20/40 mesh sand (Concentration: 2 lb/ft^2) at different compaction pressures plotted against time. Higher compaction observed with higher compaction pressure. Grain rearrangement is believed to contribute initial 2% compaction as can be seen from the common initial slope in all the three cases and subsequent compaction is attributed to the particle crushing.

In all the three cases, we observe two distinct slopes: 1) the common initial slope of 2% compaction and 2) increase in compaction observed with increasing compaction pressure. It is believed that initial 2% compaction is due to the rearrangement of grains and the subsequent compaction is due to the particle crushing.

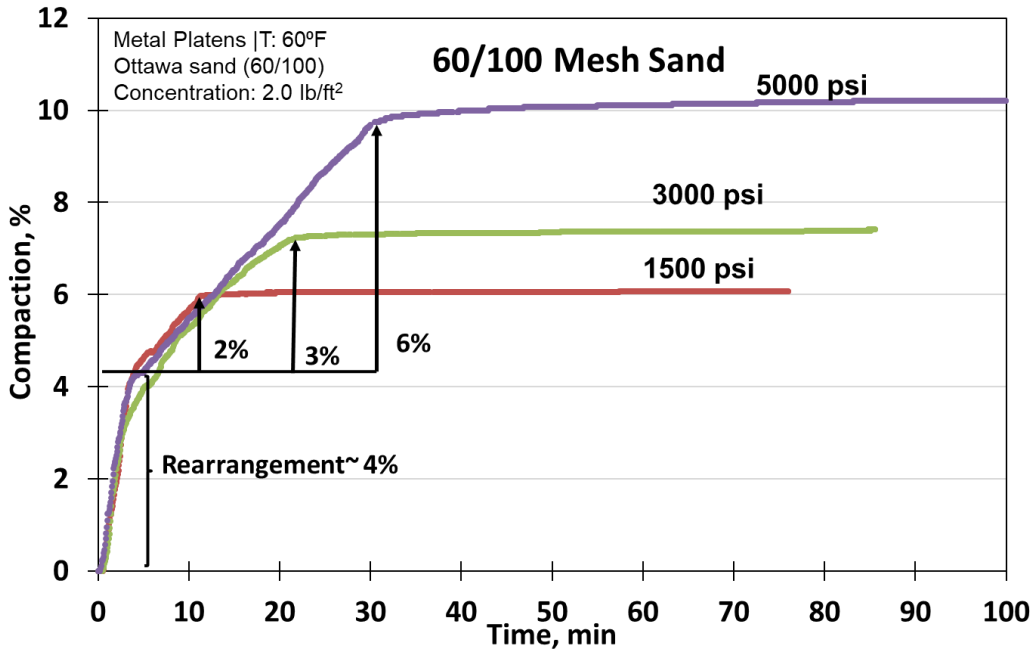

Figure 18: Compaction percentage of 60/100 mesh sand (Concentration: 2 lb/ft^2) at different compaction pressures plotted against time. Higher compaction is observed with higher compaction pressure. Grain rearrangement is believed to contribute initial 4% compaction as can be seen form the common initial slope in all the three cases and subsequent compaction is attributed to the particle crushing.

Fig. 18 shows the results of the dry crush test conducted with 60/100 mesh sand at a concentration of 2 lb/ft^2 at 60 ^{o}F. The proppant compaction has been studied as a function of confining pressure. At 1500, overall 6% compaction is observed. At 3000 psi, 7% compaction and at 5000 psi, compaction of 10% is observed. Again, we observe the two distinct slopes in all the three curves. The initial slope which is common to all the three cases, with overall 4% compaction is believed

to be due to the grains rearrangement. Subsequent compaction is mainly attributed to particle crushing.

In case of 60/100 mesh, we again observe higher overall compaction with higher compaction pressure. However, comparing the overall compaction of 20/40 mesh sand with 60/100 mesh sand, we observe higher compaction with 60/100 mesh sand at each confining pressure (**Fig. 19**).

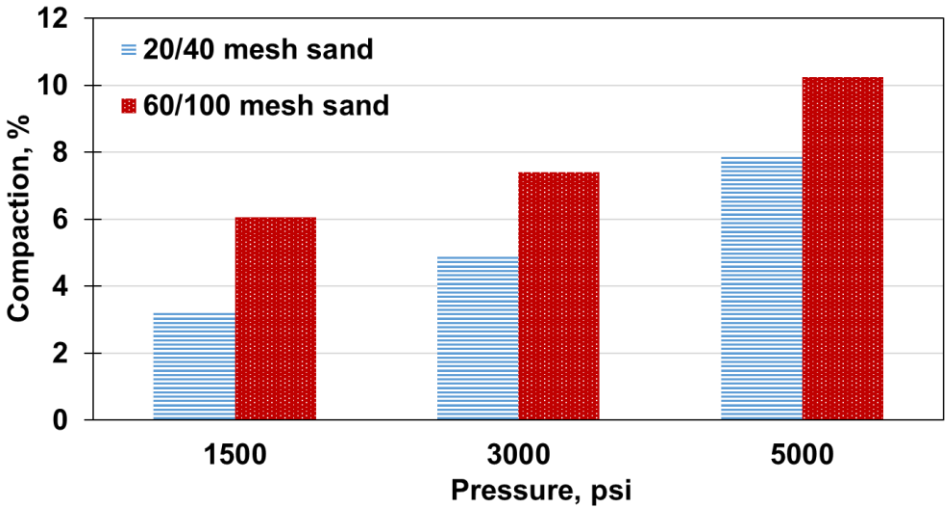

Figure 19: Bar graph representing the overall compaction with 20/40 and 60/100 mesh Ottawa sand (concentration: 2 lb/ft^2) at three different confining pressures of 1500, 3000 and 5000 psi. Increase in compaction observed with increase in compaction pressure in both the cases. However, at each confining pressure, greater compaction is observed with 60/100 mesh sand as compared to 20/40 mesh sand.

It should be noted here that these compactions are only due to initial loading at room temperature under no flow conditions. Additionally, during flow under reservoir conditions, the crushed particles will further move in the direction of flow leading to porosity and permeability reduction. To quantify the amount of crushing and fines generation, particle size analysis has been done after each experiment.

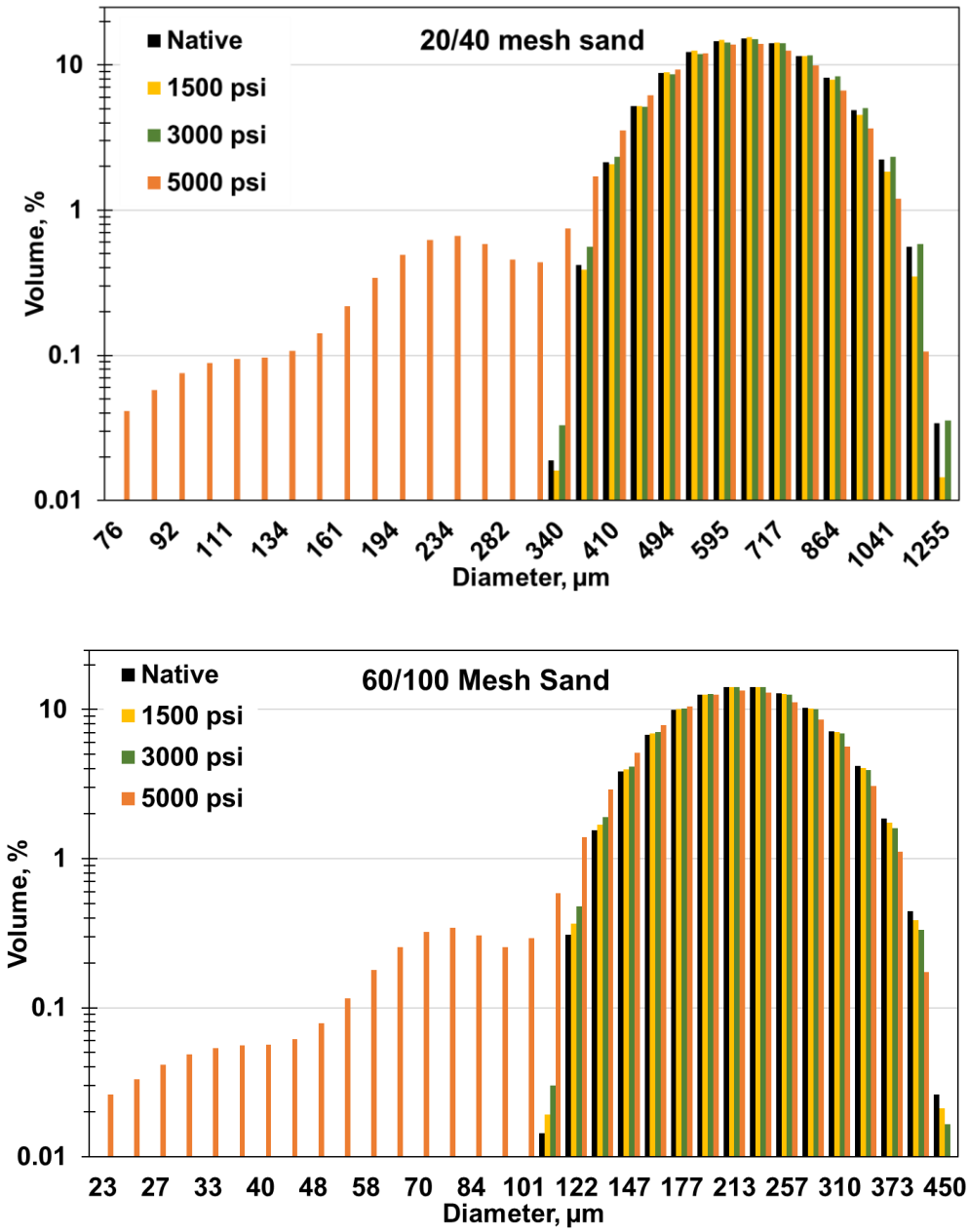

Figure 20: Particle size analysis after each dry crush tests with 20/40 sand (top) and 60/100 sand (bottom) at compaction pressure of 1500, 3000 and 5000 psi. The x-axis represents the particle size in microns and y-axis represents the volume percent corresponding to each particle size. Significant crushing obtained at a compaction pressure of 5000 psi compared to 1500 and 3000 psi.

Fig. 20 shows the particle size analysis of all the three pressure tests with 20/40 sand (top) and 60/100 sand (bottom). The x-axis of the plot represents the particle size in microns and the y-axis represents the volume percentage corresponding to each particle size. For both the proppants, black bars represent the native particle size distribution. Yellow bars indicate the particle size distribution obtained after crushing at 1500 psi, green at 3000 psi and orange at 5000 psi.

In both the plots, we observe negligible amount of crushing and fines generation at 1500 and 3000 psi. However, we observe significant levels of fines generation at 5000 psi as shown by orange bars corresponding to smaller particle sizes. The cumulative volume percentage of particles less than 40 mesh (in case of 20/40 sand) is observed to be 11% compared to the volume of fines smaller than 100 mesh (in case of 60/100 mesh proppant) of 13%.

Fig. 21 shows the comparison of the particle size analysis of 20/40 sand with 60/100 mesh sand at 5000 psi. **Fig. 21 (top)** shows the native particle size distribution of each proppant before the start of the experiment and the **Fig. 21 (bottom)** shows the distribution of fines below 175 microns observed after each experiment. Significant amount of fines, up to 8.3%, is observed in case of 60/100 mesh compared to 1.2% with 20/40 sand.

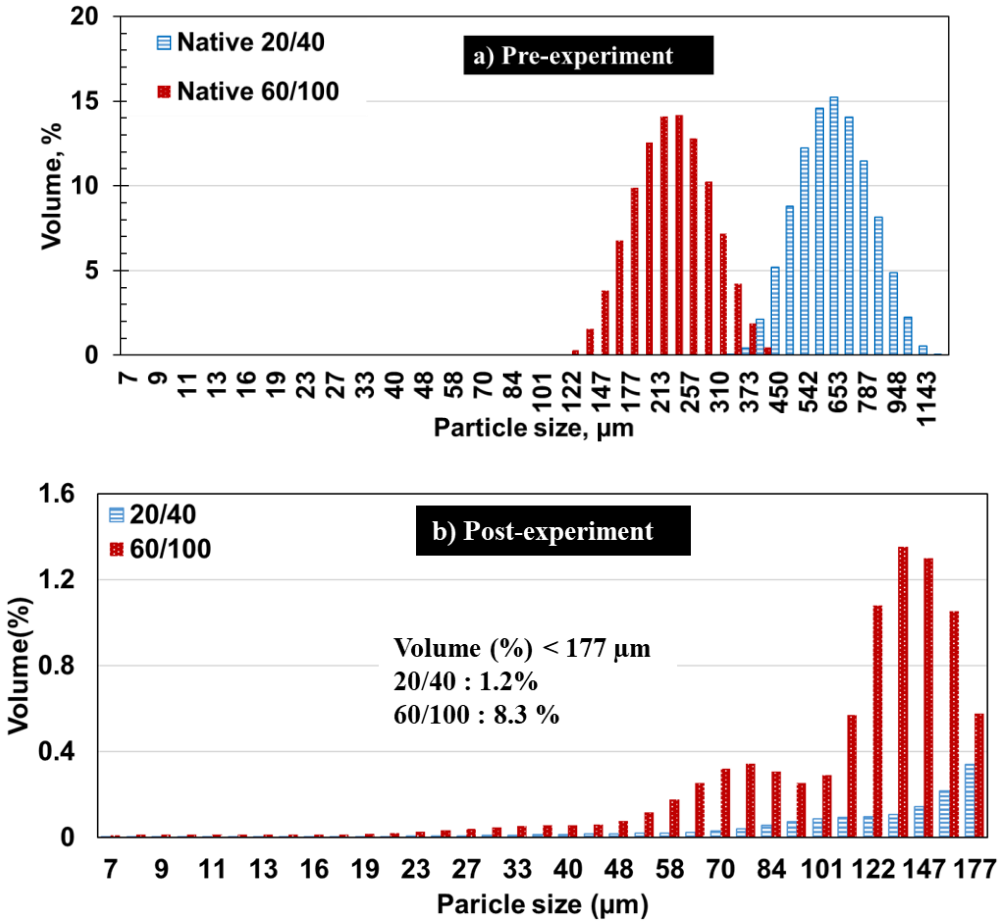

Figure 21: Particle size distribution of 20/40 and 60/100 mesh sand before the start of the experiment (top) and volume of fines generation after the dry crush test at 5000 psi (bottom). In both the plots, x-axis represents the particle size in microns and y-axis represents the volume percentage corresponding to each particle size. 7 times higher volume % of fines (particle size < 177 µm) is observed with 60/100 sand compared to 20/40 mesh sand.

3.2. Effect of proppant concentration on permeability

To understand the impact of proppant concentration on permeability and the damage mechanisms behind the decrease in permeability, experiments were conducted with proppant concentration of 3 lb/ft^2 and 4 lb/ft^2 with 60/100 mesh Ottawa sand, and the results have been compared with the lower proppant concentration of 2 lb/ft^2 (Mittal 2017). The proppant pack of the required concentration was placed between the Hastelloy platens. The proppant pack was then subjected to an axial load of 5000 psi using the loading rate of 100 psi/min. The temperature of the conductivity cell was maintained at 250 ^{o}F. The brine composed of distilled water mixed with 3% NaCl and 0.5% KCl was flowed at a rate of 3 ml/min.

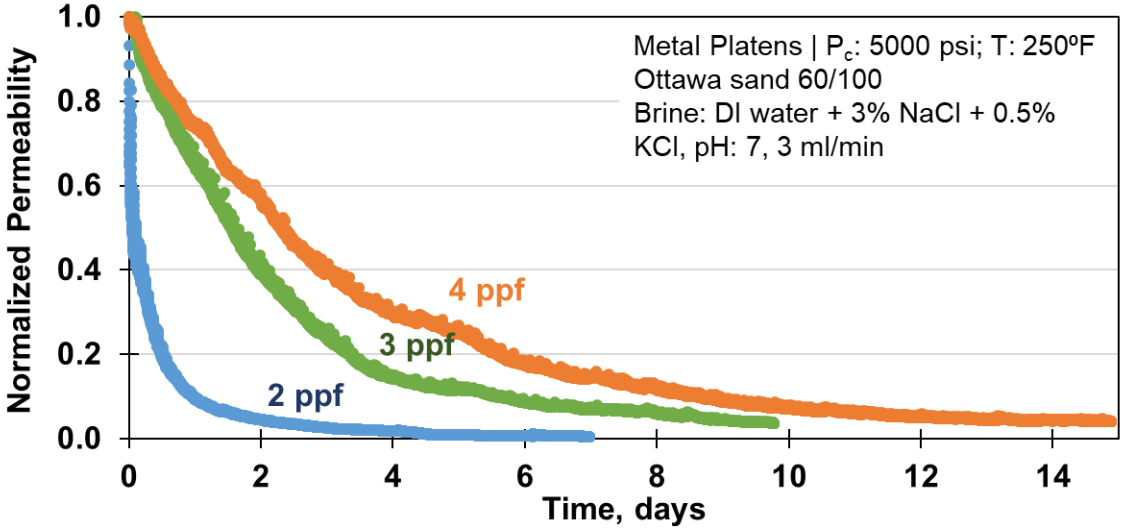

Figure 22: Normalized permeability variation over time with different proppant concentration. 60/100 mesh sand subjected to axial load of 5000 psi at a loading rate of 100 psi/min. Temperature 250 ºF was maintained throughout the experiment and the brine composed 3% NaCl and 0.5% KCl was flowed at a rate of 3 ml/min. Steeper decline in permeability observed with proppant concentration of 2 lb/ft^2 as compared to concentration of 3 lb/ft^2 and 4 lb/ft^2.

The permeability comparison with the three different proppant concentration is shown in the **Fig. 22**. The permeability with lower concentration of 2 lb/ft^2 drops precipitously within few days of the start of flow. However, higher permeability observed with higher proppant concentration. The change in permeability with varying proppant concentration with respect to change in porosity has been plotted in **Fig. 23**. The trendline has been fitted during the linear decline portion of the curve where the slope of 0.64, 0.95 and 1.2 are observed with the proppant concentration of 4, 3 and 2 ppf respectively. We observe increasing slope with lower proppant concentration. This indicates that with lower proppant concentration the rate of permeability decline will also increase.

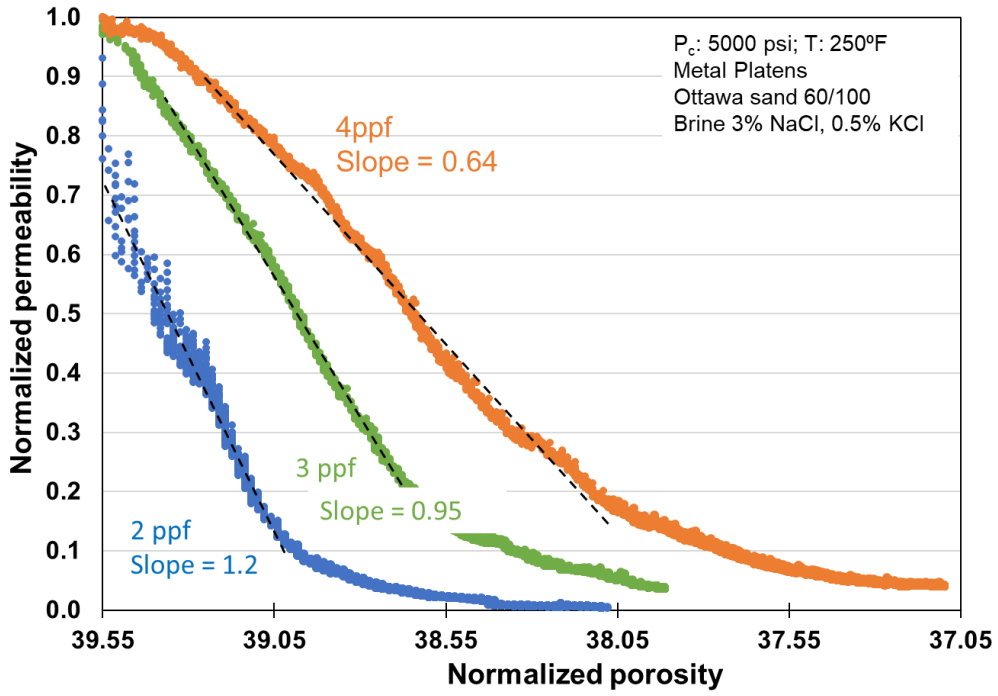

Figure 23: Normalized permeability vs. normalized porosity for the three different proppant concentrations. The dotted black lines indicate the trendline fitted in the linear portion of the permeability decline. With lower concentration higher slope is observed which indicates higher rate of permeability decline with lower proppant concentration.

Over the unit drop in porosity from 39.55% to 38.55%, we observed that permeability declined up to 98% in case of the 2 lb/ft^2 concentration. However, the decline of 80% is observed with proppant concentration of 3 lb/ft^2 and 60% permeability decline is observed with 4 lb/ft^2 concentration.

After the completion of each flow experiment, particle size analysis was done on the proppants. **Fig. 24** shows the particle size distribution obtained from each experiment. In the plot, the x-axis represents the grain diameter in µm and the y-axis (logarithmic scale) represents the volume percent corresponding to grains diameter. The black bars represent the particle size distribution of 60/100 mesh sand before the start of each experiment where the average grain diameter is ~220 µm. The blue bars represent the particle size distribution after the experiment with 2 lb/ft^2, green bars represent 3 lb/ft^2 and orange bars represent the 4 lb/ft^2 experiment.

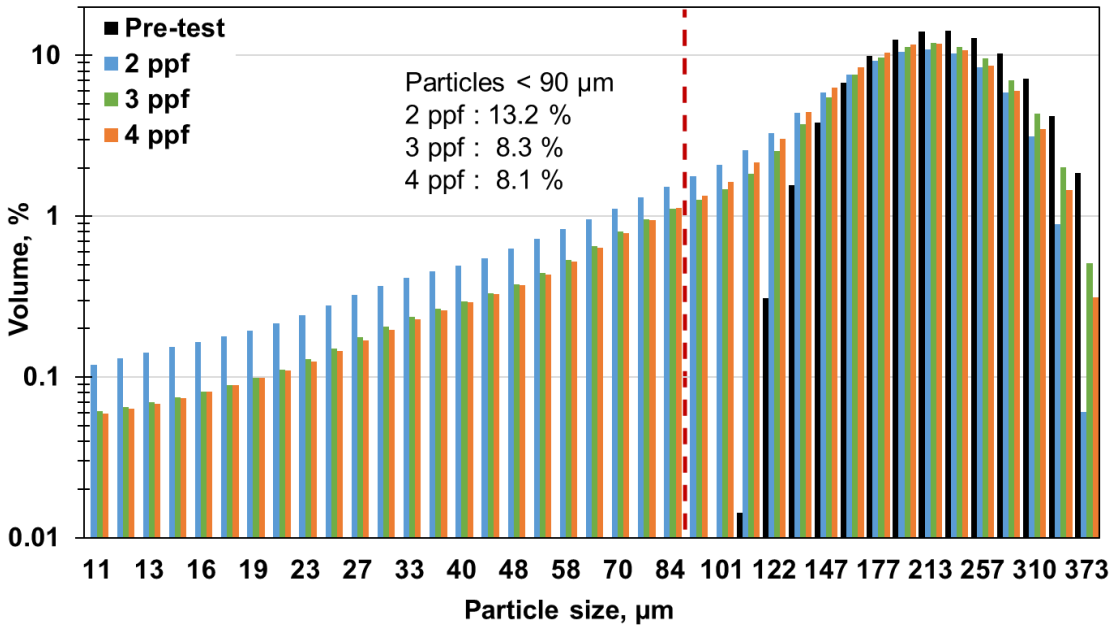

Figure 24 : Particle size analysis results of the three experiments conducted with different proppant concentrations. Particle size in µm is plotted on the x-axis and the corresponding volume percentage is plotted on y-axis. Significant levels of crushing are observed in all cases. However, the level of crushing is observed to be greater in case of lower proppant

concentration as indicated by blue bars compared to higher proppant concentration indicated by green and orange bars.

Significant level of crushing and fines generation is observed as indicated by the bars corresponding to grain diameter less than 150 µm (100 mesh) at all proppant concentrations. However, volume percent of fines generation is observed to be greater for lower proppant concentration of 2 lb/ft^2 as compared to the higher concentrations of 3 lb/ft^2 and 4 lb/ft^2. This suggests that higher level of crushing occurs at lower proppant concentration.

The SEM image of the native 60/100 mesh Ottawa sand is shown in the **Fig.25**. Using analysis of SEM images, roundness and circularity has been calculated.

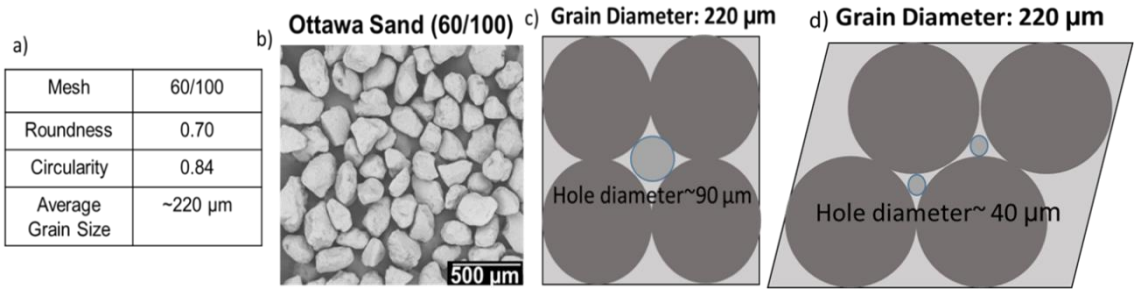

Figure 25: SEM image of native 60/100 mesh Ottawa sand (b). Using the 2-dimensional view of proppant, roundness and circularity were calculated (a). c). Assuming the ideal cubic packing of spherical grains of diameter 220 µm, maximum diameter of particle size which can be accommodated in the pore space is calculated to be ~90 µm and for rhombohedral packing it is~40 µm (d). Any particles larger than these values will plug the pores and reduce the porosity and permeability.

Assuming the ideal cubic packing of the perfectly spherical grains, the maximum diameter of the grains which can be accommodated in the space between proppant is calculated to be ~90 µm for cubic packing and for rhombohedral packing, this size reduces to ~40 µm. The finer particles will have the tendency to block the pores and cause porosity and permeability reduction. From the particle size analysis, shown in the **Fig.24**, the volume percentage of fines smaller than 90 µm was

calculated. A larger volume of fines ~13% is observed in case of lower proppant concentration (2 lb/ft^2) compared to ~8% in case of higher proppant concentration (4 lb/ft^2). It should be noted that the percentages of fines are similar (~8%) in both the cases of higher proppant concentration of 3 lb/ft^2 and 4 lb/ft^2.

Taneja (2016) reported dry crush tests with different proppant concentration conducted with 20/40 sand placed across the metal platens (**Fig.26**). At a lower concentration of 1 lb/ft^2, he observed uniform crushing throughout the proppant pack. However, at higher concentration of 4 lb/ft^2, non-uniform crushing primarily concentrated at the metal interface was observed. We believe that at higher concentration, a non-crushed portion is left in the center which will cause less decrease in porosity and permeability. However, at lower concentration, this non-crushed zone is reduced which leads to sharp decline in permeability.

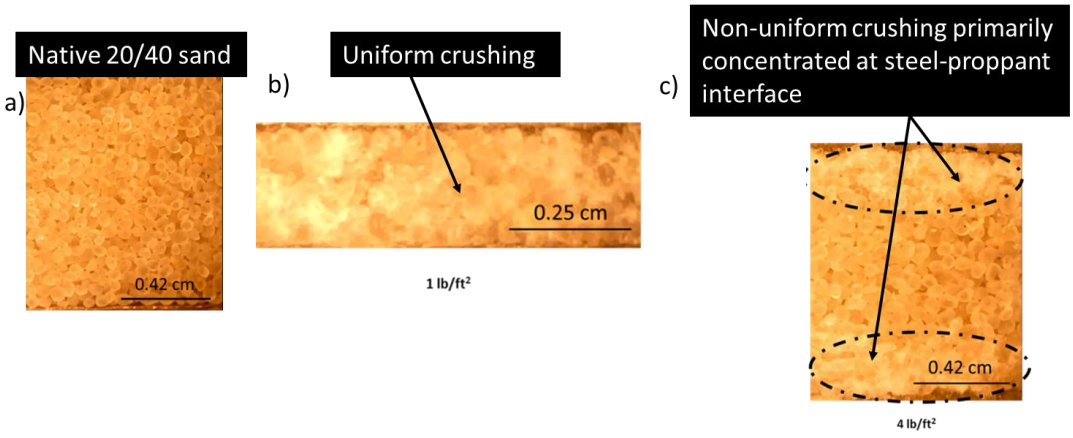

Figure 26: Dry crush tests results of 20/40 Ottawa sand crushed between metal platens with different proppant concentrations (Taneja 2016). a) Image showing native 20/40 Ottawa sand; b) image showing uniform particle crushing observed at lower proppant concentration of 1 lb/ft^2 c) image showing non-uniform crushing primarily concentrated at metal interface observed at higher concentration. Note the presence of non -crushed zone in the center due to greater proppant thickness at high proppant concentration of 4 lb/ft^2.

3.3.Effect of proppant type on permeability

It has been widely acknowledged that premium proppants such as ceramic proppants will provide higher fracture conductivity compared to silica sand. However, mechanisms leading to differences in conductivity remains unclear. Therefore, to study the effect of proppant type on fracture conductivity, experiments have been conducted using ceramic proppant and the results have been compared with the experiments conducted with silica-based sand (Mittal 2017) under similar test conditions.

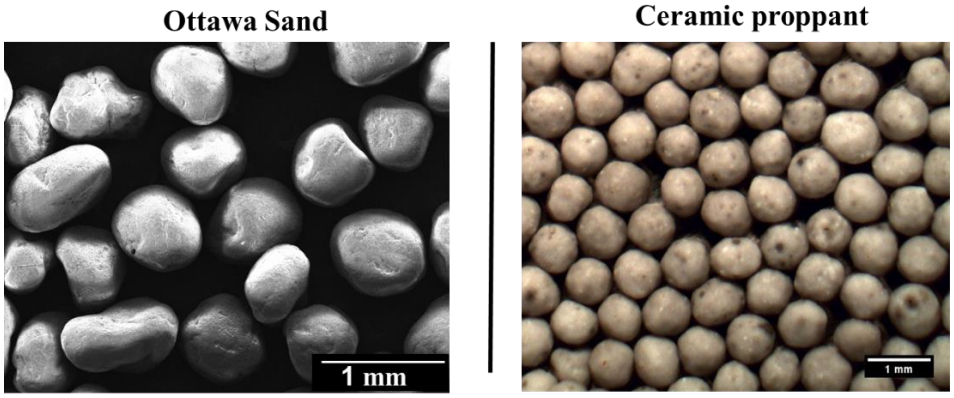

Type	Ottawa sand	Ceramic proppant
Roundness	0.7-0.8	0.9
Sphericity	0.8	0.9

Figure 27: Image analysis of 20/40 Ottawa (silica-based) sand and ceramic proppant. Comparing both we see ceramic proppant has higher sphericity and roundness compared to Ottawa sand.

The physical properties of both the ceramic and silica proppant were studied before the experiment. To characterize the properties like sphericity and roundness, SEM images were taken and analyzed as shown in the **Fig. 27**. We observed ceramic proppant has a higher sphericity and roundness compared to silica-based Ottawa sand. Pre-test particle size analysis shows that Ottawa sand has a wider distribution of particles sizes than the ceramic proppant of the same mesh **Fig. 28a.** Dry

crush tests have been conducted by placing the proppant between the metal platens at a concentration of 2 lb/ft^2. The proppant pack was subjected to an axial loading of 5000 psi loaded at a rate of 100 psi/min at room temperature. Particle size analysis shows that Ottawa sand undergoes significant crushing with cumulative volumes of fines generated around~ 9.7%. However, ceramic proppant shows almost zero crushing and no fines generation (**Fig. 28 b-c**.). But ceramic proppant shows some level of crushing when water flows for 3 days through the proppant pack after loading to 5000 psi suggesting a water weakening effect (Gupta et al. 2019). This necessitates the study of flow through experiment to understand the behavior of both the proppant and rock-proppant interaction under reservoir conditions.

a.)

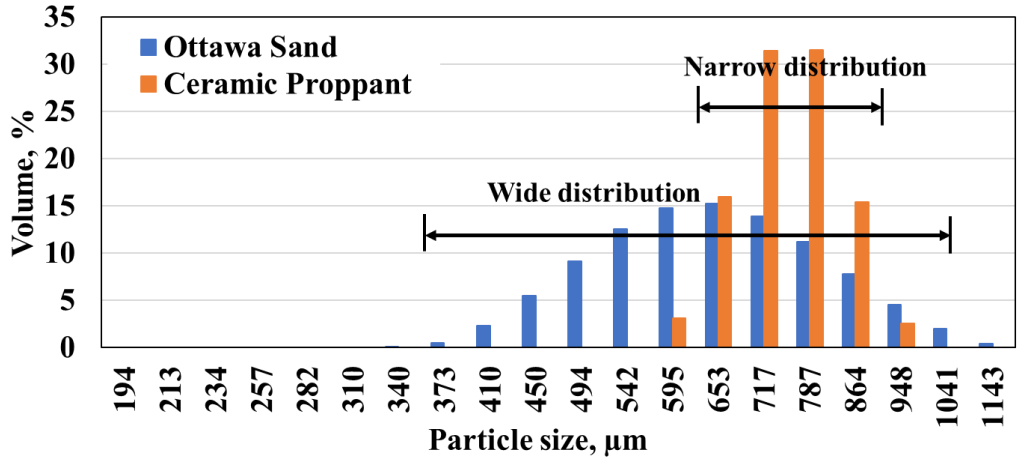

b.)

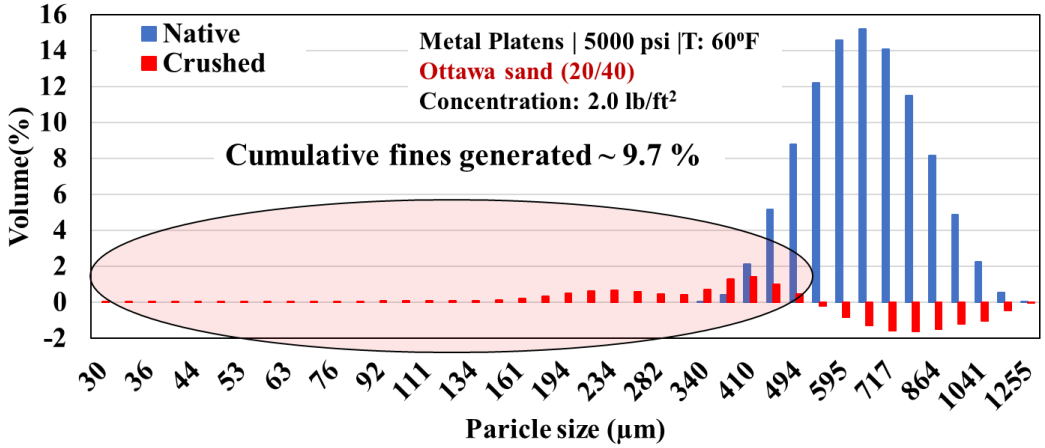

c.)

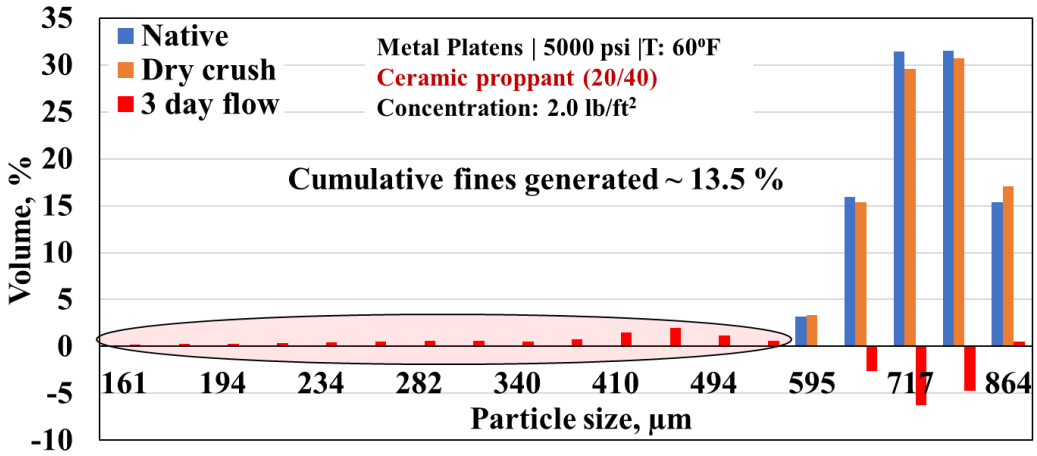

Figure 28: Particle size analysis comparisons of ceramic and Ottawa sand. a.) Native particle size analysis showing wide distribution for Ottawa sand and more uniform, narrow distribution of ceramic proppant. b.) dry crush test with Ottawa sand showing significant crushing with cumulative volume ~9.7% fines generation. c). Dry crush test with ceramic proppant showing almost no crushing at 5000 psi. However, after flow period of 3 days, cumulative fines generated are about ~13.5%.

Flow through experiments have been conducted by placing the proppant at a concentration of 1.5 lb/ft^2 between shale platens subjected to an axial load of 5000 psi and 250 ^{o}F. Brine composed of distilled water, 3% NaCl and 0.5% KCl was flowed through the proppant pack. Shale platens machined from the Eagle Ford formation were used in both the experiments. The FTIR mineralogy shown in the **Fig. 29** suggests the sample used in the experiment was rich in clays (58%), with 41% carbonates and 1% other minerals. The Total Organic Carbon (TOC) content was ~5.1 wt.% and helium crushed porosity was ~9.4%.

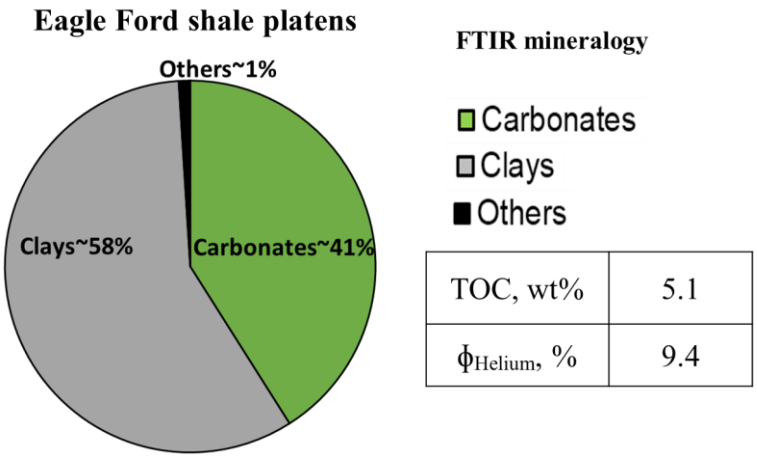

Figure 29: FTIR mineralogy of the Eagle Ford shale sample shows the presence of 41% carbonates, 58% clays and 1% other minerals. The helium crushed porosity is 9.4% and the Total Organic Carbon (TOC) is 5.1%.

The permeability comparison of both the proppant types with time is shown in **Fig. 30**. After the flow experiment of 2 days, a greater decline in permeability with Ottawa sand is observed whereas ceramic proppant shows relatively higher permeability. However, permeability with ceramic proppant declines at a faster rate compared to the Ottawa sand. After, 11 days of flow, the permeability with ceramic proppant becomes lower than that of Ottawa sand.

a.)

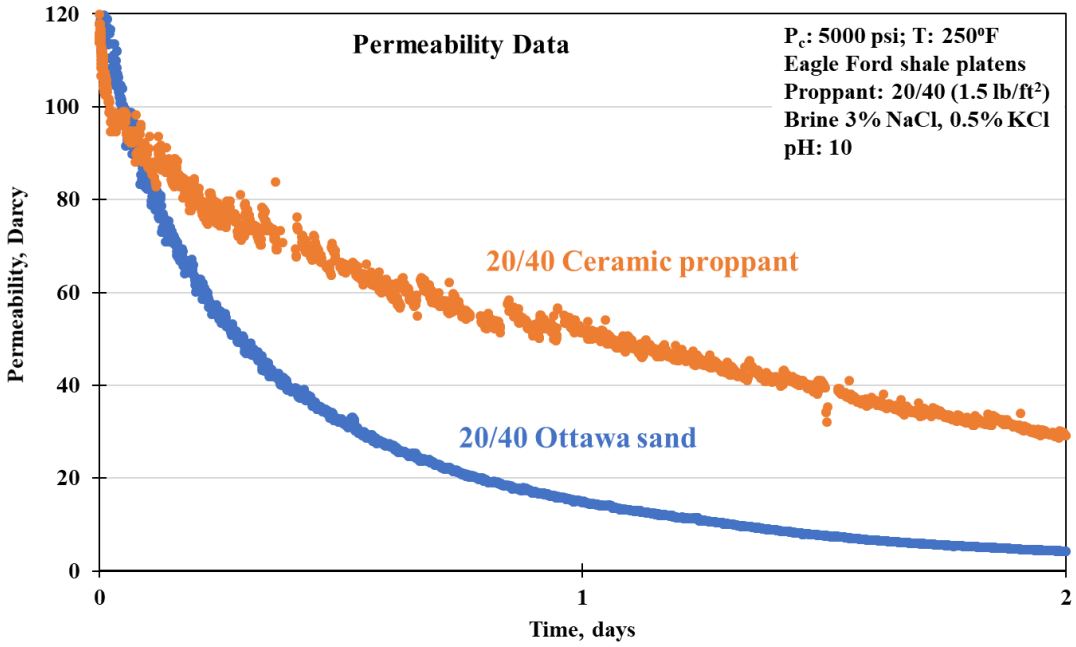

b.)

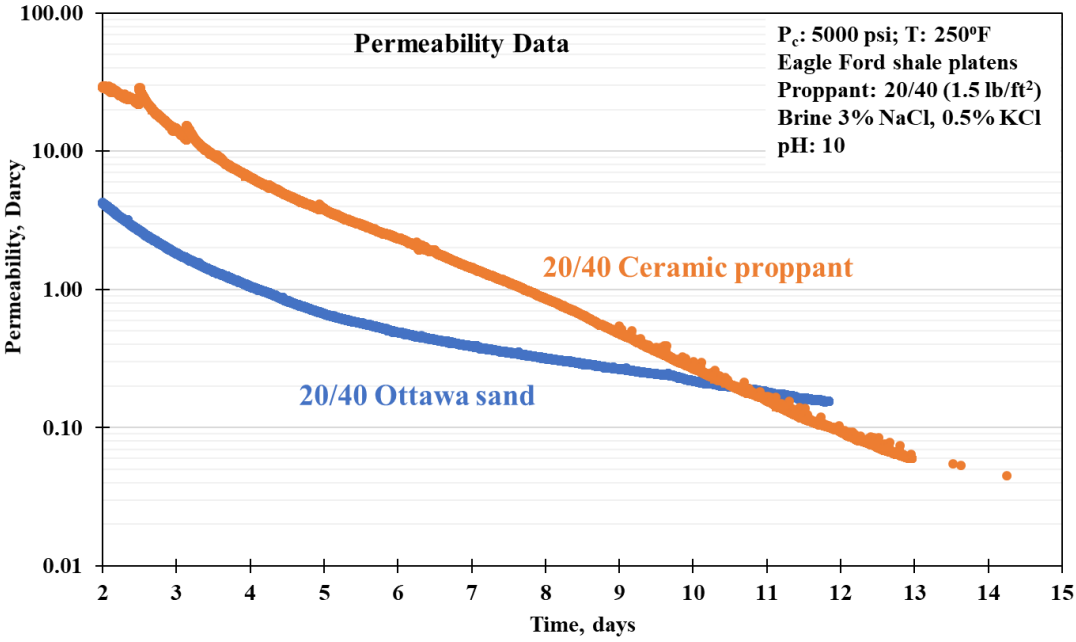

Figure 30: Permeability comparison of 20/40 Ottawa sand and ceramic proppant over time with Eagle Ford shale platens. Within a short period of 2 days, a greater decline in permeability with 20/40 Ottawa sand is observed compared to the ceramic proppant. However, permeability with ceramic proppant declines at a faster rate and becomes lower than Ottawa sand after the flow period of 11 days.

LVDT data was used to determine the proppant pack width reduction over time as shown in **Fig. 31**. Here, step 1 indicates the initial condition when the cell is at zero applied stress. Moving from step 1 to step 2, an axial load of 5000 psi is applied at a loading rate of 100 psi/ min and temperature was raised to 250 ^{o}F. At the end of step 2, flow is started and maintained at a rate of 3 ml/min. Step 3 indicates the condition of 5000 psi and 250 ^{o}F and flow of 8 days. We observe up to 64% compaction with Ottawa sand compared to 30% compaction with the ceramic proppant. Comparing the above compaction with metal platens where compaction is only due to grain rearrangement and crushing, we calculated the compaction due to embedment in the above two cases. We observed 14% compaction due to embedment in case of ceramic compared to 48% compaction with Ottawa sand.

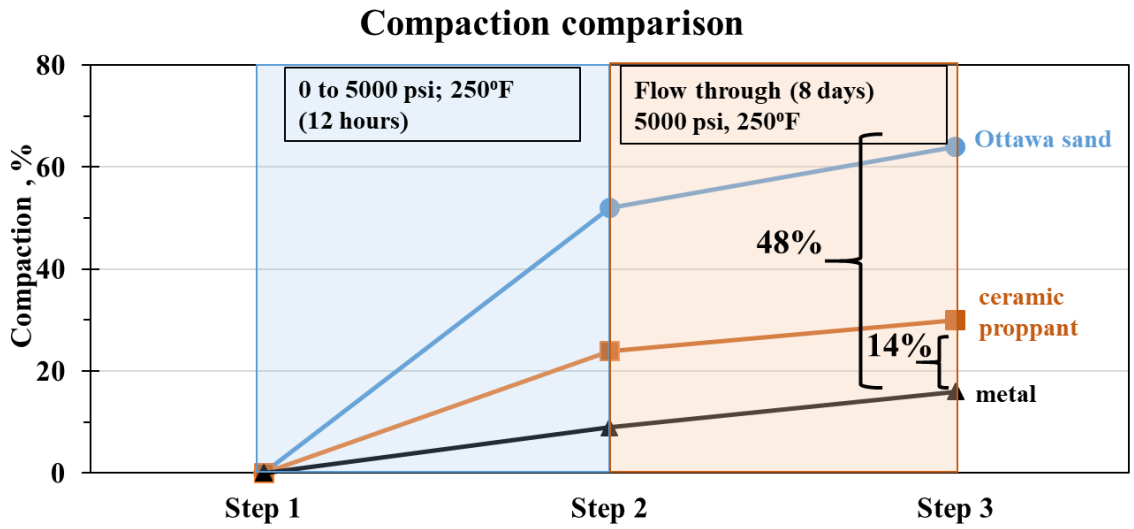

Figure 31: Compaction measured using LVDTs for both the experiments with different proppant types. After the flow period of 8 days, Ottawa sand shows overall higher compaction (~62%) compared to ceramic proppant (~30%). Comparing the compaction with the experiment conducted with metal, the component of embedment has been calculated. Lower embedment ~14% is observed with ceramic proppant compared to 48% with Ottawa sand.

The embedment depth has been characterized using profilometer surface scanning. Shown in the **Fig. 32** is the profilometer scan of the surface of the platens after the experiment. The green color indicates the baseline zero depth/height. Cooler colors (blue) indicate embedment due to loading and hotter colors (red) indicate extrusion of surface near the embedment. We observed embedment depth up to 350 µm with Ottawa sand compared to 225 µm for ceramic proppant. It should be noted here that with ceramic proppant embedment is more uniform and circular throughout the surface compared to irregular and angular embedment with Ottawa sand. Ceramic proppant appears to extrude the shale surface at its boundaries due to its high strength. Also, the uniform and circular embedment suggest the uniform load distribution among the well-rounded, high strength grains leading to overall lower embedment compared to the Ottawa sand.

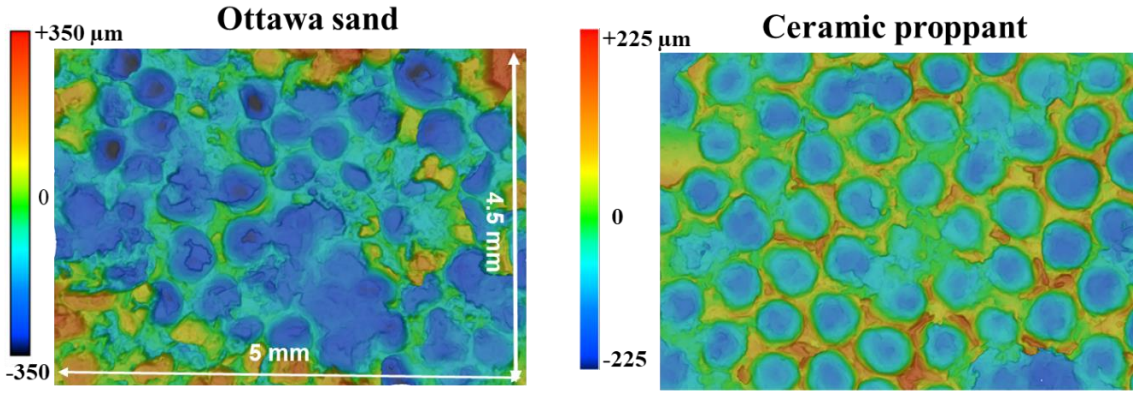

Figure 32: Laser profilometer scan of Eagle Ford shale platen with 20/40 Ottawa sand (left) and 20/40 ceramic proppant (right) after the long-term flow through testing. With Ottawa sand, embedment depth up to 350 µm is observed as compared to 225 µm for the ceramic proppant. The embedment is recorded at a proppant (concentration: 1.5 lb/ft^2) placed between the Eagle Ford shale platens at an axial stress of 5000 psi and 250 ^{o}F when alkaline brine (pH: 10) is flowed.

After the completion of the flow through test, the shale and proppant pack were further examined under SEM to evaluate the mechanical and chemical changes. **Fig. 33a** shows the top platen

surface with a uniform layer of ceramic proppants embedded in Eagle Ford shale surface. Looking at the individual grain in **Fig. 33 (b-f)**, we note the presence of well-rounded ceramic proppant grains with chemically precipitated sodium chloride salt and diagenetic clay coating growth at the surface. This observed salt coating is primarily due to cooling of the brine after the completion of the experiment.

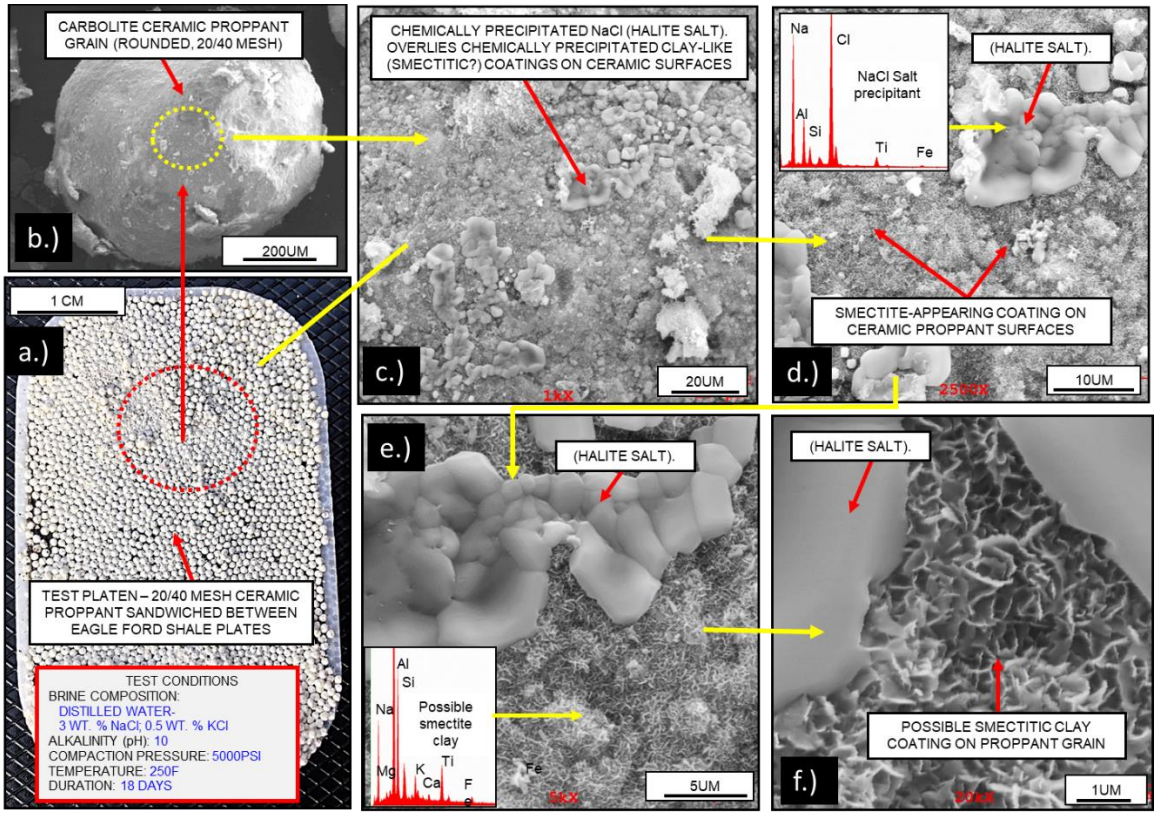

Figure 33: SEM image of the experiment (duration: 18 days) conducted with ceramic 20/40 proppant (concentration: 1.5 lb/ft^2) on Eagle Ford shale platens at a stress of 5000 psi and 250 ^{o}F flowing an alkaline fluid (pH: 10). Uniformly embedded layer of ceramic proppant grains is seen on the shale surface. Individual proppant grains are well rounded and show the growth of diagenetic smectite clay coating on their surfaces.

Fig. 34 (a-b) shows the ceramic proppant embedded deep into the shale surface and some of the proppant undergoes mechanical fracturing due to the application of high stress (5000 psi)

throughout the experiment. Extensive growth of diagenetic smectite clay coating on the outer surface of proppant grains was also observed which was further verified by EDS (**Fig. 34(c-e)**).

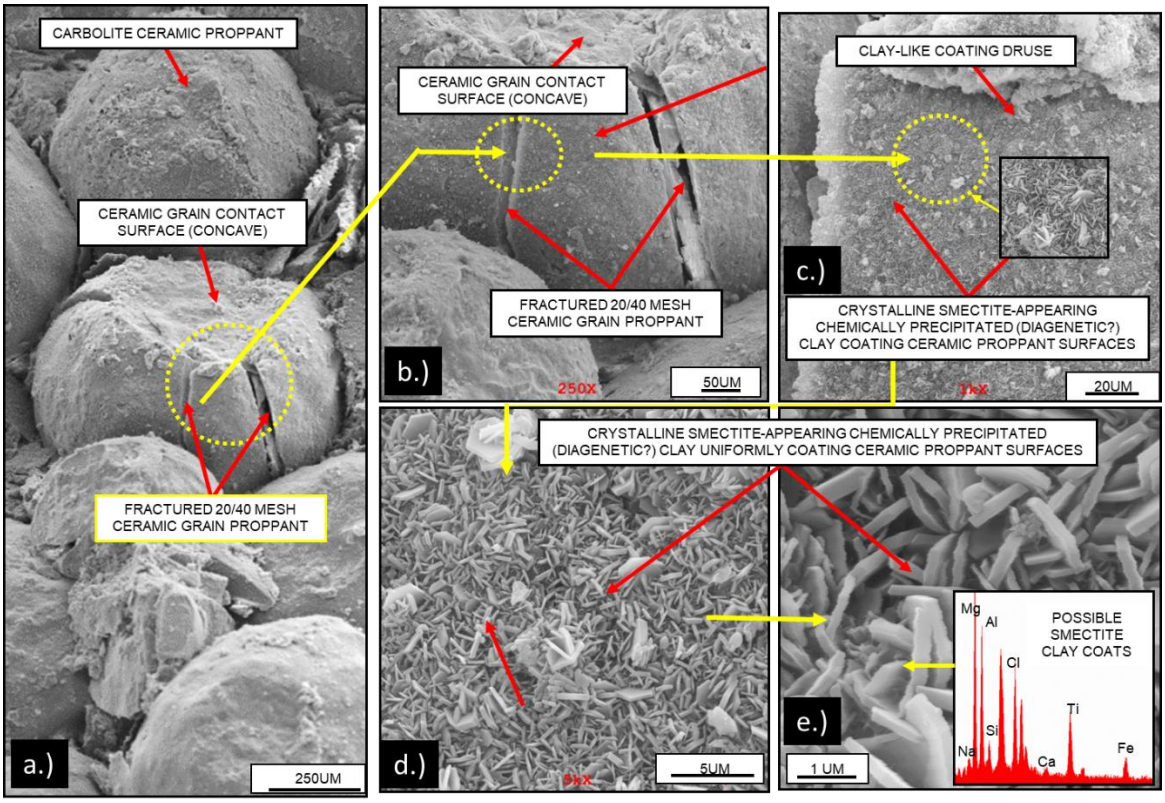

Figure 34: SEM images of the experiment (duration: 18 days) conducted with 20/40 ceramic proppant with Eagle Ford shale platens at a stress of 5000 psi and 250 ºF when the brine composed of distilled water, 3% NaCl, 0.5% KCl was flowed. Deeply embedded ceramic proppant grains can be seen (a) along with some instances of individual grain fracturing (b). The proppant grains show the presence of chemically precipitated clay coating on their surfaces (c-e).

Beside the extensive coating of diagenetic clay on the proppant grain surfaces, the presence of clay coating infilling the interior surface of fractures in the ceramic proppant was also observed (**Fig. 35 a-c**). These growths in the interior surface of the proppant indicates the growths occurs after the mechanical fracturing of the ceramic proppant grains.

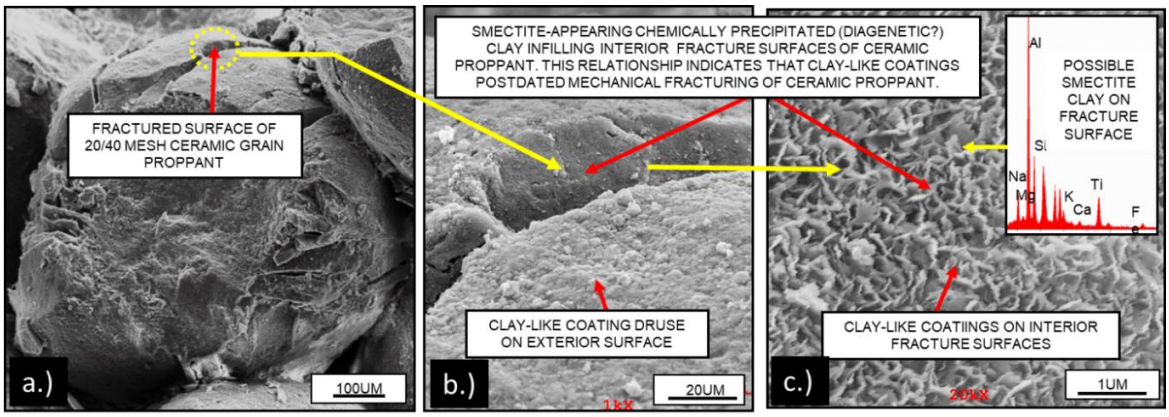

Figure 35: SEM images of the experiment (duration: 18 days) with 20/40 ceramic proppant with Eagle Ford shale platens showing the growth of diagenetic smectite clay in the interior surface of the fractured proppant grain. This indicates the clay growth postdated the mechanical fracturing of the ceramic proppant.

SEM image with 20/40 silica-based Ottawa sand conducted under similar test conditions of 5000 psi, 250 ^{o}F and the alkaline (high pH:10) environment (Mittal 2017) is shown in the **Fig.36**. Extensive proppant crushing due to mechanical fracturing of relatively low strength quartz proppant grains is observed. The embedment of the proppant in the shale surface and the disrupted shale surface near the embedded proppant boundary can also be seen in the **Fig. 36b**. Although higher degree of proppant crushing observed with silica based 20/40 Ottawa sand compared to the ceramic proppant, there is no evidence of any diagenetic growth observed with Ottawa sand.

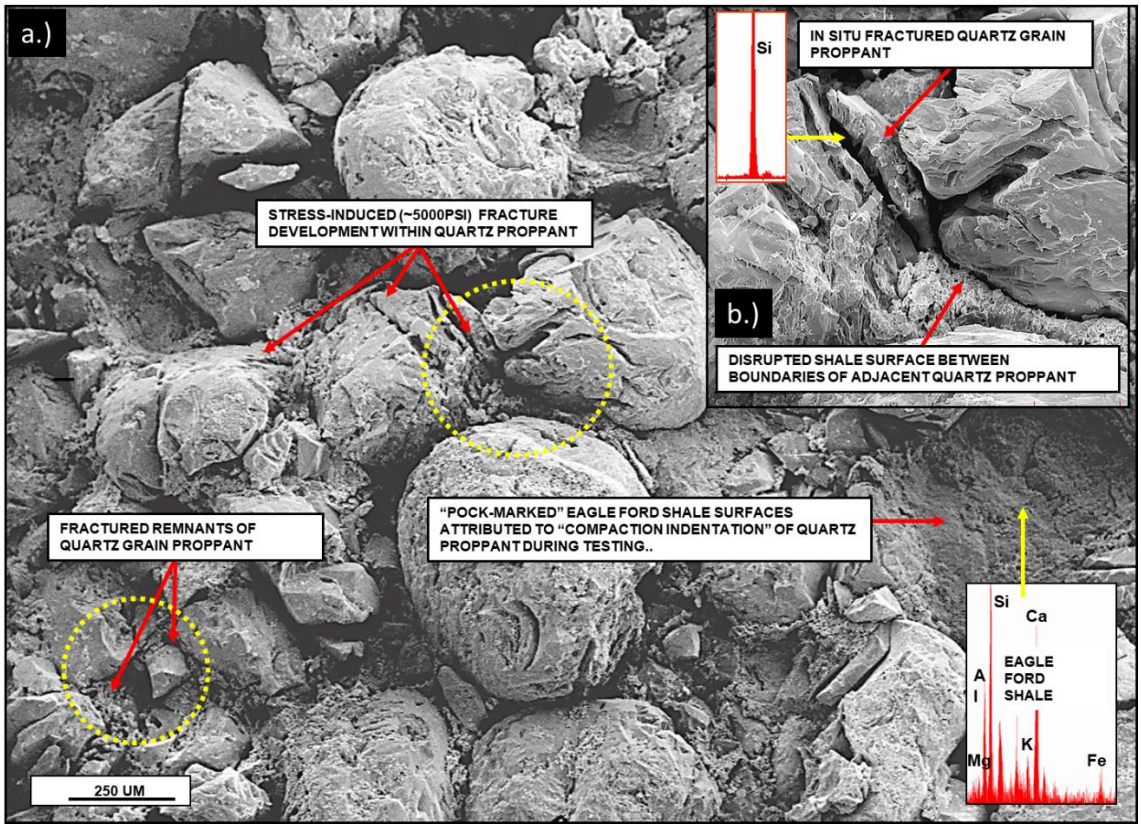

Figure 36: SEM images of the experiment (duration: 30 days) conducted with 20/40 Ottawa sand (concentration: 1.5 lb/ft^2) at a stress of 5000 psi, 250 ºF. High pH (~10) brine composed of DI water mixed with 3% NaCl, 0.5% KCl and 0.05 molar sodium carbonate was flowed at a rate of 3 ml/min throughout the experiment. Extensive mechanical fracturing of Ottawa sand observed along with proppant embedment and shale surface extrusion. However, no evidence of diagenetic growth was observed (Mittal 2018).

3.4.Effect of particle size on fracture conductivity

The experiments with Meramec formation platens and three different proppant sizes: 20/40, 40/70 and 60/100 mesh size Ottawa sand were conducted. FTIR mineralogy suggests that Meramec samples have 11% clay, 56% quartz, 22% feldspar and rest other minerals (**Fig. 37)** and the average grain size is ~40 µm. Mittal, (2017) found that coarse proppant 20/40 has higher roundness and circularity compared to finer sand 60/100 which appears more angular and have lower sphericity. Due to difference in these properties, proppants of different sizes tend to exhibit different overall crushing and compaction as studied and discussed in detail in section 3.1. However, all the tests in section 3.1 were conducted with metal platens where major compaction occurs due to grain rearrangement and crushing. During hydraulic fracturing, the proppants are pumped in to the formation where the proppant can also get embedded in to the formation adding to the further reduction in fracture width.

Experiments were conducted with platens machined from rock samples obtained from the Meramec formation (Oklahoma). Three different experiments with different proppant sizes including 20/40, 40/70 and 60/100 were conducted where proppant packs with concentration of 1.5 lb/ft^2 were subjected to an axial load of 5000 psi and 250 ^{o}F. Brine composed of distilled water with 3% NaCl, 0.5% KCl was flowed at a rate of 3 ml/min throughout the experiment.

The conductivity comparison of all the three proppant sizes is shown in the **Fig. 37**. 20/40 proppant exhibit higher conductivity (~2000 md-ft) at the beginning of the flow and even after 6 days of flow, the conductivity remains high (~850 md-ft). The conductivity tends to decrease as we move from coarser to finer mesh proppant. The 40/70 mesh proppant starts with a conductivity of (~350 md-ft) and drops up to (200 md-ft) after the flow period of 6 days and 60/100 shows the lowest

conductivity of all the three proppant sizes with a starting conductivity of (~180 md-ft) which drops rapidly within few days of flow and at the end of 6 days of flow conductivity (~45 md-ft) was observed (**Fig.37**).

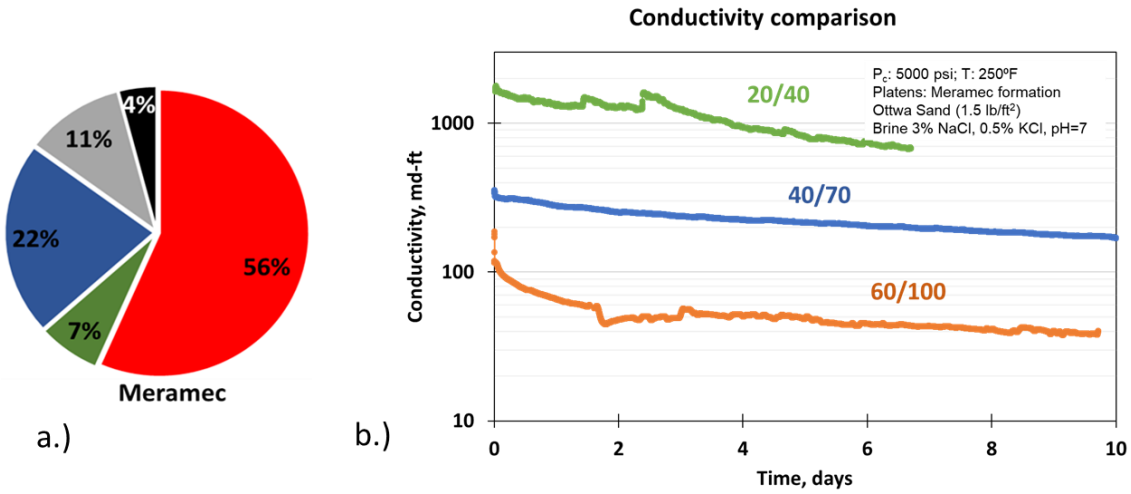

Figure 37: a) FTIR mineralogy of Meramec. b) Conductivity comparison of all the three proppant sizes: 20/40, 40/70 and 60/100. All the three experiments were conducted under similar conditions except for proppant size. The conductivity with coarser proppant 20/40 starts with higher initial value compared to the finer mesh sands 40/70 and 60/100. Over the flow period of 6 days, the conductivity with 20/40 was much higher compared to 40/70 and 60/100 with 60/100 showing the lowest conductivity.

The LVDT data was used to measure the proppant pack width reduction over time. **Fig. 38**. Shows the percentage compaction of the proppant pack over the different stages of the experiment.

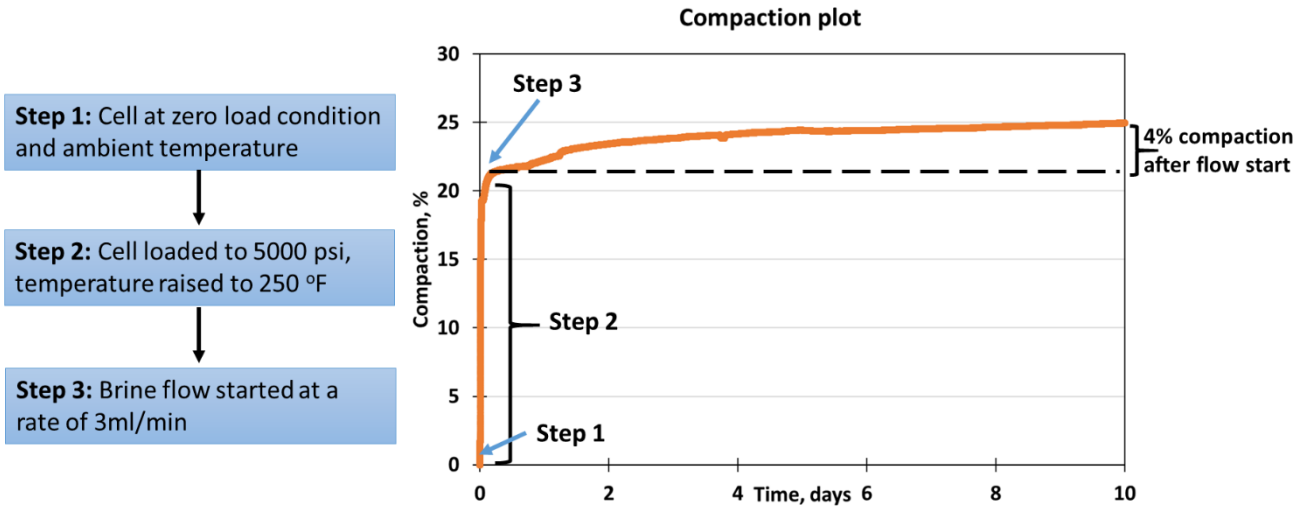

Figure 38: The normalized compaction of the 60/100 mesh (1.5 lb/ft2) Ottawa sand proppant pack between Meramec platens over time indicating different steps and corresponding compaction (right) and details of different steps (left) during the compaction measurement. Step 1 in the figure indicates the initial no load condition with zero compaction. Moving from step 1 to step 2, the cell is loaded to 5000 psi and temperature raised to 250 °F. Compaction of ~20% observed during and after the cell loading. At step 3, flow is started and after the flow period of 10 days total compaction of ~25% observed where 4% compaction was observed after the start of the flow.

Step 1 indicates the initial condition when the cell with required proppant pack is placed between the platens at zero load condition under ambient temperature. At this point, there is no compaction as there is no stress applied. At step 2, cell is loaded to 5000 psi at a loading rate of 100 psi/min and the temperature is increased up to 250 °F. Thereafter, cell is left for 12 hours to allow the temperature to stabilize. At step 3, brine flow at a rate of 3 ml/min is started. The compaction plot with all three steps is shown in the **Fig. 38 (right).** Compaction up to 20% observed with 60/100 mesh sand during the loading phase or step 2. After the flow period of 10 days, the total of ~25% proppant pack width reduction was observed out of which 4% compaction was observed after the start of the flow. This indicates the major compaction happening during the loading phase itself and less compaction is observed during the flow period of 10 days.

The compaction comparison of all the three experiments with different proppant sizes is shown in the **Fig. 39**. All three plots start with zero compaction at step1. Moving from step1 to step 2, lower compaction (~12%) is observed with 20/40 mesh sand, and 16% with 40/70, and 21% with 60/100 mesh sand. After the flow is started at step 3, the proppant pack further undergoes compaction and at the end of flow period of 10 days, total compactions of 17% with 20/40, 20% with 40/70 and 25% with 60/100 mesh sand are observed. Overall, higher compaction with finer mesh sand is observed. These compaction helps us to understand the reason behind initial difference and subsequent decline in conductivity with different proppant sizes observed in the **Fig. 37b**.

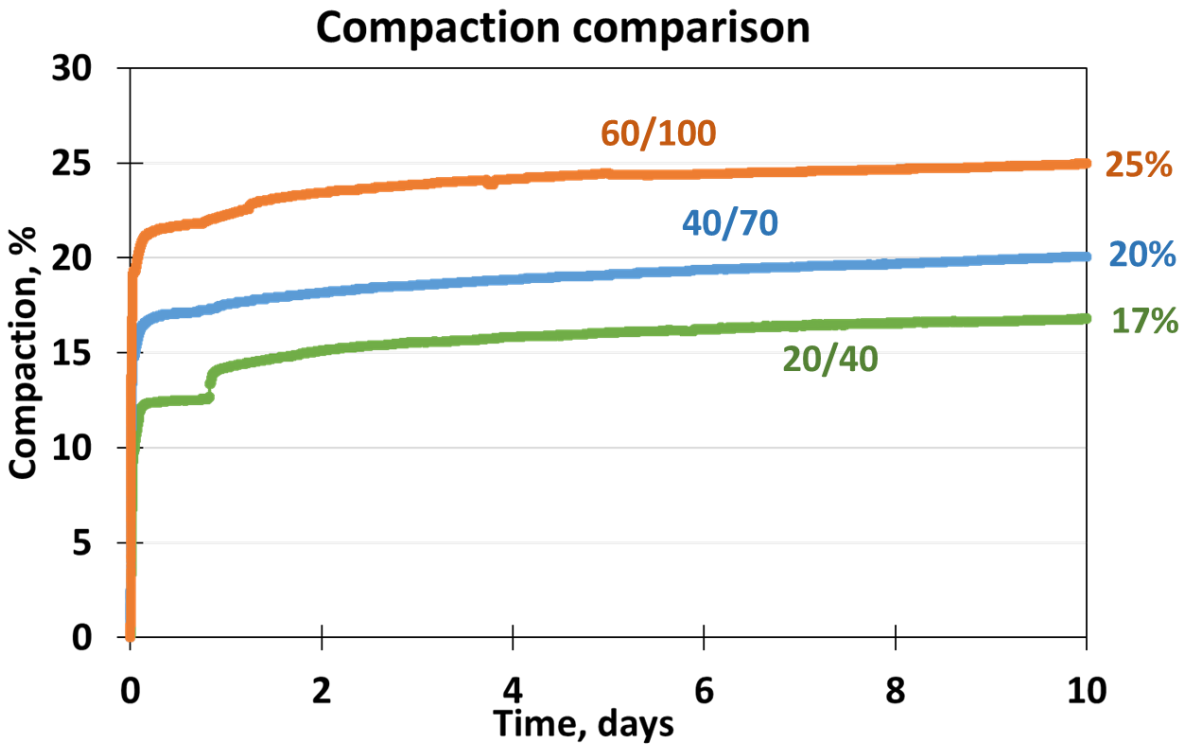

Figure 39: Comparison of compaction of Ottawa sand proppant between Meramec platens at 1.5 lb/ft2 concentration for three proppant sizes. Higher overall compaction (25%) is observed with finer mesh sand (60/100). Relatively lower compaction (20%) with 40/70 and lowest compaction (17%) is observed with 20/40 mesh sand.

The application of high stress (5000 psi) leads to the embedment of proppant grains. After the completion of each experiment the embedded proppant grains were removed from, the shale platens and the surface was examined under profilometer. The surface scans of the experiment conducted with 20/40 mesh sand are shown in the **Fig. 40**. The shale surface was polished using 1500 grit paper to obtain the smooth surface before the start of the experiment. The pre-experiment surface scans are shown in the **Fig. 40 (left)** where the green color indicates the baseline zero depth. Any embedment on the surface is indicated by the cooler (blue) colors and upliftment of the shale surface due to proppant embedment is indicated by hotter (red) color as shown in **Fig. 40 (right).**

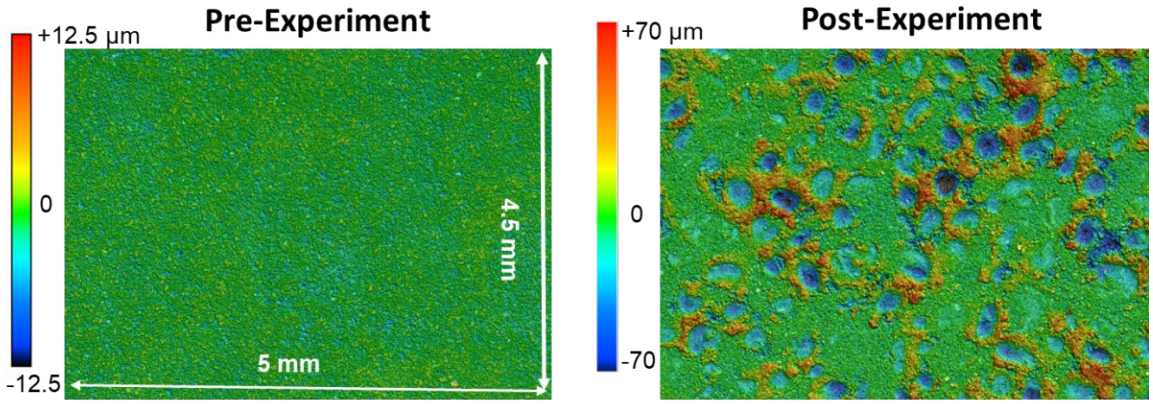

Figure 40: Surface scans of the shale before and after the test conducted with 20/40 Ottawa sand proppant placed between Meramec platens. Pre-experiment surface is shown in the left where green color indicates the baseline zero depth. Post experiment (right) shows the embedment in cool (blue) color and extrusion of shale surface due to embedment in hot colors (red).

Shale surfaces after the experiments with three different sizes of proppant with Meramec shale samples are shown in the **Fig. 41**. The shale surface with 20/40 proppant shows relatively circular and deeper embedment compared to both the 40/70 and the 60/100 mesh proppants. The deeper intrusions of 20/40 proppants lead to higher extrusion of nearby formation surfaces. The surface

with 40/70 proppant experiments shows more angular embedment and lower extrusions compared to 20/40 proppant. However, with 60/100 there is almost negligible grain embedment. 60/100 mesh proppant, being the most angular, undergoes higher rearrangement of grains and crushing leading to even finer particles generation causing lower embedment depths and negligible extrusions.

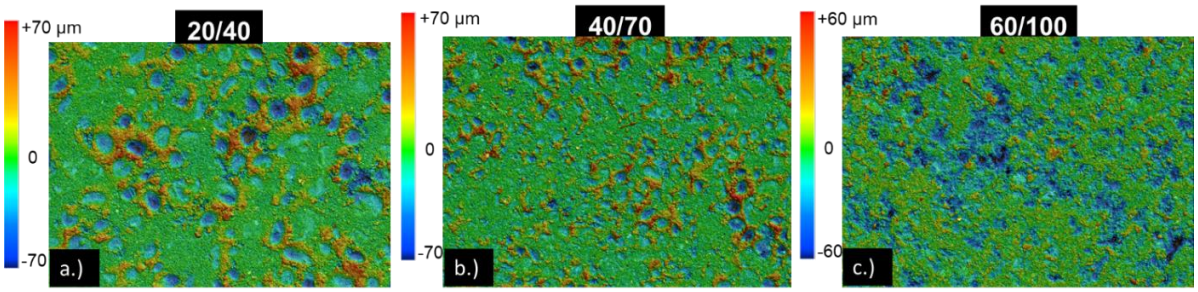

Figure 41: Post-experiment surface scan comparisons of all three experiments with different proppant sizes: a) 20/40, b) 40/70, c) 60/100. The surface profile with 20/40 indicates rounder and deeper proppant embedment depths and higher extrusions; the 40/70 shows relatively lower embedment depths and extrusions. Embedment with 40/70 appears more angular compared to 20/40. 60/100 shows very few embedments with individual grains, rather aggregated crushed fines are observed to slightly embed in the surface with almost negligible formation extrusion.

The proppant and shale surfaces were further evaluated after the experiment using SEM imaging. **Fig. 42** shows the presence of stress induced fractures of proppant grains after the experiment with 20/40 sand. **Fig. 43a** shows the tightly packed 40/70 grains due to the grain rotation and rearrangement of the angular grains during the experiment. Extensive fracturing of proppant grains and fines generation can also be seen in the **Fig. 43 (b-c).**

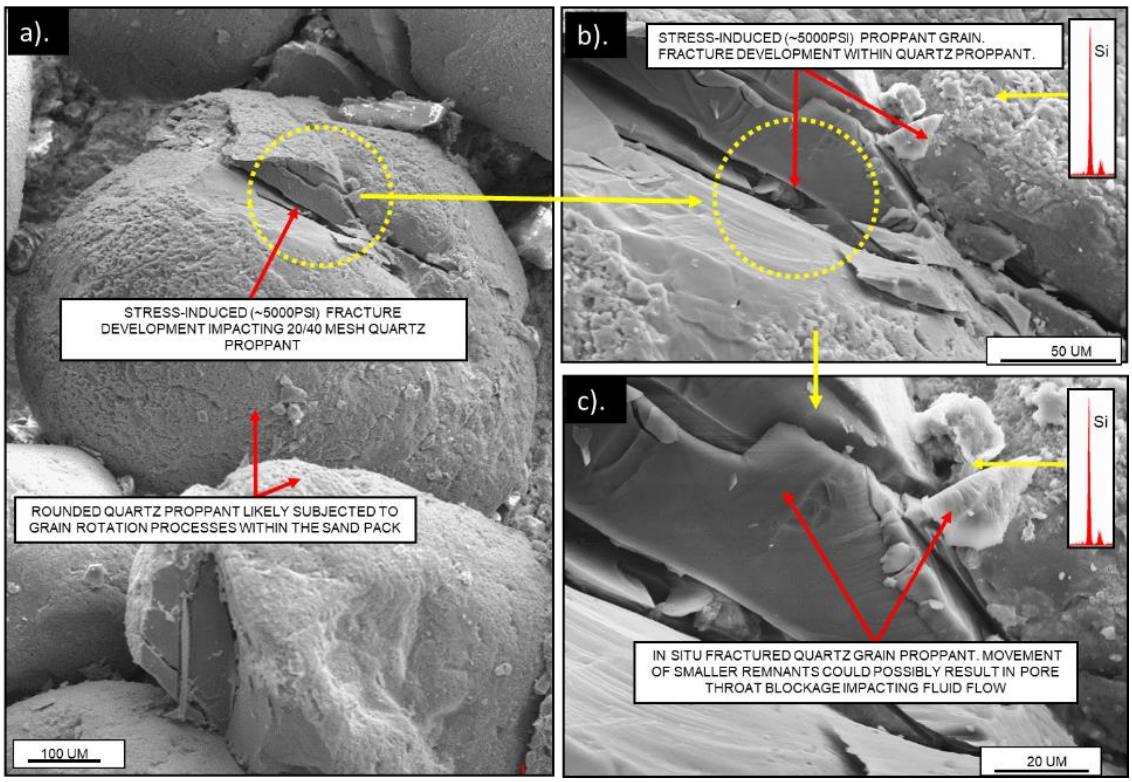

Figure 42: SEM images after the experiment conducted with 20/40 sand (concentration: 1.5 lb/ft^2) with Meramec platens. Stress induced fracture development in the proppant grains can be seen. The fracturing is due to the application of high stress (~5000 psi) throughout the experiment.

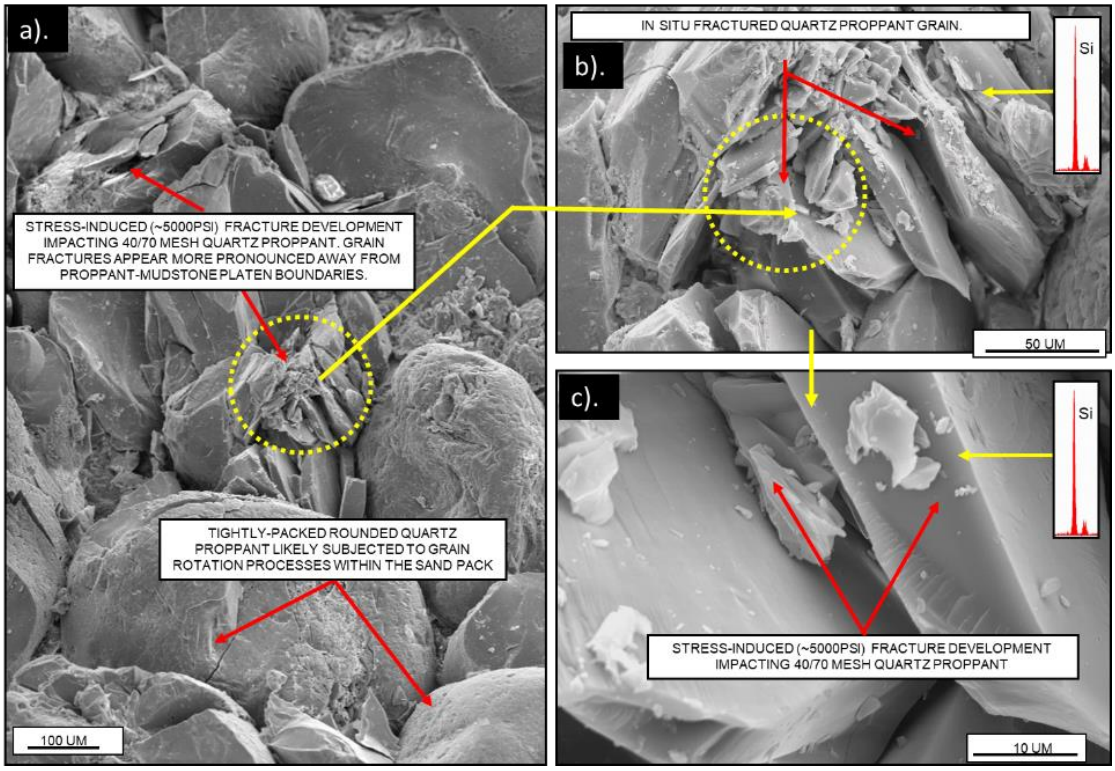

Figure 43: SEM images of the experiment conducted with 40/70 mesh proppant showing tightly packed proppant grains mostly due to grain rotation and rearrangement. Extensive fracturing of proppant grains due to high applied stress (~5000 psi) is also observed (b-c).

Fig. 44 shows, the shale surface after the experiment conducted with 40/70 mesh proppant; the proppant grains embedded on the surface exhibit less fracturing compared to the grains within the proppant pack. The disrupted shale surface due to proppant embedment can be seen in **Fig. 44b**. The disruptions of the formation further lead to the generation of fines as can be seen from the **Fig. 45 (a-c).** The fines generated from the matrix can further block the pore throats of the proppant pack and leads to the porosity and permeability reduction.

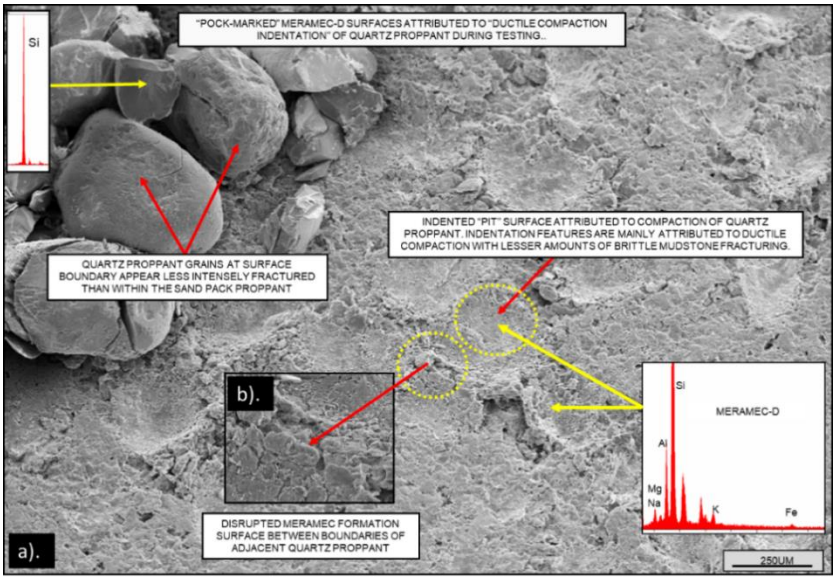

Figure 44: SEM images after the experiment with 40/70 mesh proppant. a) the shale surface shows the development of pock marks due to the proppant embedment which leads to the disruption of shale surface, b) shows disrupted material in detail.

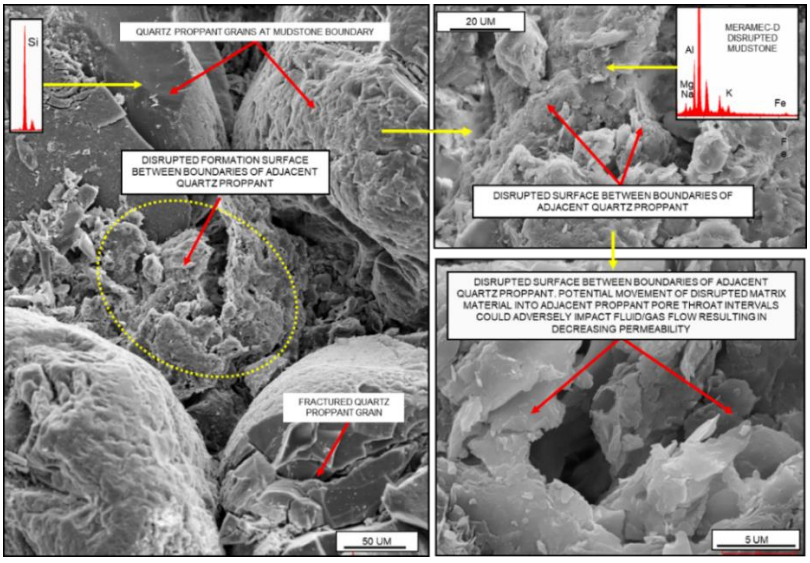

Figure 45: SEM images of the embedded proppant grains and extruded formation after the experiment with 40/70 proppant. Extruded material will lead to fines generation. These fines can block the pore throats of the proppant pack leading to the reduction in porosity and permeability.

The SEM images of the experiment conducted with 60/100 sand are shown in the **Fig. 46**. Unlike the test with 40/70, the fractured quartz grain appears more pronounce in case with 60/100 near the platen interface (**Fig. 46a**). This indicates the 60/100 mesh sand undergoes greater crushing and lower embedment compared to 40/70. The SEM images support the profilometer scan comparisons shown in **Fig. 41** where instead of individual grain embedment, like in 20/40 and 40/70, 60/100 shows multiple crushed grains embedding into the formation. These higher levels of crushing can generate larger amounts of fines. which can block the pore throats leading to the sharper decline of the permeability.

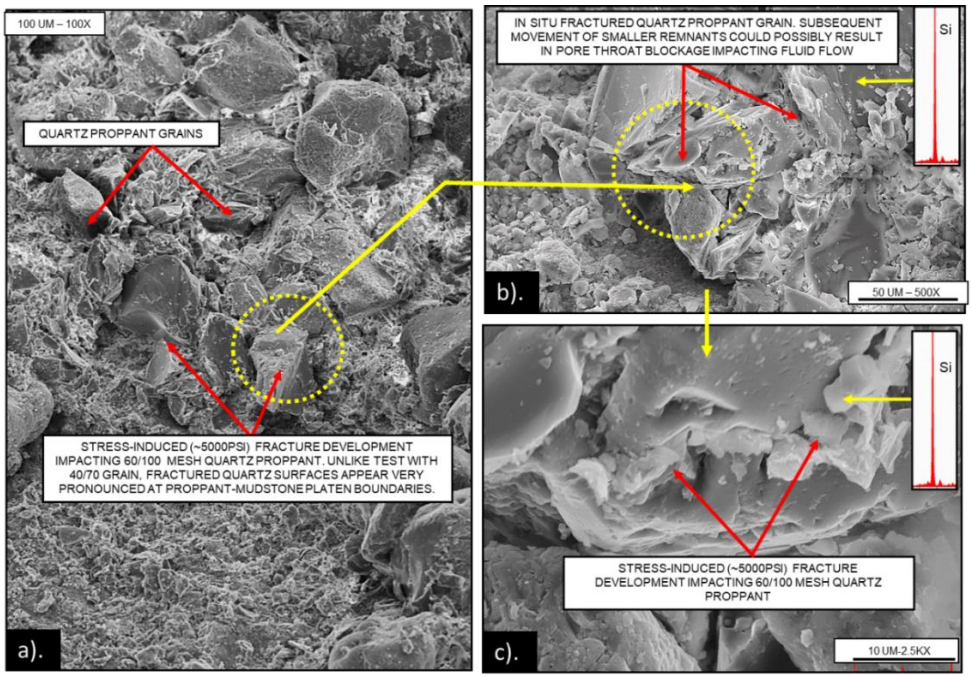

Figure 46: SEM images after the experiment with 60/100 sand with Meramec formation platens. (a) More pronounced fracturing of proppant grains near the rock-proppant interface is observed compared to the experiment with 20/40 and 40/70 proppant. (b-c) show the extensive fracturing of proppant grains and fines generation.

3.5. Effect of overburden stress on fracture conductivity

The conductivity experiments were further extended to measure the effects of overburden stress on fracture conductivity. 20/40 Ottawa sand was placed between the Eagle Ford shale platen at a concentration of 1.5 lb/ft^2 and 250 ^{o}F. Brine was flowed at a constant rate of 3 ml/min which was prepared by mixing DI water with 3% NaCl, 0.5% KCl and 0.05 molar Na_2CO_3 was added to raise the pH to 10. Basalt crushed and sieved to 20/40 mesh was also mixed with proppant to simulate the presence of volcanic components often found associated with shales (Calvin et al. 2015; Lejay at al. 2017). Keeping all the parameters same, three experiments were conducted at three different stress conditions: 1500 psi, 3000 psi and 7500 psi.

Fig. 47. Shows the fracture conductivity under different stress conditions. Keeping the permeability value observed at the start of the flow constant, conductivity is calculated using the proppant pack width reduction over time. The LVDT compaction data is used to determine the proppant pack width reduction. Lower conductivity observed with higher stress. However, conductivity is observed to decline at a very low rate over time.

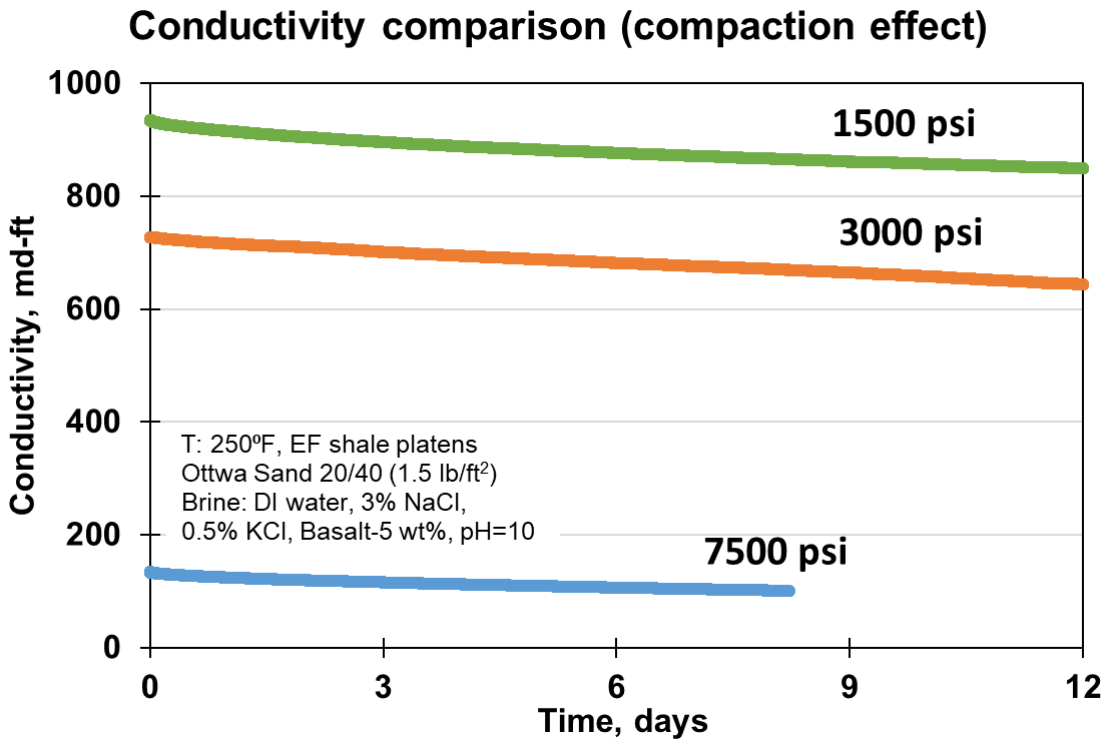

Figure 47: Fracture conductivity at three different axial stress conditions: 1500 (green), 3000 (orange) and 7500 (blue) psi. The conductivity is calculated using the proppant pack width reduction over time keeping the permeability value (permeability observed at the start of the flow) constant. Lower conductivity observed at higher stress.

Fig. 48. shows the conductivity comparison of the three experiments where dotted lines indicate the conductivity decline calculated keeping the initial permeability value constant and considering only fracture width reduction over time. Solid lines indicate the actual decline in conductivity calculated from the data which incorporates the permeability variation along with the proppant pack width reduction over time.

Higher initial conductivities are observed at stress condition of 1500 psi and 3000 psi. However, initial conductivity at 7500 psi stress is observed to be significantly lower compared to the other two stress levels. Comparing the dotted lines with the solid lines for each stress condition, we

observe that conductivity declines at a higher rate when both permeability as well as fracture width reduction is taken into consideration (solid lines).

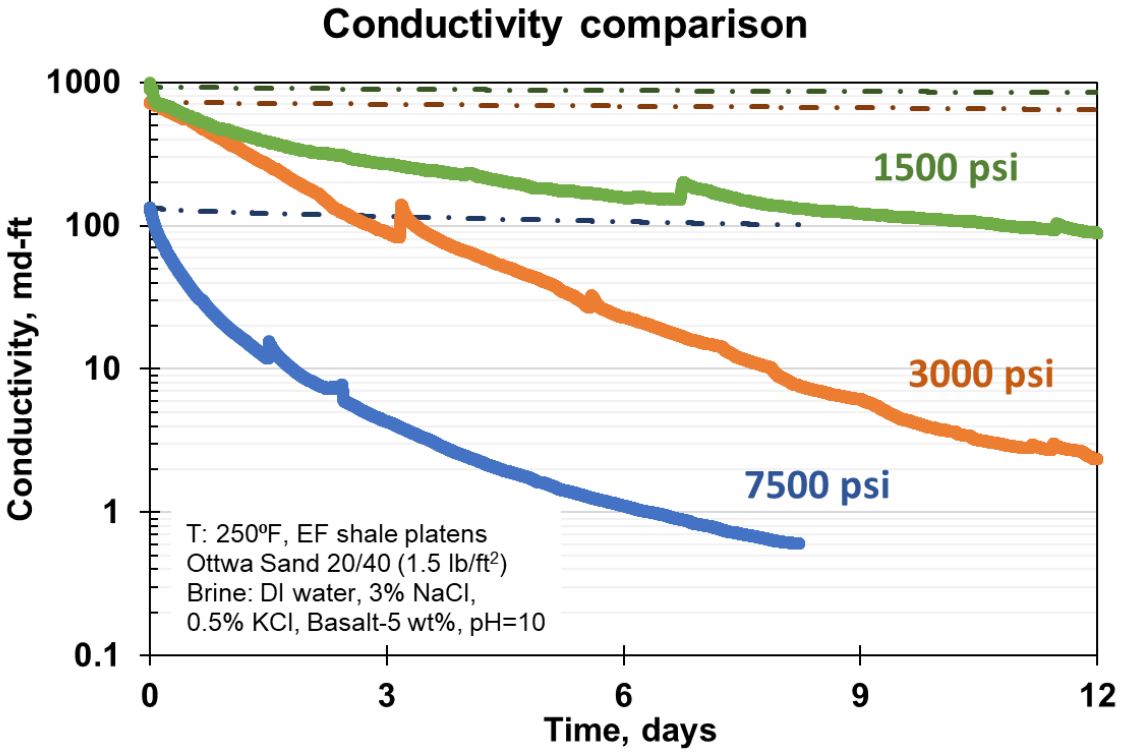

Figure 48: Comparison of fracture conductivities of three experiments conducted at three stress condition: 1500 (green), 3000 (orange) and 7500 (blue) psi keeping the other experimental conditions same. Dotted lines indicate the conductivity decline only due to proppant width reduction (keeping the initial permeability constant) and solid lines indicates the conductivity decline calculated considering proppant pack width reduction as well as permeability with time. Higher decline in conductivity observed at higher stress of 7500 psi compared to lower stress condition of 1500 and 3000 psi.

The reduction of proppant pack width over time is shown in the **Fig. 49**. Just after the loading to stresses of 1500, 3000 and 7500 psi, compaction of 11%, 14% and 30% are observed, respectively. The initial high compaction explains the high initial decline in fracture conductivity observed in the **Fig. 48**. Compaction up to 50% was observed at stress of 7500 psi over the flow period of 10 days compared to 23% and 18% at stress of 3000 and 1500 psi, respectively.

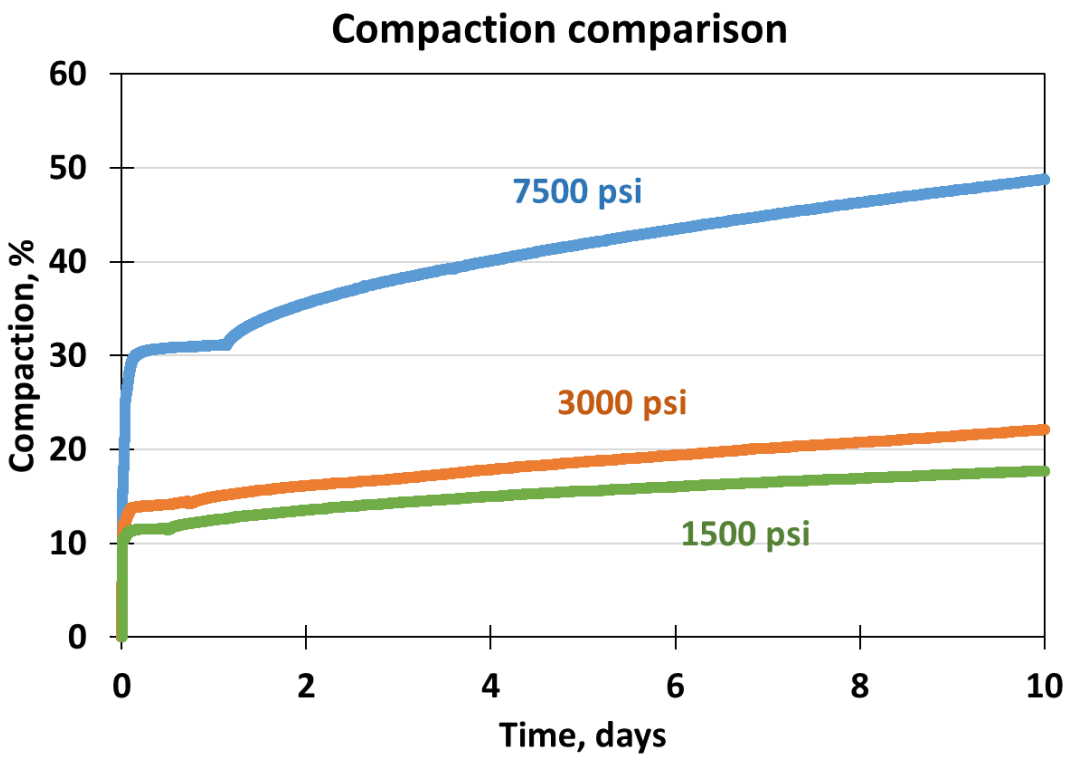

Figure 49: Compaction of proppant pack over time for the three experiments conducted at a stress of 1500, 3000 and 7500 psi. Compaction due to initial loading of the cell shows highest compaction at 7500 psi. Overall rate of compaction increases with increase in stress.

The images of proppants and shale platens after the completion of the experiments are shown in the **Fig. 50**. At 1500 psi, no instance of any proppant crushing can be seen. At 3000 psi, crushing to some extent across the surface could be seen. However, at 7500 extensive crushing of the proppant can be seen (**Fig. 50c**).

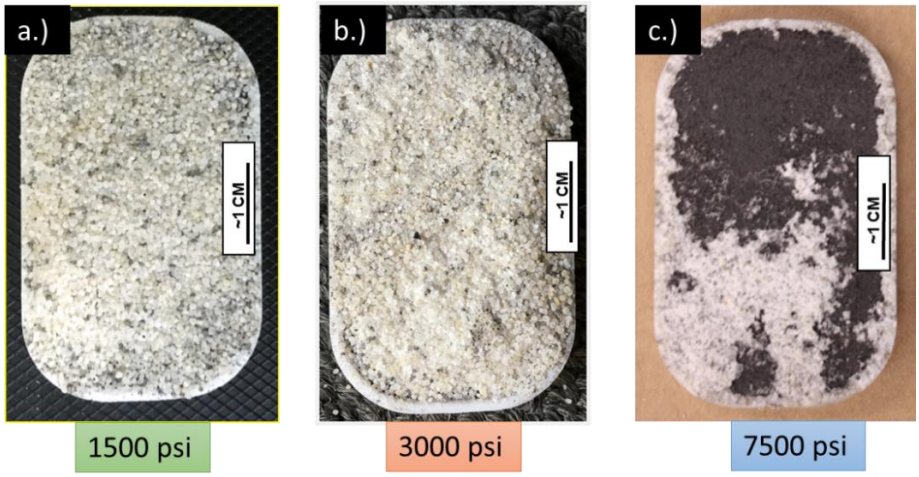

Figure 50: Images of Eagle Ford shale platens and proppant after the experiment at 1500 psi (a), 3000 psi (b) and 7500 psi (c). With increasing stress, increasing crushed particles observed.

The shale platen surfaces were also examined with profilometer. At lower stress of 1500 psi, very few instances of embedment were observed. It should be noted that maximum depth of such embedment is also limited up to 60 µm. At 3000 psi, we started to see some more instances of proppant grain embedment. The maximum depth of embedment observed to be greater (~150 µm) at a stress of 3000 psi compared to 1500 psi. However, at stress of 7500, due to extensive crushing of proppant grains and shale surface extrusion, widespread disruption of the shale surface is observed as can be seen from the **Fig. 51c**.

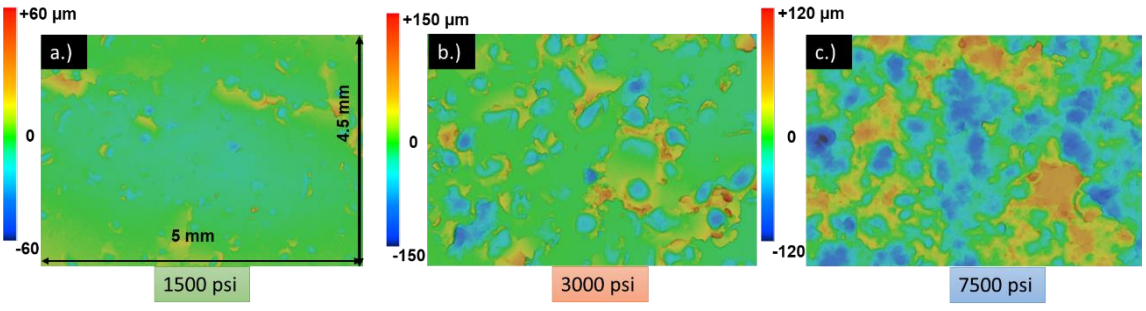

Figure 51: Surface profilometer scans of the Eagle Ford shale platens at three different stress conditions. At lower stress of 1500 psi, few embedments were observed (a). At stress of 3000

psi, relatively higher extrusion and proppant embedment were observed. However, at 7500 psi, widely disrupted shale surface is observed attributed due to highly crushed proppant grains.

Brine samples at the outlet were collected periodically and the ionic concentrations were measured. The silica content of the exit brine for all three experiments measured over the test duration is shown in the **Fig. 52**.

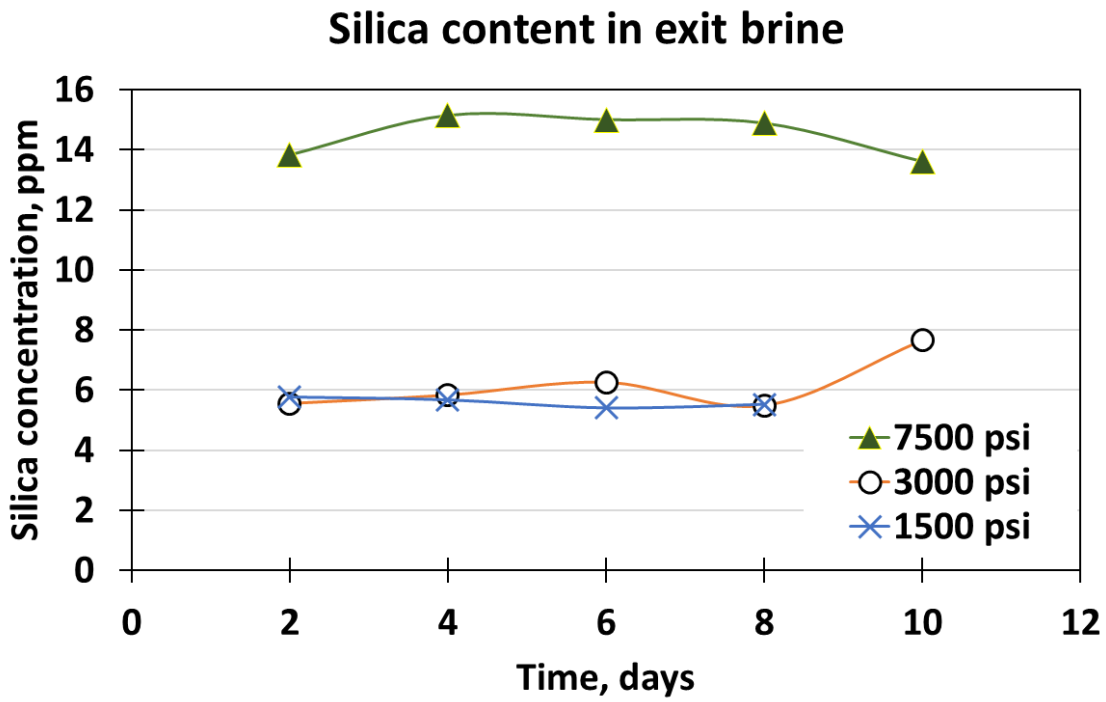

Figure 52: Silica content comparison of the outlet brine for all three load experiments conducted with 20/40 Ottawa sand (concentration: 1.5 lb/ft^2) placed between Eagle Ford shale platens. Due to extensive proppant crushing at high stress of 7500 psi, higher silica concentration observed at outlet brine compared to silica content at lower stress of 1500 and 3000 psi.

At 7500 psi the outlet brine shows significantly high silica content compared to 1500 and 3000 psi. The higher silica content is due to the high crushing and dissolution of proppant (due to greater exposed surface) at high stress under alkaline environment (~10 pH).

SEM image analysis of proppant pack after the completion of each experiment is shown in the **Fig. 53**. At lower stress, negligible or no fracturing of proppant grains is observed (**Fig. 53a**). At 3000 psi, fracturing of some proppant grains starts to appear (**Fig. 53b**) and at stress of 7500 psi, extensively fractured proppant grains are observed (**Fig. 53c**). The fractured grains with increasing stress condition create fines.

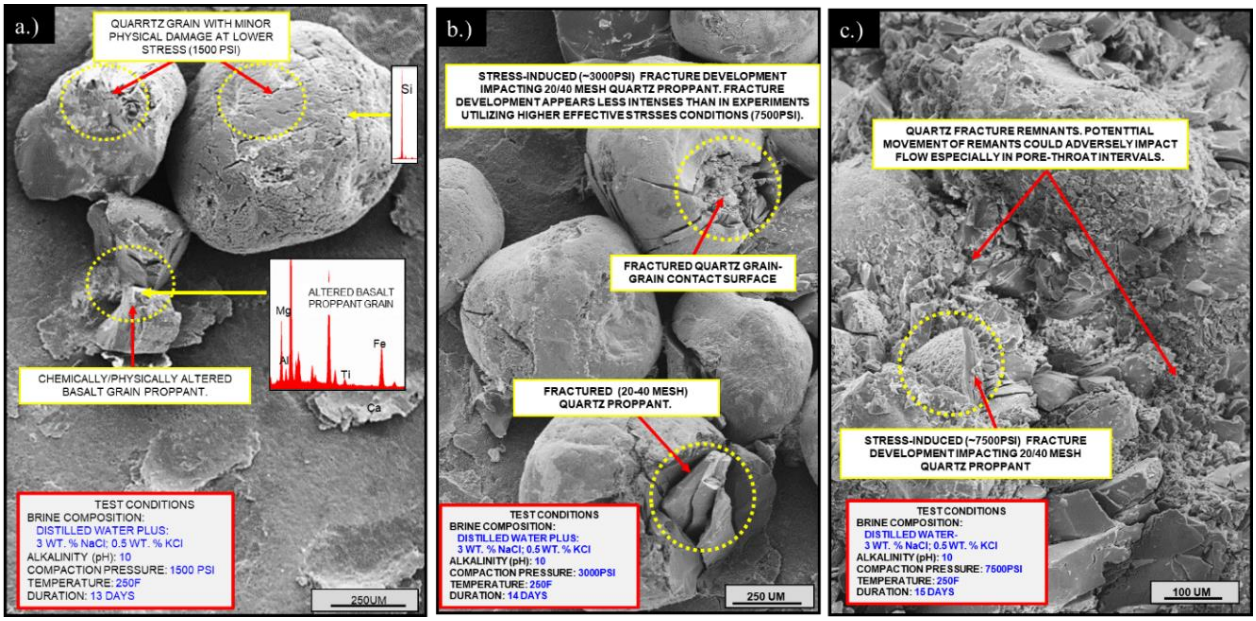

Figure 53: SEM images of the experiment conducted at (a.) 1500 psi, (b.) 3000 psi and (c.) 7500 psi stress using 20/40 Ottawa sand (concentration: 1.5 lb/ft^2) placed between the Eagle Ford shale platens. Increasing intensity of proppant fracturing observed with increased stress condition.

3.6.Effect of rock mineralogy on fracture conductivity.

Experiments have been extended to study the effect of rock mineralogy on fracture conductivity. The effect of mineralogy by using shale platens machined form two different formations Vaca Muerta and Eagle Ford were reported by Mittal (2017). For this study, Meramec formation platens have been added and the conductivity is compared to the previous study.

The FTIR results of the three formations is shown in the **Fig. 54**. The Meramec sample shows the presence of lowest amount of clay content (~11%) compared to the Vaca Muerta and Eagle Ford samples and have highest amount of quartz content. The Vaca Muerta sample has higher clay content and lower quartz content compared to the Meramec and Eagle Ford have the highest clay content (58%).

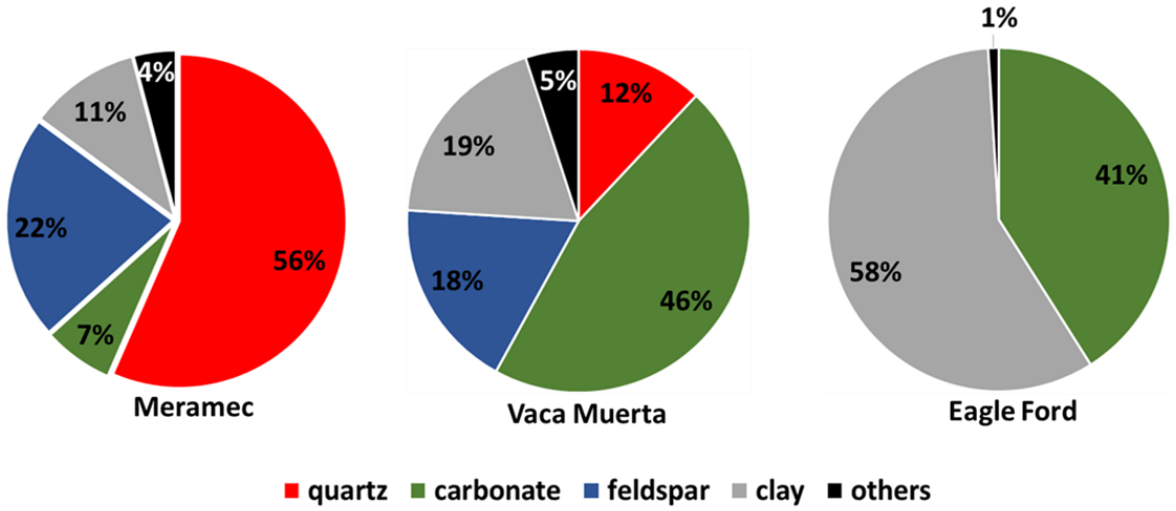

Figure 54: FTIR mineralogy of Meramec, Vaca Muerta and Eagle Ford samples. The Meramec sample has the lowest clay content (11%) and highest quartz content (56%) compared to the other two samples. However, Vaca Muerta has relatively higher clay content and lower quartz content and Eagle Ford sample shows the has the highest clay content (58%) and no quartz content.

The fracture conductivity comparison of Meramec formation with the Vaca Muerta and Eagle Ford formations is shown in the **Fig. 55**. The conductivity here is calculated only using the LVDT data keeping the permeability value (initial permeability observed at the start of the flow) constant.

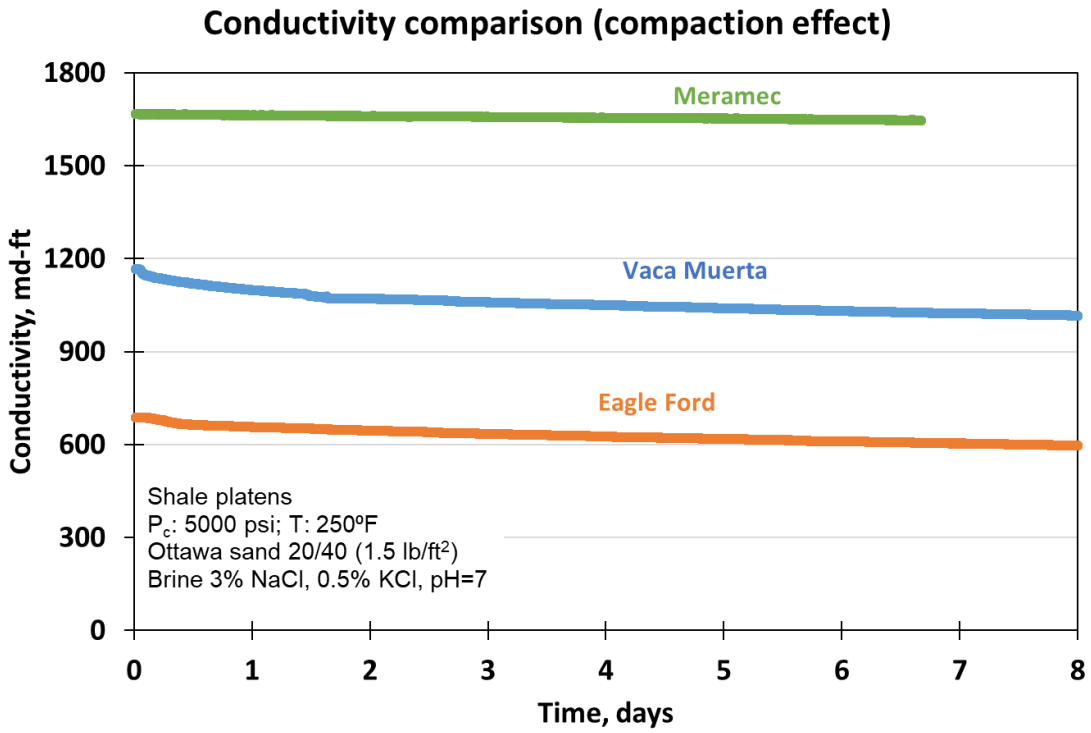

Figure 55: Fracture conductivity comparison of the experiments conducted using the three different rock mineralogy under similar test conditions of 5000 psi and 250 ºF. The conductivity is calculated using the LVDT data only to determine the contribution of fracture width reduction with time keeping the initial permeability value constant.

Fig. 56 shows the fracture conductivity comparison where the dotted lines represents the conductivity decline calculated using only proppant pack width reduction over time keeping the permeability value constant. The constant permeability value is the initial permeability observed at the start of the flow. Solid lines represent the conductivity decline calculated considering the change in permeability as well as fracture width over time.

Dotted lines show lower decline in fracture conductivity over time with each of the formations. However, comparing solid lines with dotted lines, we observe higher decline rates in each case. Meramec shows higher initially conductivity and even after the flow period of 6 days. Vaca Muerta shows relatively sharper decline in conductivity compared to Meramec, and the Eagle Ford shows highest decline of all three formations as shown by solid lines in each case.

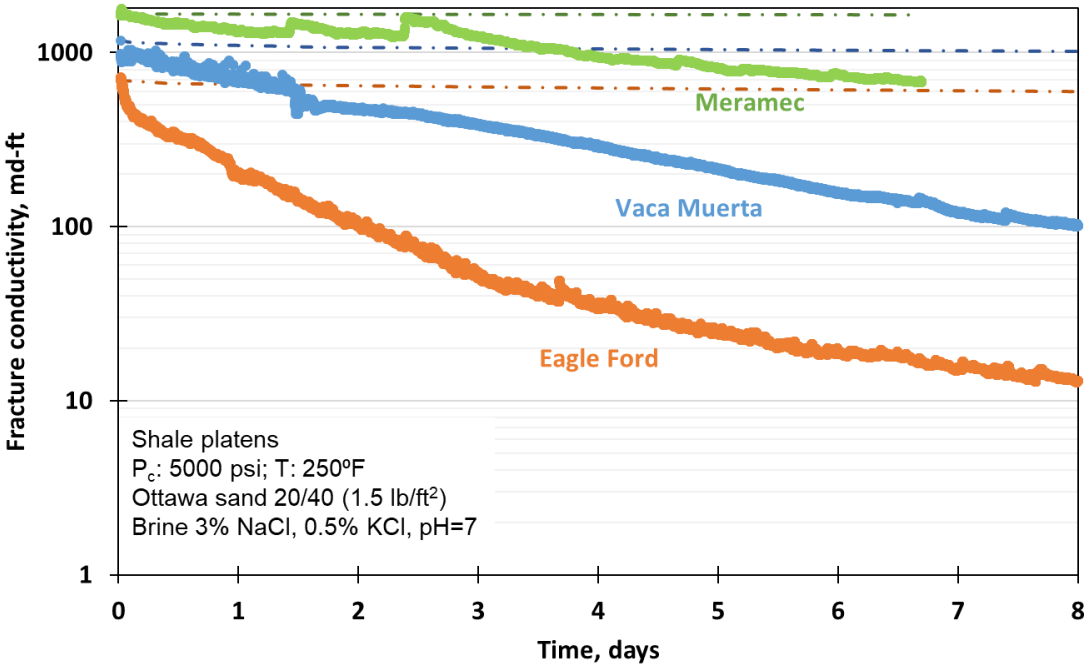

Figure 56: Fracture conductivity comparison for the three formations under similar test conditions. 20/40 Ottawa sand (Concentration: 1.5 lb/ft^2) was subjected to an axial loading of 5000 psi and 250 ºF. Dotted lines indicate the conductivity decline due only to proppant width reduction (keeping the initial permeability constant) and solid lines indicates the conductivity decline calculated considering proppant pack width reduction as well as permeability with time. Meramec fracture conductivity is greater than Vaca Muerta or Eagle Ford.

The propped fracture conductivity in all the three cases are of the order of millidarcies even after the flow period of 8 days (**Fig. 56**). However, extrapolating the above result, sharp decline in conductivity is observed in all the three cases (**Fig. 57**).

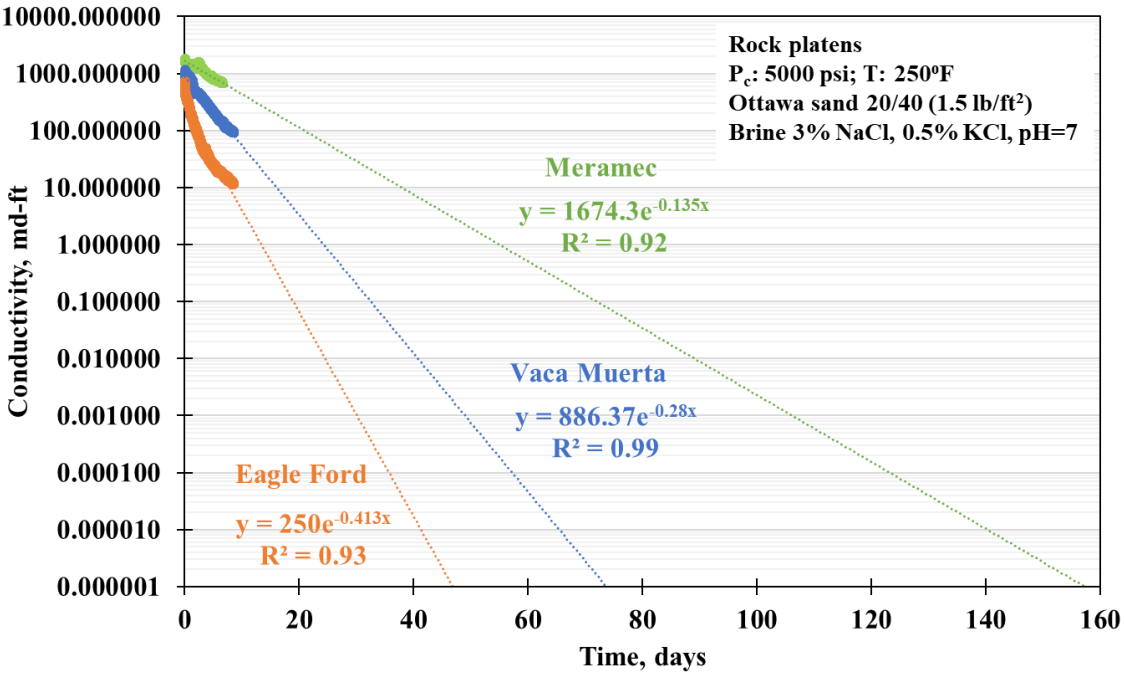

Figure 57: Extrapolation of the conductivity of all the three experiments conducted with 20/40 Ottawa sand placed between Eagle Ford, Vaca Muerta and Meramec rock platens. Conductivity declines rapidly over time.

Assuming the average matrix permeability of the three formation as 50 nd and fracture half-length of 100 ft, the dimensionless fracture conductivity (F_{CD}) has been calculated. **Fig. 58** shows the dimensionless fracture conductivity for all the three formations over time. From the plot, we see that the dimensionless fracture conductivity (F_{CD}) starts at a very high value but declines rapidly over time. The dimensionless fracture conductivity (F_{CD}) becomes less than 20 after 18 days in Eagle Ford, 35 days in Vaca Muerta and 75 days in Meramec.

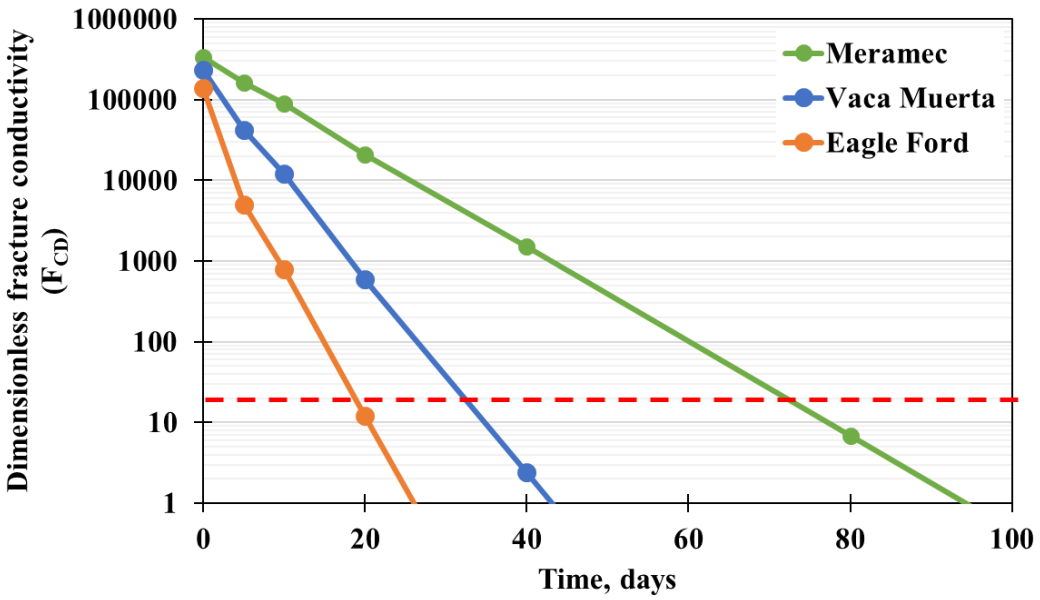

Figure 58: The dimensionless fracture conductivity (F_{CD}) over time for all the three formations calculated assuming the average matrix permeability of (50 nd) and fracture half-length (100 ft). The dimensionless fracture conductivity (F_{CD}) becomes less than 20 after 18, 35 and 75 days for Eagle Ford, Vaca Muerta and Meramec formations respectively.

Proppant pack compaction over the different phases of the experiments have been plotted in the **Fig. 59**. In the plot, step 1 indicates the initial condition when the cell was at zero load. Moving from step 1 to step 2, cell was loaded to axial stress of 5000 psi at a loading rate of 100 psi/ min and temperature was raised to 250 ^{o}F. At the end of step 2, flow was started and maintained at a rate of 3 ml/min. Step 3 indicates the condition of 5000 psi and 250 ^{o}F and flow of 6 days. We observe up to 60% compaction in Eagle Ford compared to 30% compaction in the Meramec. Higher compaction in Eagle Ford is consistent with the high reduction in fracture conductivity compared to Meramec.

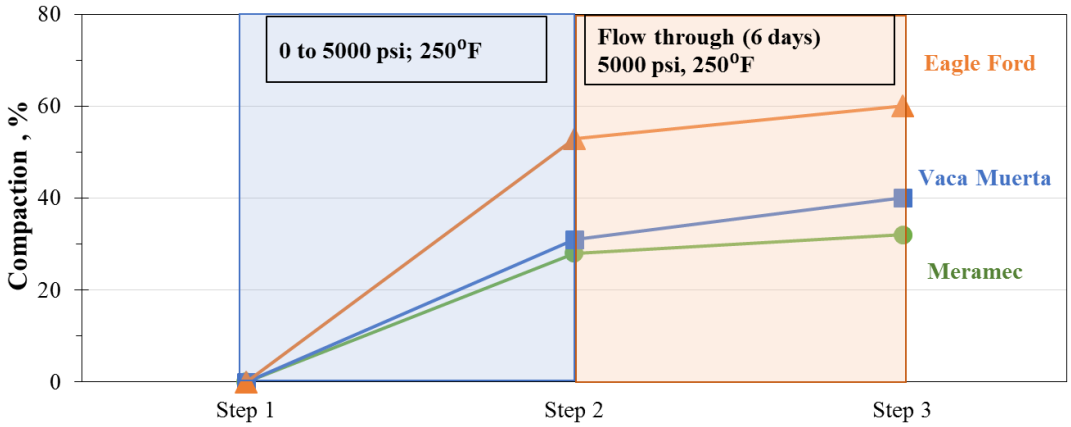

Figure 59: The compaction for the Meramec, Vaca Muerta and Eagle Ford formations plotted versus time. Over the flow period of 6 days, Meramec shows lowest compaction (~30%) compared to Eagle Ford (~60%).

After the completion of the experiment, the Meramec shale surfaces were scanned with the profilometer. Meramec samples shows very few instances of proppant embedment. Moreover, the embedment depth of the proppant was limited to the maximum of 70 µm. The comparison of profilometer scans for all three formations is shown in the **Fig. 60**. Compared to Meramec, Vaca Muerta shows higher instance of embedment along with deeper depth of embedment and extrusion (~140 µm) and Eagle Ford shows the greatest embedment depth (~350 µm).

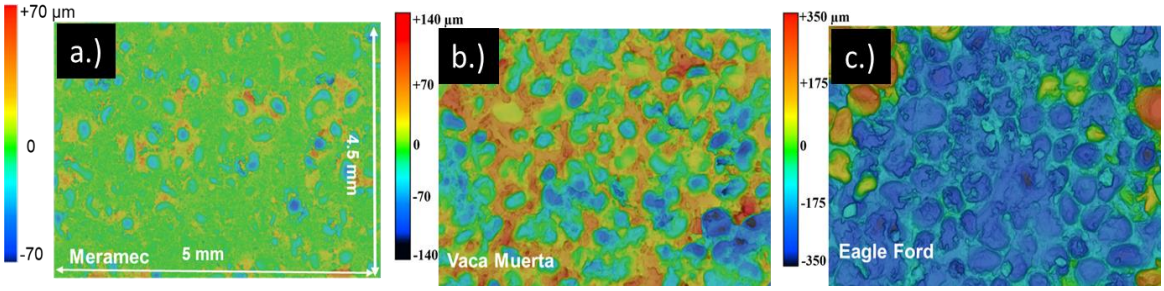

Figure 60: Profilometer scan comparison of all three formations: Meramec, Vaca Muerta and Eagle Ford. Meramec shows shallower embedment depth (~70 µm), as compared to Vaca Muerta (~140 µm) and Eagle Ford shows the deepest embedment of ~350 µm (after Mittal et al. 2018).

3.7. Evaluation of diagenetic growth

Presence of volcanics in major shale plays like Eagle Ford and Vaca Muerta have been reported in literature (Calvin et al. 2015; Lejay at al. 2017). To simulate the similar these conditions, volcanics such as obsidian and basalt have been added to our experiments. XRF results shows that the obsidian is rich in silica compared to basalt while basalt has higher calcium and magnesium ion concentrations.

Proppant diagenesis has been evaluated by conducted experiment using 20/40 mesh Ottawa sand placed between Eagle Ford shale platens. Obsidian was crushed and sieved to 20/40 mesh size and mixed by 5 wt.% with the 20/40 proppant. The results from the current experiments have been compared with the previous work done by Mittal et al. (2018) which was done on Eagle Ford shale platens using 20/40 mesh proppant mixed with 5 wt.% basalt. The confining pressure was 5000 psi, temperature was 250 ^{o}F and the brine was 5% NaCl, 0.5% KCl having the pH~10. The flow rate was maintained at 3 ml/min.

SEM analysis of the proppant pack after the experiment with obsidian shows extensive crushing of the proppant (**Fig. 61a**). The presence of alkaline environment also leads to the chemical degradation of the proppant and obsidian making obsidian surface porous (**Fig. 61b**). These chemical alterations lead to the chemically precipitated platelets on the surface. We believe that obsidian supplied the necessary ingredients for the chemical growth of these platelets ultimately leading to the secondary clay growth on the surface (**Fig. 62**).

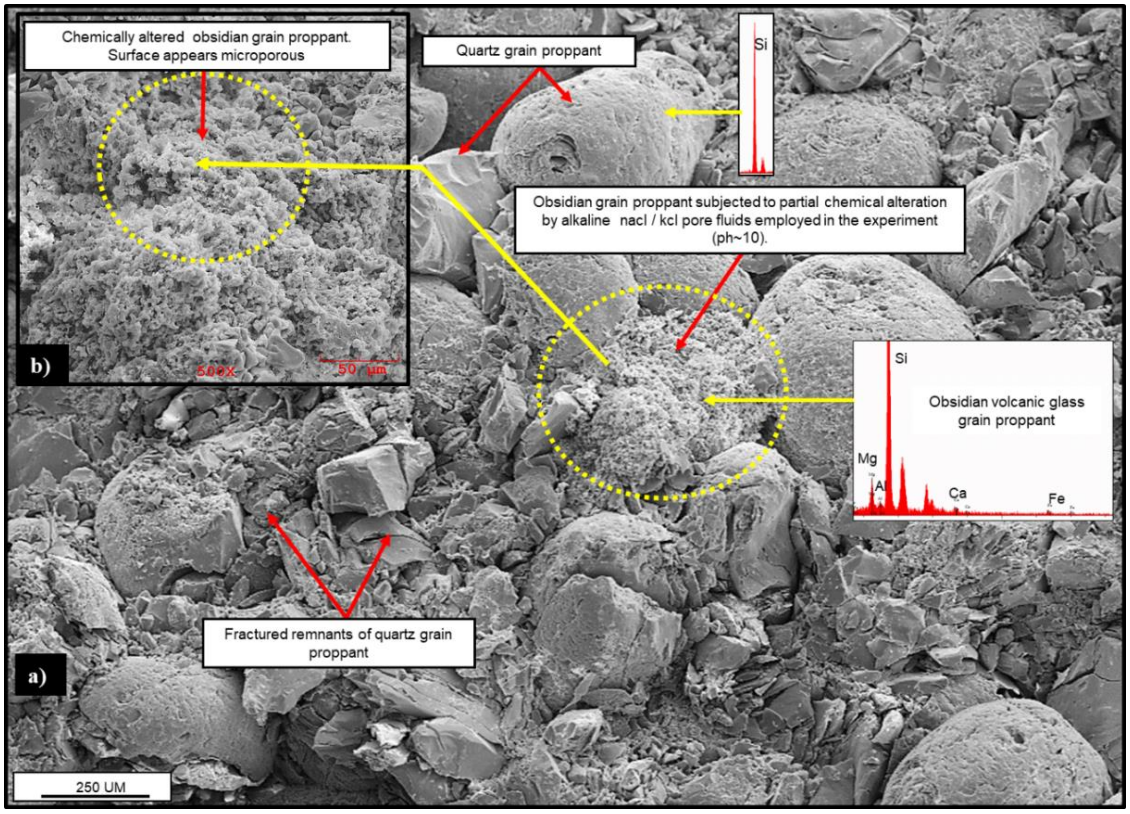

Figure 61: a) SEM images showing extensive fracturing of 20/40 mesh Ottawa sand (concentration: 1.5 lb/ft^2) placed between Eagle Ford shale platens under a stress of 5000 psi and 250 ^{o}F and alkaline environment with high pH~ 10. The experiment was conducted with 20/40 sand and obsidian for a duration of 40 days. Partial chemical alteration of obsidian grains in the alkaline environment lead to microporous obsidian surface (b).

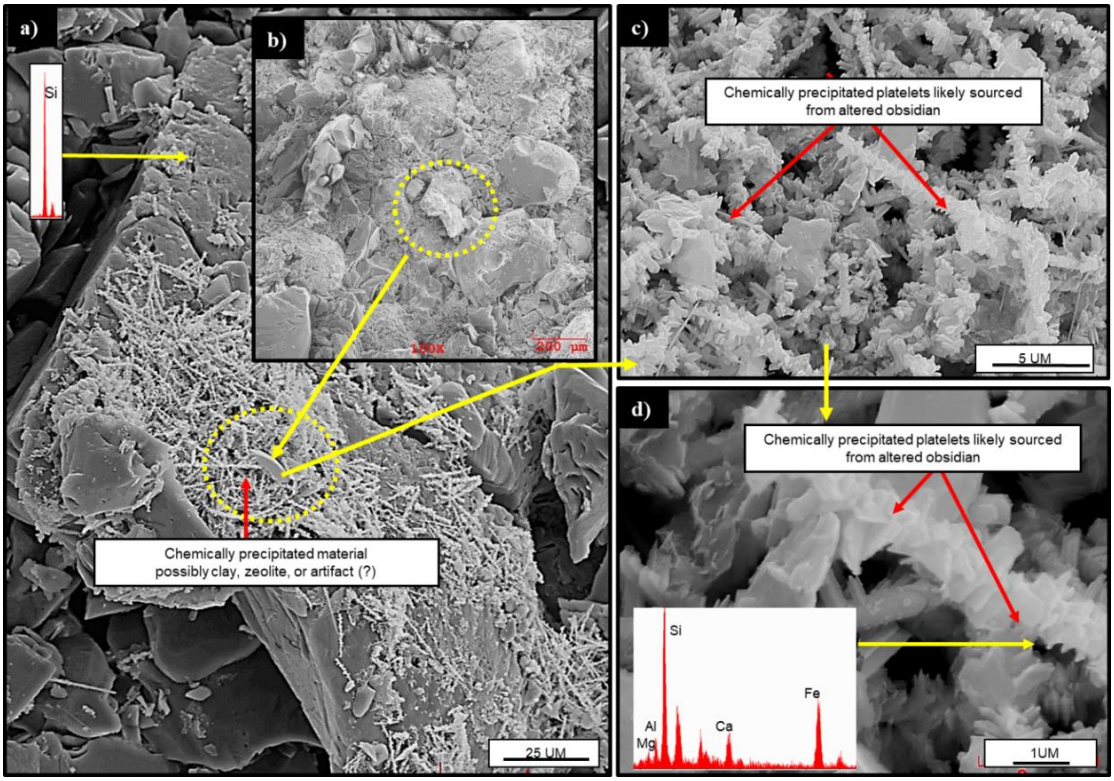

Figure 62: (a-b) SEM images showing chemically precipitated secondary clay minerals over the surface. Flow of high pH (~10) brine during the experiment (duration: 40 days) has chemically altered the obsidian grain. Note the precipitated platelets on the surface. We believed that the observed precipitation is mainly due to the chemical alteration of obsidian grains (c-d).

Fig. 63 shows the SEM images of the experiment done with 20/40 sand placed between Eagle Ford shale platens in presence of basalt over the flow period of 18 days. **Fig. 63a** shows a quartz grain with incipient clay coating. EDX confirms the clay coating shown in **Fig. 63b**. Extensive fractured proppant grains can be seen coated with microporous smectite clays in the **Fig. 63(c-d)**. Effect of high alkaline environment has further enhanced the chemical alteration of the proppant basalt grains (**Fig. 64**). The mechanical degradation and fracturing of the proppant grains exposes fresh silica surfaces and the chemically altered basalt grains further leads to the development of tubular

diagenetic zeolite-like crystals as seen in **Fig. 64a** and the growth is further confirmed using EDX in **Fig. 64(b-c).**

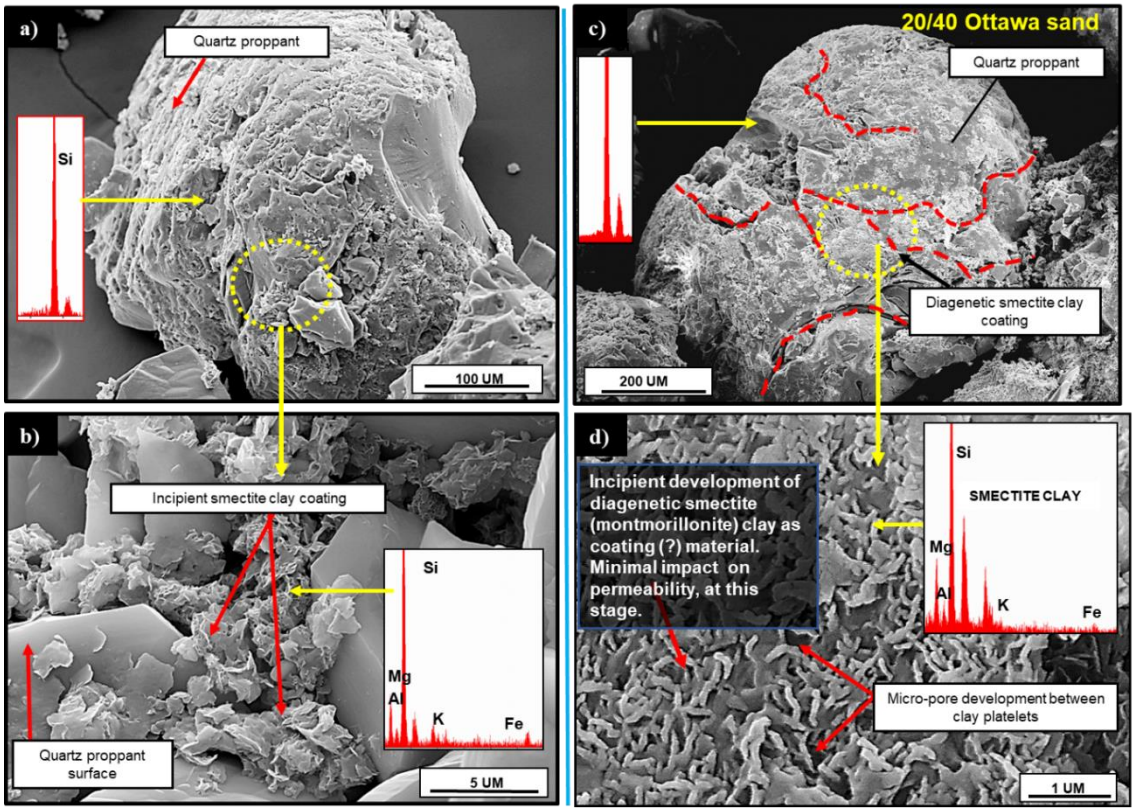

Figure 63: SEM images of 20/40 Ottawa sand (concentration: 1.5 lb/ft^2) tested at high closure stress of 5000 psi and 250 ºF placed between Eagle Ford shale platens under the alkaline environment (pH~10.5) in presence of basalt. a) Clay coating observed on the surface b) Incipient smectite growth on the proppant surface confirmed by EDX c) Extensive fracture development on the proppant grain exposing fresh silica surface to the fluid system d) Observed growth of diagenetic smectite along with associated pore development between clay platelets across the proppant surface (Mittal 2018).

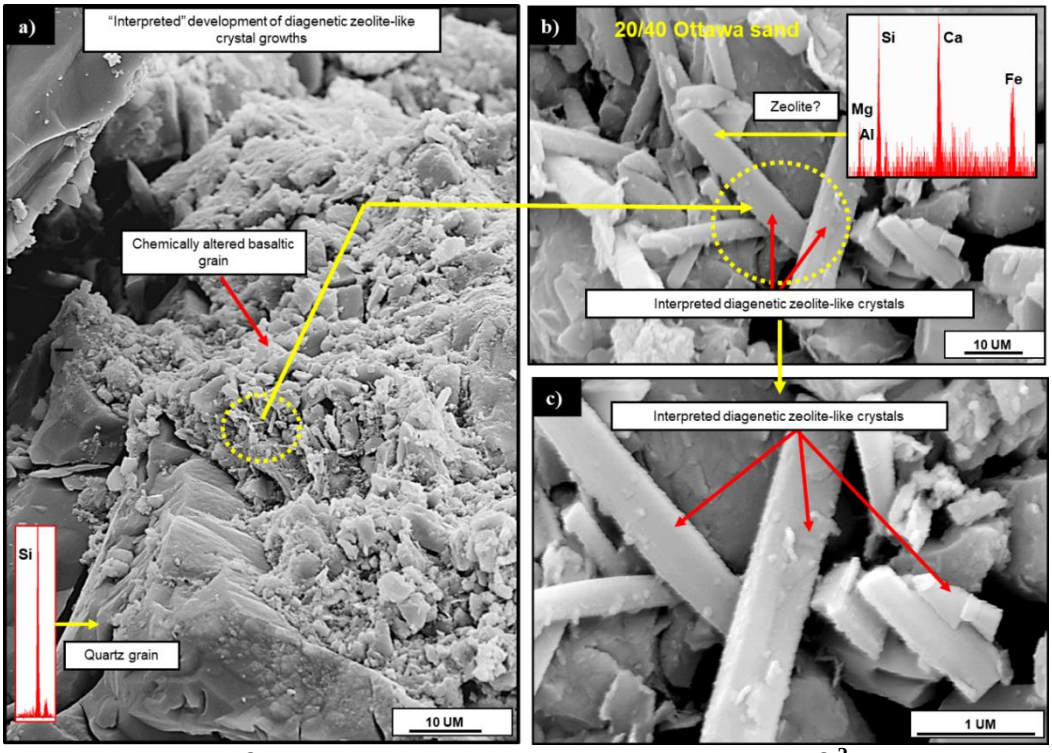

Figure 64: SEM images of 20/40 Ottawa sand (concentration: 1.5 lb/ft^2) tested at high closure stress of 5000 psi and 250 ºF placed between Eagle Ford shale platens under the alkaline environment (pH~10.5) in presence of basalt. a) Chemically altered basalt grain. b) and c) At higher magnification, tubular structures are observed. EDX confirms the growth of diagenetic zeolite-like crystals at the surface (Mittal 2018).

Comparing the results from both the tests, we observe that minor development of diagenetic growth in the form of platelets in presence of obsidian after the flow period of 40 days. On the other hand, in presence of basalt significant diagenetic growth is observed over the flow period of 18 days as shown by the SEM images (**Fig. 61 - Fig. 64**). The extent of the diagenetic growth is at incipient stage during test periods of only 18 and 40 days. However, in longer run, these growths will intensify and may plug the propped fracture leading to decline in permeability.

3.8.Discussion of results

The productivity of hydraulically fractured wells depends upon dimensionless fracture conductivity (F_{CD}) which is the ratio of fracture conductivity to the formation conductivity (McGuirer and Sikora 1960). Elsarawy et al. (2018) reviewed the importance of propped fracture conductivity in shale reservoirs and showed the importance of fracture conductivity over the short and long term well productivity through the field data observations reported by several authors (Mayerfoyer et al. 2006; Rankin et al. 2010; Vincent et al. 2011; Penny et al. 2012). Greater propped fracture conductivity is critical for well productivity and needs to be studied in detail as fracturing costs represents up to 60% of total well cost (Pope et al. 2012).

3.8.1. Effect of concentration

Proppant concentration plays an important role in the propped fracture conductivity. Higher proppant concentration in the fracture leads to lower proppant embedment and crushing (Coulter et al. 1972; Holditch et al. 1973, Palisch et al. 2009). Jaripatke et al. (2018) shows that increasing proppant concentration from 1400 lb/ft to 3000 lb/ft leads to increased production. However, the mechanisms behind the good performance with increased concentration are not fully understood.

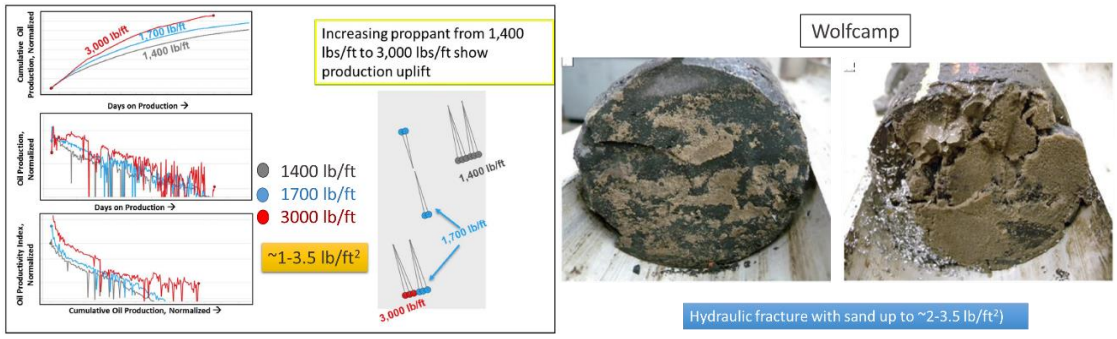

Figure 65: Field observations by Jaripatke et al. 2018 showing increase in production with increased proppant per unit lateral foot (left), drill back core showing 0.5-1 cm thick proppant in between fractures (right) (Eliot and Gale. 2018)

In the **Fig. 65** cumulative production plot shows higher production with higher proppant concentration. The concentration indicates the amount of proppant pumped per stage. Assuming different frac geometries, these concentrations (1400-3000 lb/ft) corresponds to the range of 1-3.5 lb/ft^2 proppant concentration in the fractures. Elliot and Gale (2018) reported the drill back studies done by HFTS where the cores taken from Wolfcamp near hydraulically fractured wells showed proppant thickness varying form 0.5 - 1 cm which corresponds to ~2-3.5 lb/ft^2 proppant concentration.

The experiments in this study shows up to 98% decline in proppant conductivity with unit drop in porosity with lower concentration of 2 lb/ft^2. However, with increased concentration of 4 lb/ft^2, conductivity decline up to 60% was observed with unit porosity reduction. Corroborating the results with Taneja (2016), it was found that most of the crushing happens near the interface of the proppant and rock/metal. There remains an uncrushed portion in the center which increases with increased concentration leading to lower decline in conductivity. Yang et al. 2019, observed higher production by some operators even with low strength "in-basin" sands compared with high strength white sands. Deeper analysis of completion and frac data revealed higher volume of

proppant being correlated to higher production even with low strength proppant. This could have a huge implication in completion designs where operators can save money by using relatively lower strength proppants with increased concentration to obtain similar well production.

3.8.2. Use of Ceramic proppant

Ceramic proppants are high strength synthetics developed primarily to provide high resistance to crush. They are believed to undergo less fracturing and develop fewer fines. Palisch et al. (2012) reported 34% increase in cumulative oil production after 22 months when light weight ceramic proppant (LWC) was use instead of the sand. Rankin et al. (2010) reported, through the field data analysis, 37% increase in initial production rate when ceramic proppant replaced sand. Vincent (2010) analyzed the production data over the period of 12 months of 750 horizontal wells in the Eagle Ford and showed 33% higher cumulative production with high quality ceramic proppant compared to sand or resin coated sand. However, the author also concluded significant decline in conductivity over time. In this study, we also found higher initial conductivity with ceramic proppant and significant decline in conductivity of ceramic proppant with time. After the flow period of 15 days, permeability of ceramic proppant drops even lower than Ottawa sand over the same period. Moreover, significant diagenetic growth was observed with ceramic proppant. Similar observations have been made by Ghosh et al. (2014) with ceramic proppant and Barnett shale plugs. These secondary growth minerals can reduce the conductivity over time and lead to lower production.

3.8.3. Stress dependent conductivity

Proppants are pumped during the hydraulic fracturing to keep the fractures open. At the initial stage, the fracture experiences the net effective stress which increases continuously over time due to reduction in pore pressure (Terzaghi 1925; Biot 1941). Stress dependent conductivity study between sandstones has been reported by Penny (1975). Alramahi and Sundberg (2012) designed a lab test to measure stress dependent conductivity and its effect on proppant embedment in shales of various mineralogy. However, none of the conductivity test measures the time dependence at different stresses and takes the conductivity value over the 50 hours as per API standards. In this study, stress dependent conductivity has been measured over time up to 14 days (336 hrs). A sharp decline in initial conductivity was observed which increases with increasing closure stress. However, the conductivity continues to decline over the flow period of 14 days. Often, the time dependence of fracture conductivity is estimated considering fracture width reduction over time keeping the permeability value constant. Comparing the actual permeability where both permeability as well as fracture width decline was considered and compared to the situation where only fracture width reduction is taken into consideration, we found significant conductivity decline when both permeability as well as fracture width reduction were considered. This suggests using only fracture width reduction leads to overestimation the fracture conductivity.

3.8.4. Particle size effects

Use of fine mesh sand has been increased to reduce the completion costs. Finer mesh sand (60/100) is believed to reduce leak-offs during hydraulic fracturing stimulation (Thompson 1977). However, in this study, we observed higher decline in fracture conductivity with finer mesh sand compared to coarser mesh sand. Penny (2012) studied change in well productivity due to change

in fracture conductivity using lab experiments and field data, they observed relative permeability of gas can vary between 0.05 to 0.8 depending upon the fracture conductivity. Field results showed the 7-fold increase in initial 30-day gas permeability when 20/40 mesh sand was used instead of 100 mesh proppant. The results were attributed to improved gas relative permeability due to use of 20/40 mesh sand. Although the finer mesh sand can help reduce the initial completion costs, in long run due to lower conductivity, it will require early remediation which could add to the cost.

Chapter 4: Conclusions and recommendations

1. **Effect of proppant concentration:** Permeability is observed to be strongly dependent on proppant concentration. Higher proppant concentration leads to smaller decline in permeability. Higher volume of fines observed with a lower concentration (2 lb/ft^2) compared to a higher proppant concentration (4 lb/ft^2) indicating higher crushing with lower proppant concentration.
2. **Effect of proppant type:** Higher initial permeability is observed with ceramic proppant compared to Ottawa sand placed between Eagle Ford shale platens. However, permeability with ceramic proppant declines at a faster rate compared to the Ottawa sand. Over the flow period of 14 days, permeability of ceramic proppant becomes lower than that of Ottawa sand. Moreover, significant diagenetic growth was observed with ceramic proppant and no diagenetic growth was observed with Ottawa sand. These diagenetic growths in ceramics will increase over time leading to a greater decline in permeability.
3. **Effect of proppant size:** Dry crush tests with 20/40 sand and 60/100 mesh sand placed between metal platens at three different compaction pressures show compaction increases with increasing pressure. However, at every compaction pressure greater compaction is observed with finer mesh (60/100) sand compared to coarser sand (20/40). Flow through experiments with different particle size placed between platens machined from Meramec formation shows similar results where higher conductivity observed with 20/40 sand. Conductivity starts to decrease with finer mesh sand 40/70 and lowest conductivity is observed with 60/100 mesh sand.

4. **Effect of overburden stress:** Experiments at different overburden stress conditions show that higher overburden stress leads to greater conductivity decline. At 7500 psi, initial conductivity was lower by an order of magnitude compared to the stress of 1500 psi. Fracture width reduction increased over time with increased stress. Over the flow period of 10 days, up to 50% fracture width reduction was observed. Lower compaction up to 18% and 22% was observed with experiment at lower stress of 1500 and 3000 psi, respectively. Significant crushing observed with increased stress as verified by SEM images. Exit brine composition shows higher silica dissolution in experiment with 7500 psi relative to lower stress condition of 1500 and 3000 psi.
5. **Effect of rock mineralogy:** Propped fracture conductivity measured under similar experimental conditions shows a dependency on rock mineralogy. Rock having lower clay and higher quartz content showed higher conductivity. The conductivity declines with increasing clay content. Almost negligible instance of proppant embedment observed with lower clay and high quartz content whereas high embedment with deeper depths observed with higher clay and lower quartz content.

The propped fracture conductivity is a complex function of several factors. Some of the important factors such as proppant concentration, proppant size, proppant types, overburden stress, rock mineralogy and diagenesis have been studied in detail in this study. Effect of individual factors and specific observations have been described above. Dimensionless fracture conductivity (F_{CD}) is one of the key design parameters used in numerical simulation for well stimulation. Usually, values greater than 50 is considered to be very good. In this study, we also calculated the dimensionless fracture conductivity (F_{CD}) over time for the three formations assuming the matrix

permeability (50 nd) and fracture half length (100 ft). We observed that dimensionless fracture conductivity (F_{CD}) declines rapidly over time and becomes less than 20 in 18 days for Eagle Ford, 35 days for Vaca Muerta and 75 days for Meramec.

Recommendations:

- The experiments should also be conducted with in-basin sands to evaluate their performance.
- Brine should be saturated with silica as well as volcanic ashes to simulate the *in-situ* reservoir fluid compositions.
- Sensitivities to flow rate needs to be evaluated
- Experiments should incorporate different fluid additives like friction reducer, cross-linker etc., along with NaCl and KCl in brine preparation.

References

- Beckman Coulter User Manual. 2011. Instructions for use: LS 13 320 Laser Diffraction Particle Size Analyzer.
- Biot, M.A. 1941. General theory of three-dimensional consolidation. *J app phy*, *12*(2), pp.155-164.
- Barree, R.D., Duenckel, R.J. and Hlidek, B.T. 2019. Proppant Sieve Distribution-What Really Matters? Presented in Hydraulic Fracturing Technology Conference and Exhibition, Woodlands, Texas, USA, 5-7 February. SPE-194382-MS. https://doi.org/10.2118/194382-ms
- Calvin, C., Diaz, H.G., Mosse, L., Miller, C. and Fisher, K. 2015 . Evaluating the diagenetic alteration and structural integrity of volcanic ash beds within the eagle ford shale. Presented in Unconventional Resources Conference, Calgary, Alberta, Canada, 20-22 October. SPE-175961-MS. https://doi.org/10.2118/175961-ms
- Cooke, C.E. 1973. Conductivity of Fracture Proppants in Multiple Layers. JPT, J Pet Technol 25:1101–1107. https://doi.org/10.2118/4117-PA
- Cooke, C.E. 1975. Effect of Fracturing Fluids on Fracture Conductivity. JPT, J Pet Technol 27:1273–1282. https://doi.org/10.2118/5114-PA
- Coulter, G.R., Wells, R.D 1971. Advantages of high proppant concentration in fracture stimulation. https://doi.org/10.2118/3298-pa
- Cutler, R.A., Enniss, D.O., Jones, A.H. and Swanson, S.R. 1985. Fracture Conductivity Comparison of Ceramic Proppants. Soc Pet Eng J 25:157–170. https://doi.org/10.2118/11634-PA

- Davies, J.P., y Davies, D.K. 1999. Stress-Dependent Permeability: Characterization and Modeling. Presented in Annual Technical Conference and Exhibition, Houston, Texas, 3–6 October. SPE-56813-MS. https://doi.org/10.2118/56813-MS
- Duenckel, R. J., Conway, M.W., Eldred, B. and Vincent, M.C. 2011. Proppant Diagenesis-Integrated Analyses Provide New Insights into Origin, Occurrence, and Implications for Proppant Performance. Presented in Hydraulic Fracturing Technology Conference and Exhibition, Woodlands, Texas, USA, 24–26 January. SPE-139875-MS. https://doi.org/10.2118/139875-MS
- Duenckel, R., Moore, N., O'Connell, L., Abney, K., Drylie, S. and Chen, F. 2016. The science of proppant conductivity testing-lessons learned and best practices. Presented in Hydraulic Fracturing Technology Conference, Woodlands, Texas, USA, 9-11 February. SPE-179125-MS. https://doi.org/10.2118/179125-ms
- Duenckel, R.J., Barree, R.D., Drylie, S., O'Connell, L.G., Abney, K.L., Conway, M.W., Moore, N. and Chen, F. 2017 Proppants-What 30 years of study has taught us. Presented in Annual Technical Conference and Exhibition, San Antonio, Texas, USA, 9-11 October. SPE-187451-MS. https://doi.org/10.2118/187451-ms
- EIA. 2016. Annual energy outlook 2016. https://www.eia.gov/outlooks/aeo/
- EIA. 2018. Annual energy outlook 2018. https://www.eia.gov/todayinenergy/detail.php?id=34732
- EIA. 2019. Annual energy outlook 2019. https://www.eia.gov/outlooks/aeo/

- Elliott, S.J. and Gale, J.F. 2018. Analysis and distribution of proppant recovered from fracture faces in the HFTS slant core drilled through a stimulated reservoir. Presented in Unconventional Resources Technology Conference, Houston, Texas, USA, 23-25 July. URTEC-2902629-MS. https://doi.org/10.15530/urtec-2018-2902629
- Elsarawy, A.M. and Nasr-El-Din, H.A. 2018a. Propped Fracture Conductivity in Shale Reservoirs: A Review of its Importance and Roles in Fracturing Fluid Engineering. Presented in Kingdom of Saudi Arabia Annual Technical Symposium and Exhibition, Dammam, Saudi Arabia, 23-26 April. SPE-192451-MS. https://doi.org/10.2118/192451-ms
- Elsarawy, A.M. and Nasr-El-Din, H.A. 2018b. An Experimental Investigation of Proppant Diagenesis and Proppant-Formation-Fluid Interactions in Hydraulic Fracturing of Eagle Ford Shale. Presented in Trinidad and Tobago Section Energy Resources Conference, Port of Spain, Trinidad and Tobago, 25-26 June. SPE-191225-MS. https://doi.org/10.2118/191225-ms
- Fredd, C.N., McConnell, S.B., Boney, C.L. and England, K.W. 2001. Experimental study of fracture conductivity for water-fracturing and conventional fracturing applications. SPE J 6:288–298. https://doi.org/10.2118/74138-PA
- Freeman, E.R., Anschutz, D.A., Rickards, A.R. and Callanan, M.J. 2009 . Modified API/ISO crush tests with a liquid-saturated proppant under pressure incorporating temperature, time, and cyclic loading: What does it tell us? Presented in Hydraulic Fracturing Technology Conference, Woodlands, Texas, 19-21 January. SPE-118929-MS. https://doi.org/10.2118/118929-ms

- Gallagher, D.G. 2011. The hierarchy of oily conductivity. JPT, J Pet Technol 63:18–20. https://doi.org/10.2118/0411-0018-jpt
- Ghosh, S., Rai, C.S., Sondergeld, C.H. and Larese, R.E. 2014. Experimental investigation of proppant diagenesis. Presented in Unconventional Resources Conference, Calgary, Alberta, Canada, 30 September–2 October. SPE-171604-MS. https://doi.org/10.2118/171604-ms
- Gidley, J.L., Penny, G.S., McDaniel, R.R. 1995. Effect of proppant failure and fines migration on conductivity of propped fractures. SPE Prod Facil 10:20–25. https://doi.org/10.2118/24008-pa
- Gupta, I., Sondergeld, C., Rai, C. and Hofmann, R. 2018. Water Weakening: Case Study From Marcellus, Woodford, Eagle Ford and Wolfcamp. Presented in 52nd US Rock Mechanics/Geomechanics Symposium, Seattle, Washington, 17-20 June. ARMA-2018-365.
- Haynes. 2016. Hastelloy C-276 Principal Features. http://haynesintl.com/docs/default-source/pdfs/new-alloy-brochures/corrosion-resistant-alloys/c-276.pdf?sfvrsn=6
- Holditch, S.A., Ely, J. 1973. Successful Stimulation of Deep Wells Using High Proppant Concentrations. JPT, J Pet Technol 25:959–964. https://doi.org/10.2118/4118-PA
- Kale, S., Rai, C.S. and Sondergeld, C.H. 2010. Rock typing in gas shales. Presented in Annual Technical Conference and Exhibition, Florence, Italy, 19-22 September. SPE-134539-MS.

  https://doi.org/10.2118/134539-MS.

- Kassis, S. and Sondergeld, C.H. 2010. Fracture permeability of gas shale: Effect of roughness, fracture offset, proppant, and effective stress. Presented in International Oil and Gas Conference and Exhibition in China, Beijing, China, 8-10 June. SPE-131376-MS. https://doi.org/10.2118/131376-MS
- Keyence User Manual. 2014. Profile-analyzing Laser Microscope VK-X250K/X150K/X120K Series.
- Krumbein, W.C. and Sloss, L.L. 1963. *Stratigraphy and sedimentation* (No. QE571 K7 1963).
- Kumar, A., Chellappah, K., Aston, M. and Bulgachev, R. 2013 . Quality control of particle size distributions. Presented in European Formation Damage Conference & Exhibition, Noordwijk, The Netherlands, 5-7 June. SPE-165150-MS. https://doi.org/10.2118/165150-ms
- Lacy, L.L., Rickards, A.R., Bilden, D.M. 1998. Fracture width and embedment testing in soft reservoir sandstone. SPE Drill Complet 13:25–29. https://doi.org/10.2118/36421-PA
- LaFollette, R.F. and Carman, P.S., 2010. Proppant Diagenesis: Results So Far. Presented in Unconventional Gas Conference, Pittsburgh, Pennsylvania, USA, 23–25 February. SPE-131782-MS. https://doi.org/10.2118/131782-MS
- LaFollette, R.F. and Carman, P.S., 2011. Long Term Stability Of Proppants Exposed To Harsh Shale Reservoir Conditions. Presented in Hydraulic Fracturing Technology Conference, Woodlands, Texas, USA, 24-26 January. SPE-140110-MS. https://doi.org/10.2118/140110-MS

- Lee, D.S., Elsworth, D., Yasuhara, H., Weaver, J.D. and Rickman, R. 2010. Experiment and modeling to evaluate the effects of proppant-pack diagenesis on fracture treatments. J Pet Sci Eng 74:67–76. https://doi.org/10.1016/j.petrol.2010.08.007
- Lejay, A., Larmier, S., Rutman, P. and Gelin, F. 2017 . The role of porosity in the development of parallel bedded calcite filled fractures (or beef) in the Vaca Muerta: an integrated analysis from high resolution core data. Presented in Unconventional Resources Technology Conference, Austin, Texas, 24-26 July. URTEC-2668071-MS. http://dx.doi.org/10.15530/URTEC-2017-2668071.
- Liang, F., Sayed, M., Al-Muntasheri, G. and Chang, F.F. 2015 . Overview of existing proppant technologies and challenges. Presented in Middle East Oil & Gas Show and Conference, Manama, Bahrain, 8-11 March. SPE-172763-MS. https://doi.org/10.2118/172763-MS
- Mayerhofer, M.J., Lolon, E.P., Youngblood, J.E. and Heinze, J.R. 2006. Integration of microseismic-fracture-mapping results with numerical fracture network production modeling in the Barnett Shale. Presented in Annual Technical Conference and Exhibition, San Antonio, Texas, USA, 24-27 September. SPE-102103-MS. https://doi.org/10.2118/102103-MS
- McDaniel, B.W. 1986. Conductivity testing of proppants at high temperature and stress. Presented in California Regional Meeting, Oakland, California, USA, 2-4 April. SPE-15067-MS. https://doi.org/10.2118/15067-MS
- McGuire, W.J., Sikora, V.J. 1960. The Effect of Vertical Fractures on Well Productivity. J Pet Technol 12:72–74. https://doi.org/10.2118/1618-g

- Mittal, A., Rai, C.S. and Sondergeld, C.H. 2017a. A Study of Propped-Fracture Conductivity: Impairment Mechanisms Under Laboratory Conditions. Presented in SPWLA 58th Annual Logging Symposium, Oklahoma City, Oklahoma, USA, 17-21 June. SPWLA-2017-CC.
- Mittal, A., Rai, C.S. and Sondergeld, C.H. 2017b. Laboratory Investigation of Proppant-Pack Conductivity: Eagle Ford and Vaca Muerta Shale. Presented in Unconventional Resources Technology Conference, Austin, Texas, 24-26 July 2017. https://doi.org/10.15530/urtec-2017-2670951
- Mittal, A., Rai, C. and Sondergeld, C. 2018a. Experimental Proppant Conductivity Observations: Evaluating Impact of Proppant Size and Fluid Chemistry on Long-Term Production in Shales. Presented in Annual Technical Conference and Exhibition, Dallas, Texas, USA, 24-26 September. SPE-191741-MS. https://doi.org/10.2118/191741-MS
- Mittal, A., Rai, C.S. and Sondergeld, C.H. 2018b. Proppant-conductivity testing under simulated reservoir conditions: Impact of crushing, embedment, and diagenesis on long-term production in shales. SPE J 23:1304–1315. https://doi.org/10.2118/191124-pa
- Montgomery, C.T., Smith, M.B. 2010. Hydraulic fracturing: History of an enduring technology. JPT, J Pet Technol 62:26–32. https://doi.org/10.2118/1210-0026-jpt
- Murphey, J.R. and Totty, K.D., Halliburton Co, 1989. Continuously forming and transporting consolidatable resin coated particulate materials in aqueous gels. U.S. Patent 4,829,100.
- Palisch, T.T., Duenckel, R.J., Bazan, L.W., Heidt, J.H. and Turk, G.A. 2007 . Determining realistic fracture conductivity and understanding its impact on well performance-theory

and field examples. Presented in Hydraulic Fracturing Technology Conference, College Station, Texas, U.S.A, 29-31 January. SPE-106301-MS. https://doi.org/10.2118/106301-MS

- Palisch, T.T., Duenckel, R.J., Chapman, M.A., Woolfolk, S. and Vincent, M.C. 2009. How to Use and Misuse Proppant Crush Tests--Exposing the Top 10 Myths. Presented in Hydraulic Fracturing Technology Conference, Woodlands, Texas, 9-21 January. SPE-119242-MS. https://doi.org/10.2118/119242-MS
- Palisch, T., Duenckel, R., Wilson, B. 2015. New technology yields ultrahigh-strength proppant. SPE Prod Oper 30:76–81. https://doi.org/10.2118/168631-PA
- Penny, G.S., Crafton, J.W., Champagne, L.M. and Zelenev, A.S. 2012. Proppant and fluid selection to optimize performance of horizontal shale fracs. Presented in Hydraulic Fracturing Technology Conference, Woodlands, Texas, USA, 6-8 February. SPE-152119-MS. https://doi.org/10.2118/152119-MS
- Penny, G.S., 1987. An evaluation of the effects of environmental conditions and fracturing fluids upon the long-term conductivity of proppants. Presented in Annual Technical Conference and Exhibition, Dallas, Texas, USA, 27-30 September. SPE-16900-MS. https://doi.org/10.2118/16900-MS
- Pope, C.D., Palisch, T. and Saldungaray, P. 2012. Improving completion and stimulation effectiveness in unconventional reservoirs–Field results in the eagle ford shale of North America. Presented in European Unconventional Resources Conference & Exhibition, Vienna, Austria, 20-22 March. SPE-152839-MS. https://doi.org/10.2118/152839-MS

- Rankin, R.R., Thibodeau, M., Vincent, M.C. and Palisch, T. 2010. Improved production and profitability achieved with superior completions in horizontal wells: a bakken/three forks case history. Presented in Annual Technical Conference and Exhibition, Florence, Italy, 19-22 September. SPE-134595-MS. https://doi.org/10.2118/134595-MS
- Raterman, K.T., Farrell, H.E., Mora, O.S., Janssen, A.L., Gomez, G.A., Busetti, S., McEwen, J., Davidson, M., Friehauf, K., Rutherford, J. and Reid, R. 2017. Sampling a stimulated rock volume: an eagle ford example. Presented in Unconventional Resources Technology Conference, Austin, Texas, 24-26 July. URTEC-2670034-MS. https://doi.org/10.15530/URTEC-2017-2670034
- Raysoni, N., Pinto, M. and Kothamasu, R. 2013. Insights into the Relationship between Single Grain and API/ISO Crush Strength when applied to Proppants with or without Diagenesis. Presented in 47th US Rock Mechanics/Geomechanics Symposium, San Francisco, California, 23-26 June. ARMA-2013-171.
- Raysoni, N. and Weaver, J. 2012a. Long-term proppant performance. Proc - SPE Int Symp Form Damage Control 1:162–177. https://doi.org/10.2118/150669-ms
- Raysoni, N. and Weaver, J.D. 2012b. Selection of proppants for long-term stability. Presented in Hydraulic Fracturing Technology Conference, Woodlands, Texas, USA, 6-8 February. SPE-150668-MS. https://doi.org/10.2118/150668-MS
- Rivers, M., Zhu, D. and Hill, A.D. 2012. Proppant fracture conductivity with high proppant loading and high closure stress. Presented in Hydraulic Fracturing Technology Conference, Woodlands, Texas, USA, 6-8 February. SPE-151972-MS. https://doi.org/10.2118/151972-MS

- RP61, A.P.I., Recommended Practices for Evaluating Short-Term Conductivity, 1989. *Washington, DC: API*.
- RP56, A.P.I., Recommended Practices for Testing Sand Used in Hydraulic Fracturing Operations, 1995. *Washington, DC: API*.
- Rystad Energy. ShaleWellCube, 2019. Editor: Artem Abramov. Available from: https://www.rystadenergy.com/products/shale-solutions/shalewellcube/
- Schubarth, S. and Milton-Tayler, D. 2004. Investigating how proppant packs change under stress. Presented in Annual Technical Conference and Exhibition, Houston, Texas, 26-29 September. SPE-90562-MS. https://doi.org/10.2118/90562-MS
- Sondergeld, C.H., and Rai, C.S. 1993. A New Concept in Quantitative Core Characterization. The Leading Edge. 12 (7): 774-779.
- Simo, H., Pournik, M. and Sondergeld, C.H. 2013. Proppant Crush Test: A New Approach. Presented in Production and Operations Symposium, Oklahoma City, Oklahoma, USA, 23-26 March. SPE-164506-MS. https://doi.org/10.2118/164506-MS
- Stephenson, C.J., Rickards, A.R. and Brannon, H.D. 2003. Is Ottawa Still Evolving? API Specifications and Conductivity in 2003. Presented in Annual Technical Conference and Exhibition, Denver, Colorado, 5-8 October. SPE-84304-MS. https://doi.org/10.2118/84304-MS
- Tang, Y. and Ranjith, P.G. 2018. An experimental and analytical study of the effects of shear displacement, fluid type, joint roughness, shear strength, friction angle and dilation angle on proppant embedment development in tight gas sandstone reservoirs. Int J Rock Mech Min Sci 107:94–109. https://doi.org/10.1016/j.ijrmms.2018.03.008

- Tang, Y., Ranjinth, P.G., Perera, M. and Rathnaweera, T.D. 2018. Influences of proppant concentration and fracturing fluids on proppant-embedment behavior for inhomogeneous rock medium: An experimental and numerical study. SPE Prod Oper 33:666–678. https://doi.org/10.2118/189984-PA
- Taneja, S., Rai, C. S. and Sondergeld, C. H. 2016. Experimental Study of Proppant Pack Deformation, Master's Thesis, The University of Oklahoma. https://hdl.handle.net/11244/44933
- Terzaghi, K. 1925. Principles of soil mechanics. *Engineering News-Record*, *95*(19-27), pp.19-32.
- Thompson, J.C. 1977. The Theory, Methods of Application and Results of the Use of 100 Mesh Sand in Stimulating Permian Basin Formations. Presented in Permian Basin Oil and Gas Recovery Conference, Midland, Texas, 10-11 March. SPE-6374-MS. https://doi.org/10.2118/6374-MS
- Underdown, D.R., Sparlin, D.D. and Day, J.C. 1980. A Plastic Pre-Coated Gravel For Controlling Formation Sand (February 1980). Presented in Offshore South East Asia Show, Singapore, 26-29 February. SPE-8850-MS. https://doi.org/10.2118/8850-MS
- Vincent, M.C. 2010. Refracs: Why do they work, and why do they fail in 100 published field studies? Presented in Annual Technical Conference and Exhibition, Florence, Italy, 19-22 September. SPE-134330-MS. https://doi.org/10.2118/134330-MS
- Weaver, J.D., Parker, M., van Batenburg, D.W. and Nguyen, P.D. 2007. Fracture-related diagenesis may impact conductivity. SPE J 12:272–281. https://doi.org/10.2118/98236-PA

- Weaver, J., Rickman, R. and Luo, H. 2008. Fracture Conductivity Loss Due to Geochemical Interactions Between Man-Made Proppants and Formations. Presented in Eastern Regional/AAPG Eastern Section Joint Meeting, Pittsburgh, Pennsylvania, USA, 11–15 October. SPE-118174-MS. https://doi.org/10.2118/118174-MS
- Xu, T., Zheng, W., Baihly, J., Dwivedi, P., Shan, D., Utech, R. and Miller, G. 2019. Permian Basin Production Performance Comparison Over Time and The Parent-Child Well Study. Presented in Hydraulic Fracturing Technology Conference and Exhibition, Woodlands, Texas, USA, 5-7 February. SPE-194310-MS. https://doi.org/10.2118/194310-MS
- Yang, A., Carbrey, R., Abramov, A. and Ramos-Peon, A. 2019 . Effect of Proppant Design on Production Decline of Shale Wells. Presented in Unconventional Resources Technology Conference, Denver, Colorado, 22-24 July. URTEC-2019-440-MS. https://doi.org/10.15530/urtec-2019-440
- Yasuhara, H., Elsworth, D., Polak, A. 2003. A Mechanistic Model for Compaction of Granular Aggregates Moderated by Pressure Solution. J of Geoph Res 108 (B11): 1-13. 2530. http://dx.doi.org/10.1029/2003JB002536.

Appendix-A

1. Assembling Proppant-pack

1.1. Cleaning

Before starting the experiment, use ethanol to clean silica gel from all the threads of conductivity cell and fittings.

1.2 Assembly of Proppant-Pack (see Fig. 1 for reference)

a) Fig. 1 shows the metal bracket (cuboid with space to push proppant-pack into conductivity cell). The metal block (tall metal piece fitting inside the bracket) is used to push the rock and metal platens into the cell. Install the Teflon sleeves (white color sleeve) on Hastelloy seal and rock sample (see Fig. a).

b) Use the metal bracket to insert the Hastelloy sleeve at an angle and flatten it out. Using the manual hydraulic press in department machine room and metal block, push the platen-sleeve combination to the bottom ensuring it is flat (follow the procedure in Fig. 2,3, and 4). Also insert the rock sample with Teflon sleeve using similar procedure at the same time.

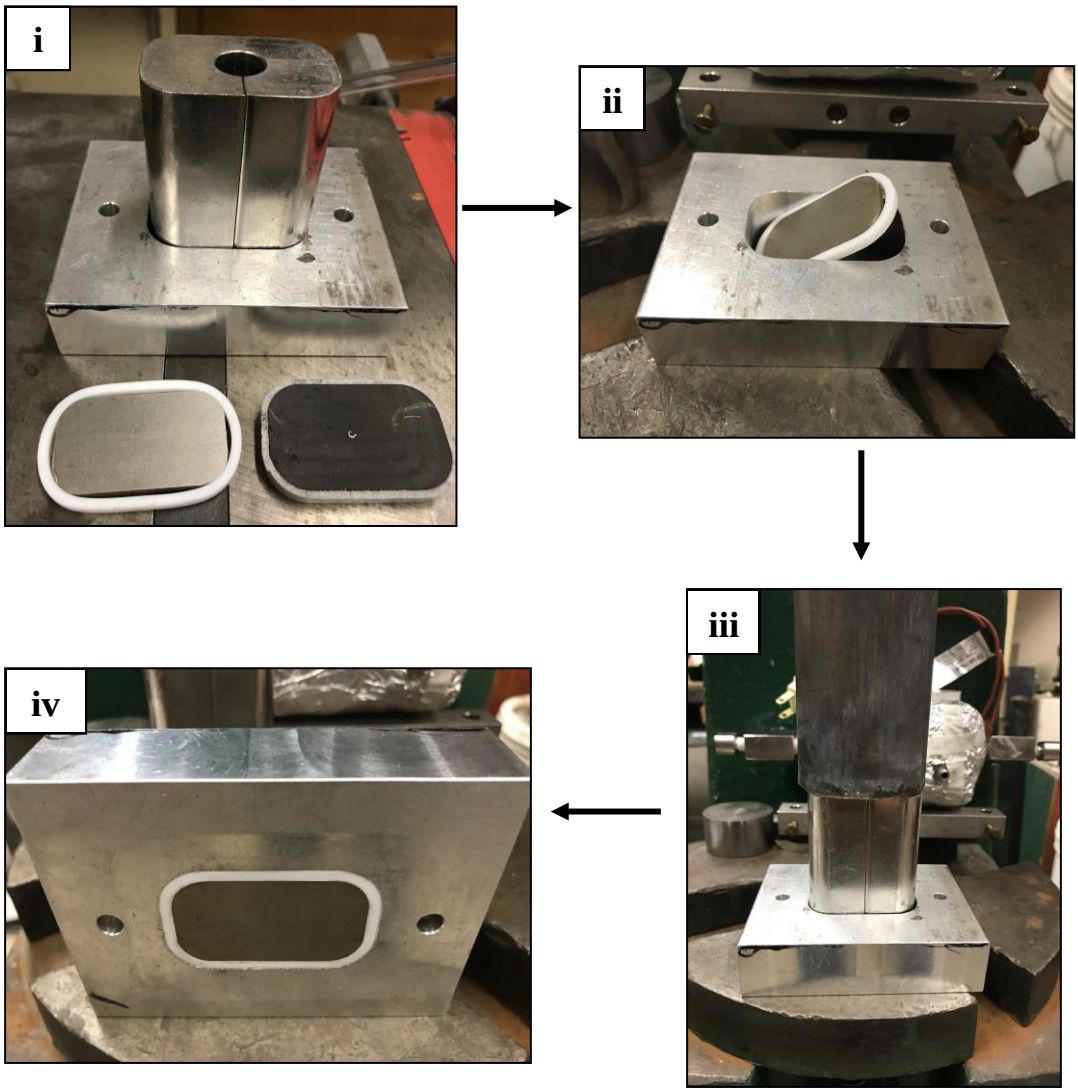

Fig. 1: Images for section 1.2 (assembly of proppant-pack)

1.3. Installing lower part of proppant-pack (see Fig. 2 for reference)

i. Use the metal ring (highlighted in yellow in Fig. i) to adjust the proppant-pack thickness being tested. Use the metal bracket to push the rock-sleeve and seal-sleeve combinations into the conductivity cell using the hydraulic press.

ii. The rock-platen should be placed so that the port for fluid flow is not blocked in conductivity cell (see Fig. iv).

iii. HFT superglue specifically has been observed to be effective in sticking the Hastelloy mesh to the conductivity cell body (Fig. v). Cut appropriately sized Hastelloy mesh and apply superglue to the ends (longer mesh cut-out can be helpful in providing more surface area for it to glue properly) (see Fig. vi).

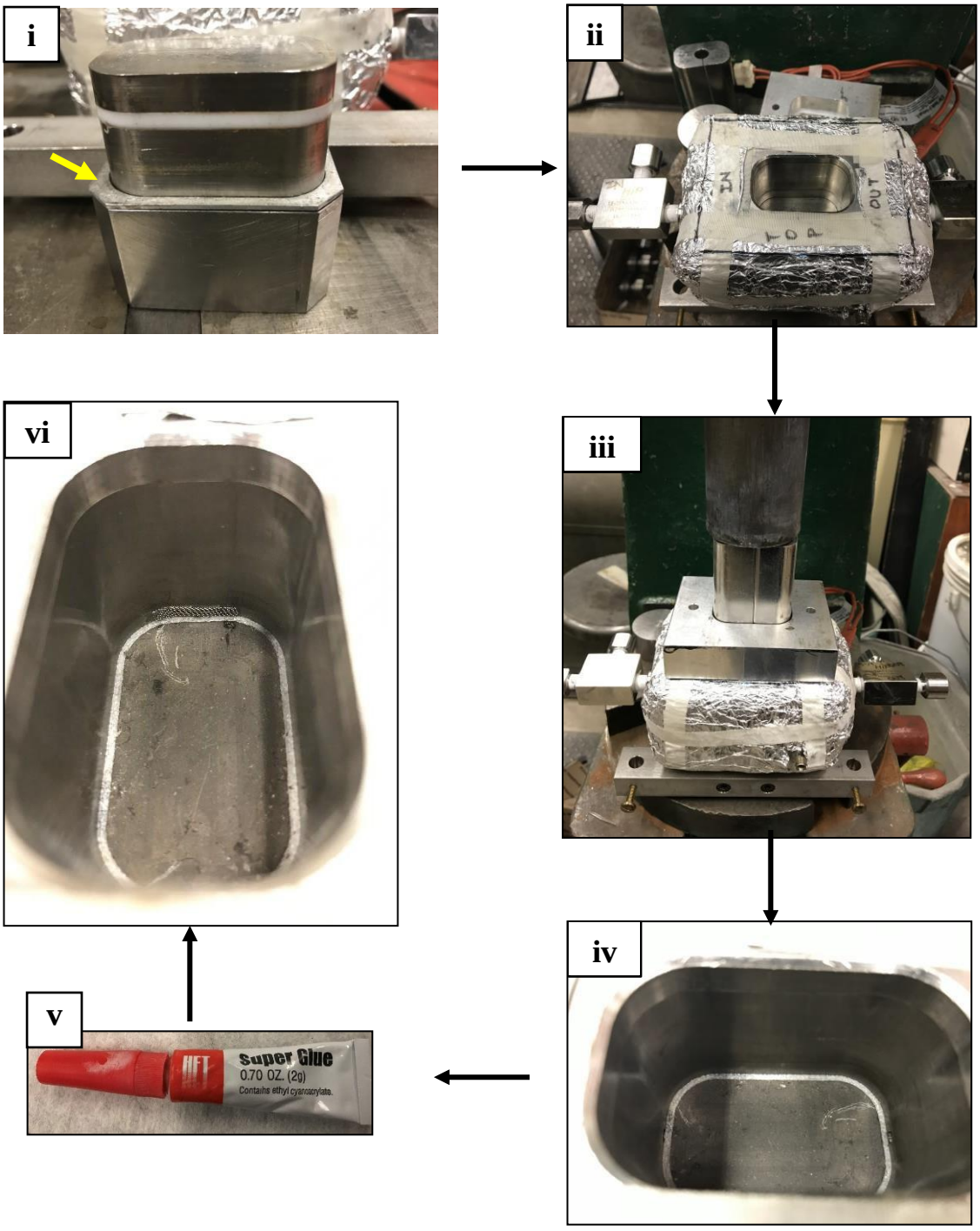

Fig. 2: Images for section 2.3 (installing lower part of proppant-pack)

1.4. Dial gauge for base height measurement (see Fig. 3 for reference)

Note:

→Make sure the alignment of dial gauge is not altered during the measurement

→Take multiple readings for checking repeatability, and also three readings moving from inlet towards outlet

a) Use a leveler to make sure the dial gauge is locked in vertical measurement.
b) Adjust dial gauge to measure the base height or zero error. Try to keep this reading as small as possible. This would enable measuring a thick proppant-pack. Do not change the orientation or alignment of dial gauge until the assembly of proppant-pack is completed.
c) Once the proppant is put in, use the metal block with Hastelloy sleeve (**measure the thickness of Hastelloy seal before starting all these measurements**) combination to compact the proppant-pack at 300 psi using the automated press in mechanical room (see Fig. v). The directions for software are discussed later.

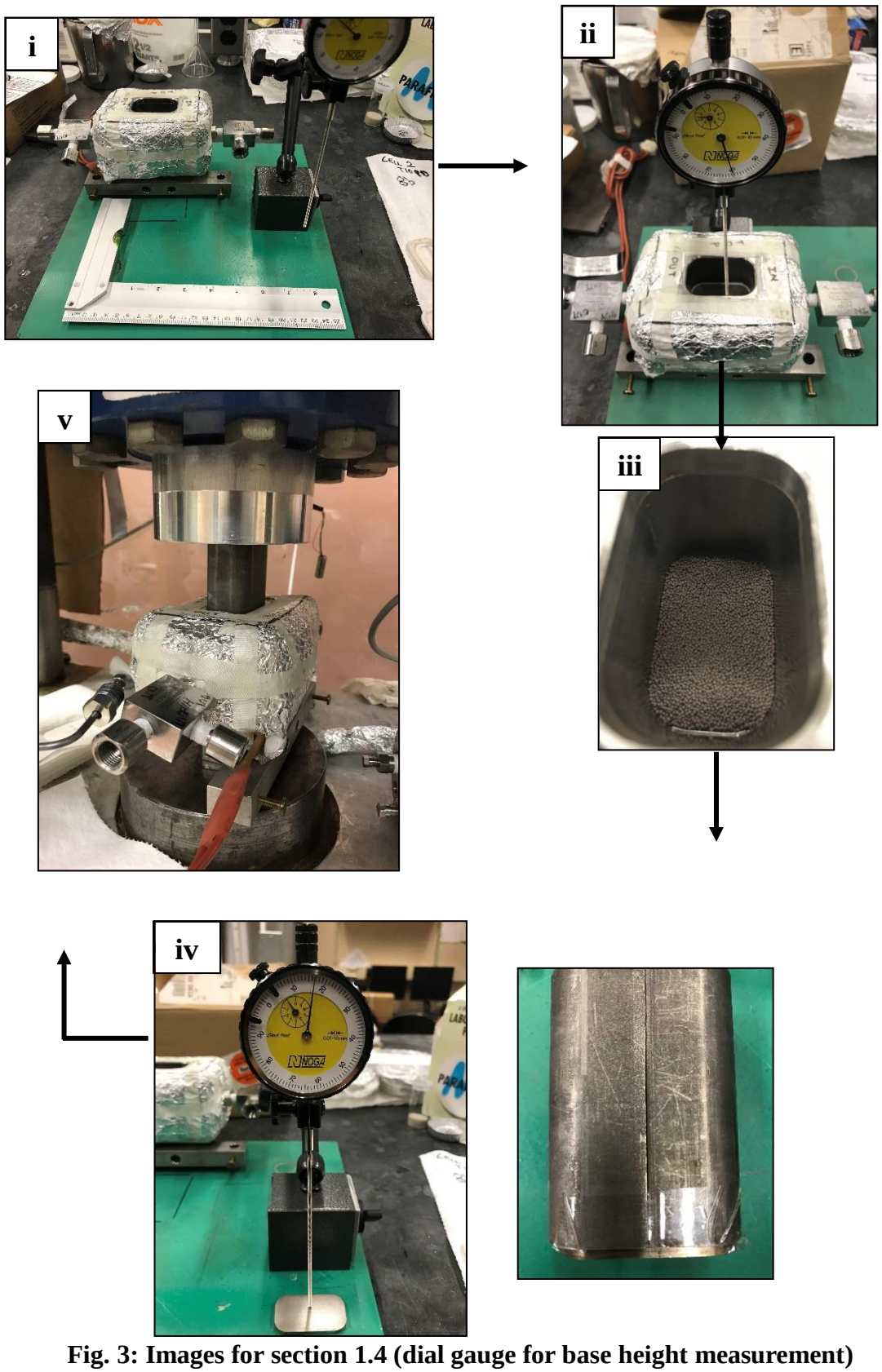

Fig. 3: Images for section 1.4 (dial gauge for base height measurement)

1.5. Proppant-pack thickness measurement: Dial gauge (see Fig. 4 for reference)

a) After compacting to 300 psi for 15 minutes, measure the proppant thickness using dial gauge.

b) Attach a nut on the seal used earlier (see Fig. i). Lay the seal on top of proppant-pack and use dial gauge for the measurement. **Note** that the dial gauge is required to be in same alignment setting throughout to measure proppant-thickness at different stages (see Fig. ii).

c) **Proppant thickness** = **Final measurement** (measurement in step b in section 1.5) – **thickness of Hastelloy seal** (measurement in step c in section 1.4) – **zero error** (measurement in step b in section 1.4)

d) Once the thickness has been determined, install the top part of proppant-pack. Place the rock, seal and steel spacer in the order mentioned from bottom to top in the metal bracket. Use the metal block to push these into the conductivity cell. Note that by placing all these three parts on top of another, an attempt is made to avoid any air gaps between these platens (see Fig. iii and iv).

e) Install the top part of the conductivity cell and place the cell between the pistons of hydraulic press. Make sure the LVDT cores and the **matching** assembly are sliding through the top part of conductivity cell.

f) Before starting the experiment, click on the setup button in the LVDT box (see software

section). Adjust the LVDTs at both the ends till a reading of -0.0999 is obtained. Make sure that sliding the LVDTs in the direction of compaction of proppant-pack, the values for LVDT move from -0.1 to 0 to +0.1. Bring back the LVDT to -.0999 position. Now, a screwdriver can be used to tighten the LVDTs in place using the nuts on the side (see Fig. iv). Note that there is no load on the conductivity cell at this point.

g) The LVDT numbers at this stage are representative of the proppant-pack thickness measured in step c (section 1.5)

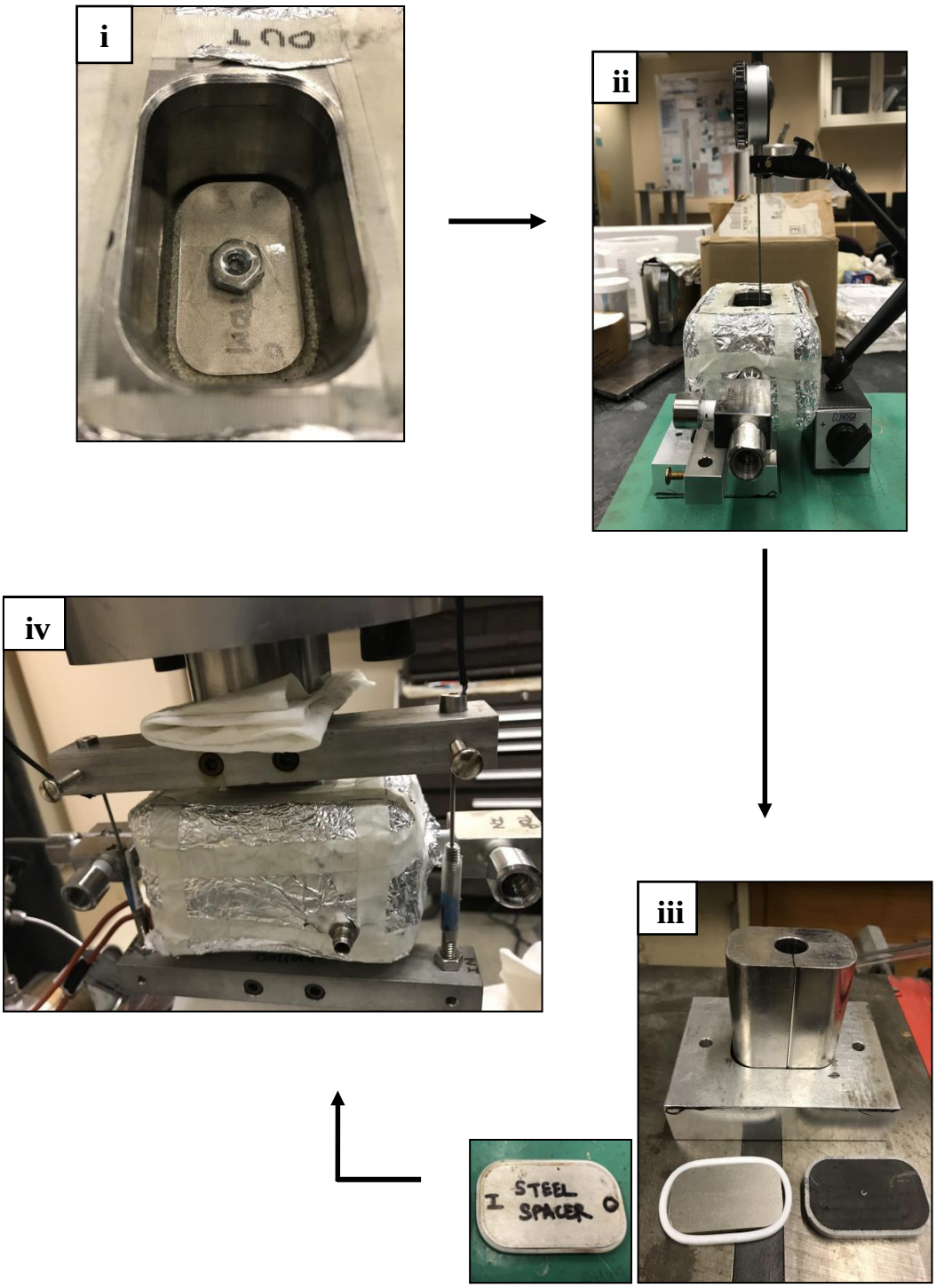

Fig. 4: Images for section 1.5 (proppant-pack thickness measurement)

2. Software Settings

2.1. Open the "Load Control" folder on desktop.

2.2. Open the selected Visual basic project (highlighted in the image below).

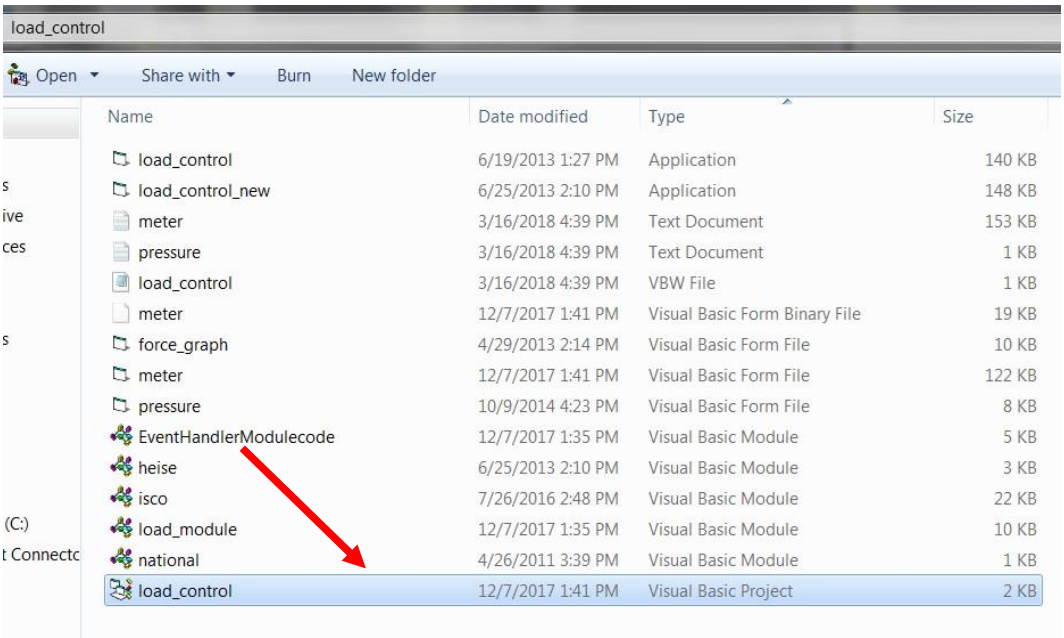

2.3. Click the play icon to run the code (highlighted in red).

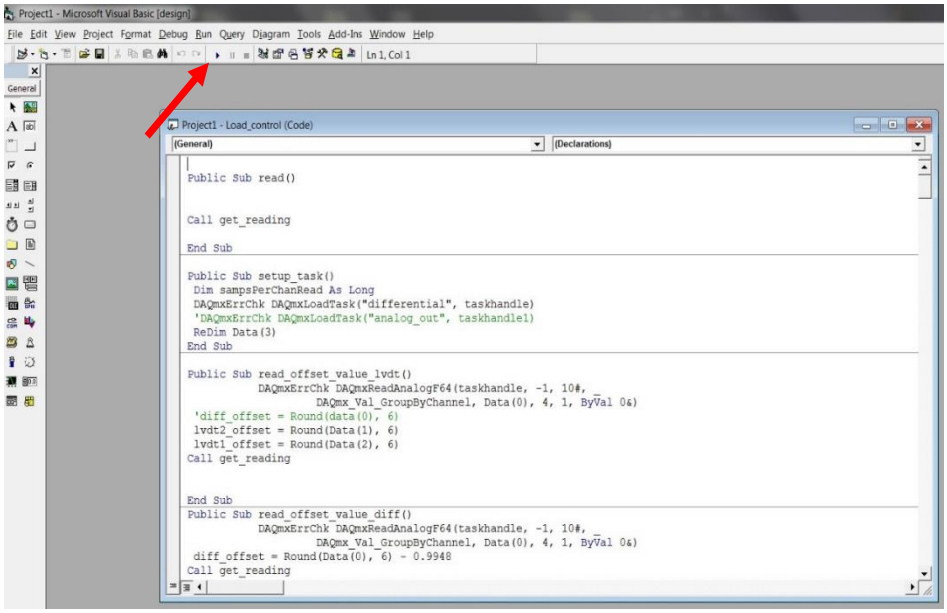

2.4. Window for the software will open. with input parameters will open. Enter the desired parameters in the tabs highlighted with red arrows and hit “Start”. The snapshot below shows the numbers for reference.